Atmospheric concentration of black carbon in the western Arctic

Master Thesis
submitted by

Kristina Conrady

Supervisors:

Prof. Dr. K. Heinke Schlünzen
Meteorologisches Institut, Universität Hamburg

Dr. Andreas Herber
Alfred-Wegener-Institut Helmholz-Zentrum
für Polar- und Meeresforschung, Bremerhaven

Meteorologisches Institut
Fachbereich Geowissenschaften
Universität Hamburg

Hamburg, Oktober 2013

Abstract

Black carbon (BC) influences the Arctic climate by altering the radiation budget. Measurements of atmospheric BC concentration are rare in the Arctic. Furthermore, literature providing information about the current BC concentration or about its evolution refers almost exclusively to ground measurements. Using Polar Airborne Measurements and Arctic Regional Model Simulation Project (PAMARCMiP) data of 2009, 2011 and 2012, an inventory of the current BC concentration is made in this thesis. It is made before the onset of the commercial utitlsation in the Arctic. Besides the horizontal and vertical distribution of BC concentration and its temporal variation, possible source areas are identified and surrogate parameters are sought.

Mean BC concentration is about $26\,\text{ng/m}^3$ in 2009 and doubles approximately to $52\,\text{ng/m}^3$ in 2011 and almost doubles again to $102\,\text{ng/m}^3$ in 2012. In contrast to previous results, the vertical distribution of BC concentration analysed in this thesis reveals no height dependency in most cases. Regional differences exist in 2011, while the horizontal distribution is rather homogeneous in 2009. The trajectory analysis reveals air masses including a high amount of BC origin of Eurasia, while air masses transported over the Arctic Ocean, the North Atlantic or northern Canada include a lower amount of BC. Neither ozone concentration, nor particle concentration, nor AOD, nor albedo are exposed to be a surrogate parameter for BC concentration.

Further measurements of this kind are necessary to observe the evolution of BC concentration in the Arctic and to force regulations like definitions of thresholds. Additionally, an increase in data density is essential to enhance the reliability of the results.

Kurzfassung

Schwarzer Kohlenstoff, englisch "black carbon" (BC), beeinflusst das arktische Klima in dem es den Strahlungshaushalt verändert. Messungen der atmosphärischen BC-Konzentration in der Arktis existieren nur vereinzelt und Literatur, die Aufschluss über die aktuellen BC-Konzentrationen oder deren zeitliche Entwicklung gibt, bezieht sich nahezu ausschließlich auf Stationsdaten. Bevor die kommerzielle Nutzung der Arktis im großen Umfang einsetzt, wird in dieser Arbeit eine Bestandsaufnahme der gegenwärtigen BC-Konzentrationen anhand von Daten der Polar Airborne Measurements and Arctic Regional Model Simulation Project (PAMARCMiP) Kampagnen der Jahre 2009, 2011 und 2012 präsentiert und diskutiert. Neben der horizontalen und vertikalen Verteilung der BC-Konzentration und ihrer zeitlichen Änderung, werden mögliche Quellregionen identifiziert und nach Parametern gesucht, die Rückschlüsse über die BC-Konzentration ermöglichen.

Die mittlere BC-Konzentration beträgt 2009 $26\,\mathrm{ng/m^3}$, verdoppelt sich zunächst bis 2011 auf $52\,\mathrm{ng/m^3}$ und dann nochmal auf $102\,\mathrm{ng/m^3}$ im Jahre 2012. Im Gegensatz zu Untersuchungen von Daten aus früheren Jahren, zeigt die vertikale Verteilung der BC-Konzentrationen der hier untersuchten Daten in den meisten Fällen keine Höhenabhängigkeit. Regionale Unterschiede der BC-Konzentration existieren 2011, während sie 2009 kaum vorhanden sind. Die Trajektorienanalyse zeigt, dass Luftmassen mit hohen BC-Konzentrationen vermutlich aus Eurasien in die Arktis transportiert werden, während Luftmassen, die über den Arktischen Ozean, den Nordatlantik oder Nordkanada transportiert wurden, eher geringere BC-Konzentrationen aufweisen. Weder Ozonkonzentration, Teilchenkonzentration, Aerosol-optische Dicke noch Albedo werden als Proxyparameter für die BC-Konzentration identifiziert.

Weitere Messungen dieser Art sind notwendig, um die Entwicklung der BC-Konzentration in der Arktis zu dokumentieren und Regelungen, wie zum Beispiel die Festlegung eines Grenzwertes, zu forcieren. Dafür ist aber auch eine Erhöhung der Datendichte unerlässlich, um die Belastbarkeit der Ergebnisse zu erhöhen.

Contents

1 Introduction

In comparison with all other particulate species located in the atmosphere, black carbon (BC) is the one with the most efficient ability to absorb visible light (AMAP, 2011). Ramanathan and Carmichael (2008) estimate a global BC forcing of about $0.9\,\mathrm{W/m^2}$, thus, as much as 55% of the CO_2 forcing. Therefore, it is larger than the forcing resulting from other greenhouse gases like CH_4, CFCs, N_2O or tropospheric ozone (Ramanathan and Carmichael, 2008). However, its atmospheric lifetime is around days to weeks and, therefore, much less than the CO_2 lifetime (*U.S. EPA*, 2012). Hence, a reduction in BC would lead to a rapid response in terms of its impact on climate.

Beside its distinctive ability to absorb short-wave radiation, BC influences the properties of clouds and the albedo of the surface it is deposited. The reduction of albedo by BC, the so-called "BC snow/ice albedo effect", leads to warming, while the other effects of BC on climate are not well quantified (*U.S. EPA*, 2012). Therefore, the globally averaged net climate effect of BC might lead to either warming or cooling. Regarding the net effect on the Arctic climate only, the BC snow/ice albedo effect plays a greater role compared to the other effects. Thus, BC is assumed to have a warming effect on the Arctic climate, especially if the surface albedo is high during spring. This effect combined with temperatures not far below the freezing point of water might induce melting and, in turn, lead to further warming. That is why the vulnerability in terms of warming and melting effects of BC makes the Arctic unique.

The amount of BC, especially in the Arctic atmosphere, is poorly analysed. With the onset of extensive commercial use of the Arctic, the amount of BC in the Arctic atmosphere will increase, assuming no BC reducing techniques. That includes Arctic shipping like marine transport, fishing and tourism, as well as offshore production of resources and military use. The current amount of BC in the Arctic atmosphere is not known, neither the probable evolution in BC concentration in the Arctic. But these two values are important to estimate the current and the future impact of BC on Arctic climate.

It is estimated that the retreat of sea-ice in the Arctic will soon allow the use of the Northwest Passage and the Northern Sea Route, which in turn increases the number of BC sources along these shipping routes. Most probably, pollutants emitted in the lower Arctic atmosphere remain in the Arctic, since the stratification is usually stable in polar regions. BC located in lower altitudes has a warming effect (AMAP, 2011), while it has a dimming effect in higher altitudes (Ramanathan and Carmichael, 2008). Therefore, not merely the total amount of BC in the Arctic atmorphere is important to know, but rather the knowledge of the vertical distribution of BC is essential in order to determine the impact of BC on Arctic climate.

This thesis is structured as follows. In Chapter 2, the term "black carbon" is explained, its characteristics are described and its impact on Arctic climate is outlined. Furthermore, BC sources and some published BC concentrations are listed. In Chapter 3, black carbon instruments are introduced, the campaigns, the used data originates, and the data analysis is described.

The aim of this thesis is to give an impression of the current BC concentration in the Arctic atmosphere and to show how the BC concentration has been developing since 2009. Therefore, the horizontal and vertical distribution of refractory black carbon (rBC) is analysed. Since no data are available for the eastern part of the Arctic, only the western part is investigated.

The used data sets have been recorded during three Polar Airborne Measurements and Arctic Regional Model Simulation Project (PAMARCMiP) campaigns in the years 2009, 2011 and 2012. Before analyses of these data are possible, the parameters which are of concern are merged in one data set and are cleaned afterwards. To reveal the current atmospheric rBC concentration in the western Arctic, different analyses are made and described in Chapter 4. Previous analyses show a height dependency of BC concentration, thus, the vertical distribution of rBC is investigated in this thesis. Furthermore, the temporal variation of the vertical rBC concentration is analysed, as well as, the spatial differences. Additionally, the horizontal distribution of rBC concentration is analysed. As described for the vertical distribution, the temporal and spatial variation of rBC concentration are investigated.

Using a backward trajectory model and a particle dispersion model, possible source areas are determined in Chapter 4, as well. In this context, three examples of vertical profiles of rBC concentration are chosen. Backward trajectories ending at the measur-

ing points of these profiles are calculated. Results of a particle dispersion model are used for comparative purposes. In order to support the interpretation of the model results, the general synopses of the weather for the chosen cases are compared to the backward trajectories.

Measurements of parameters describing the BC amount are rare, especially in the Arctic. A proxy parameter is sought in order to draw inferences about BC, if no BC data are available. To find possible dependencies, correlation analyses for rBC concentration and Ozone concentration, particle concentration, aerosol optical depth and albedo are made and described in Chapter 5. The four parameters are included in the mentioned data sets and are part of the measurements of at least one PAMARCMiP campaign.

The conclusions follow in Chapter 6.

2 Black carbon in the atmosphere

2.1 What is "black carbon"?

The question what "black carbon" is cannot be answered easily. Although, black carbon (BC) plays a major role in the Earth's climate system and influences air quality, there is no unambiguous definition of the term "black carbon" in the research community. Additionally, the distinction against the term "soot" is not clarified. In some papers, soot is determined as a part of BC, e.g. IPCC (2007a) (p. 810), in others it is used vice versa (Horvath, 1993; Moosmüller et al., 2009; Ramanathan and Carmichael, 2008; Schwarz et al., 2006; *U.S. EPA*, 2012). Furthermore, in the Intergovernmental Panel on Climate Change (IPCC, 2007b) (p. 135), for instance, these two terms are partly used synonymously.

Among others, Buseck et al. (2012), Bond et al. (2013) and Petzold et al. (2005) consider these problems and propose definitions and recommendations for the use of the term "black carbon". In Buseck et al. (2012), a problem-solving approach is presented. They introduce the term "ns-soot", where "ns" signifies carbon nanospheres. They define, that ns-soot is comprised of nanospheres, which are typically smaller than 100 nm in diameter and arranged in acinoform (grape-like) morphologies. BC is then described as "an ensemble of carbonaceous materials that strongly absorb visible light" (Buseck et al., 2012), which not only contains ns-soot, but also other light-absorbing carbonaceous materials. In terms of particle morphology, it is an useful approach but in this thesis, it is not further used.

Bond et al. (2013) determine BC by itemising its characteristics. They mention the strong ability of BC to absorb visible light, BC is refractory with a volatilisation temperature near 4000 K, the insolubility of BC in water, organic solvents and other components of atmospheric aerosol and that BC is an aggregate of small spherules. The characteristics of BC are discussed in detail in Section 2.2.

Petzold et al. (2005) recommend a terminology which is related to a measuring technique or a kind-of-use. They determine BC as "a useful qualitative description when referring to light-absorbing carbonaceous substances in atmospheric aerosol" and they recommend to use more specific terms for quantitative utilisation. These terms are equivalent black carbon (EBC), refractory black carbon (rBC) and soot. Data derived from optical absorption methods (Chapter 3), should be referred to as EBC, since those methods require a conversion of light absorption coefficient into mass concentration. In contrast, the term rBC should be used regarding data derived from incandescence-based methods (Chapter 3). Petzold et al. (2005) recommend to only use the term "soot" to describe the formation of carbonaceous particles, namely incomplete combustion, and not for atmospheric aerosol.

In the current literature, the nomenclature of carbonaceous particles and carbonaceous matter in airborne particles is characterised by inadequate definitions and distinct ambiguities. The terminology invented by Petzold et al. (2005) is used in this thesis, because they clearly distinguish between the terms "BC" and "soot" which is still seldom found in literature. Since an incandescence-based method is used, the recommended term for measurements derived from incandescence-based methods, "refractory black carbon" (rBC), by Petzold et al. (2005) is chosen for data analysis.

2.2 Characteristics of black carbon

Based on the described vagueness in definition, it is not straightforward to specify the characteristics of BC. BC is formed during incomplete combustion of fossil fuels, biofuels and biomass (Fig. 2.1). Incomplete combustion means, there is no complete conversion of the fuels or biomass into CO_2 and water, due to a lack of oxygen and/or too low temperatures. Incomplete combustion occurs in several kinds of burning processes. Following Bond (2007), the main four source categories are a) diesel engines used for transport or industrial applications, b) residential solid fuels, namely wood and coal, c) forest and savanna burning, both natural and for slash-and-burn land clearance and d) industrial processes. During these burning processes, small carbon spherules of diameters $d < 10\,\mathrm{nm}$ up to $50\,\mathrm{nm}$ are formed and accumulated in aggregates. The light-absorbing carbonaceous substances included in this aerosol is in this text called "black carbon" or "BC". The emitted BC particles are insoluble in water and common organic solvents and, therefore, they are not washed out from the atmosphere due to

wet deposition (AMAP, 2011). However, the aggregates' morphology facilitates sorption of other species (Petzold et al., 2005), they get hydrophilic and accessible for wet deposition. The formation of aggregates starts at or shortly after emission and the aggregates get internally or externally mixed. Therefore, hardly any pure BC particles exist in the atmosphere, particularly in the Arctic atmosphere. The particles grow via coagulation during transport. Their size distribution is a function of formation mechanism and atmospheric processes during transport. The more efficient the fuel burn, the smaller the particles. Usually, the particles are assigned to the Aitken mode but due to subsequent coagulation, they grow and they are found in the accumulation mode.

The composition of BC particles is partly depending on the fuel burned. Fossil fuel and biomass combustion leads to emissions of BC and organic carbon (OC), as well as SO_2, NO_x, CO and volatile organic carbon species. OC is a chemical combination of carbon and hydrogen or other elements (Petzold et al., 2013). The distinguishing features of the two combustion processes are the ratio of BC and OC and the different co-emitted species. While the ratio of BC and OC is relatively high at fossil fuel combustion and sulphate is additionally emitted, this ratio is lower at biomass burning and potassium and ammonium are additionally emitted (AMAP, 2011). The co-emitted species are important, because they can affect the way in which BC is altered. That involves the degree of hygroscopicity, the manner of acting as cloud condensation nuclei (CCN), the atmospheric lifetime, as well as absorption and scattering properties.

As mentioned before, BC is removed from the atmosphere via wet deposition. Additionally, dry deposition acts as a sink for atmospheric BC. In regions with low precipitation amounts, like the Arctic, dry deposition is an important process. Lifetime of BC strongly depends on the deposition rates of the areas the particles are transported through. It usually has a short atmospheric lifetime between days and weeks (Cape et al., 2012). The sedimentation rate is lowest for particles of the accumulation mode (Nilsson and Rannik, 2001) and, therefore, for the grown BC particles. For larger particles, the sedimentation rate increases with particle size, while the sedimentation rate decreases with particle size for smaller particles. Thus, the sedimentaion rate might be lower in the Arctic compared to the global average, which might lead to longer atmospheric lifetimes of BC in the Arctic.

One of the most important properties of BC is the strong ability to absorb light in the spectral range of visible light. The mass specific absorption coefficient, also called mass absorption cross section (MAC), at $\lambda = 550\,\text{nm}$ is greater than $5\,\text{m}^2/\text{g}$ (Petzold et al., 2013). The MAC is only slightly wavelength-dependent and holds for freshly

formed particles. The effect of this property is discussed in Section 2.3. As mentioned before, BC particles can consist of a BC core and a coating of different possible components. The coating may alter the optical properties of BC. Light absorption is enhanced, if the BC core is coated with scattering material, which is shown theoretically by Fuller et al. (1999) and observed experimentally by, for instance, Schnaiter et al. (2005) and Zhang et al. (2008).

Two other specific particles absorbing visible light are brown carbon (BrC) and dust (Bond et al., 2013). BrC is a subset of organic aerosol and consists of a complex mixture of organic compounds. BrC and BC are similar in size but BrC absorbs light weaker than BC. Its MAC is smaller than $1\,\mathrm{m^2/g}$ for a wavelength of $\lambda = 550\,\mathrm{nm}$. Furthermore, BrC light absorbance is strongly wavelength dependent. The latter aspect and the solubility of BrC deliver the possibility to distinguish between BC and BrC. Dust in comparison to BC and BrC has the weakest light absorption, namely around $0.009\,\mathrm{m^2/g}$ for a wavelength of $\lambda = 550\,\mathrm{nm}$, especially at lower wavelength. Moreover, dust particles can be distinguished from BC, since these have typical diameters larger than $2\,\mathrm{\mu m}$, a crystalline structure and contain crustal elements (Bond et al., 2013).

2.3 Impact of black carbon on Arctic climate

In terms of global surface air temperature change, BC is twice as effective as CO_2 (Hansen and Nazarenko, 2004), neglecting the ambiguity in nomenclature. BC mainly affects the Earth's radiation budget in three different ways (Fig. 2.1). The BC snow/ice albedo effect is shown in Figure 2.1a. Deposition of BC to ice/snow enhances the absorption of shortwave radiation and leads to melting and eventually to warming of the lower atmosphere and induces melting. A particular feature of the Arctic atmosphere is the stable atmospheric boundary layer. This suppresses heat exchange with upper layers and the surface temperature response is closely related to radiative fluxes at or near the surface. The BC snow/ice albedo effect superimposes the snow/ice albedo feedback (AMAP, 2011) and intensifies its effect. Hansen and Nazarenko (2004) estimate a globally climate forcing of $0.3\,\mathrm{W/m^2}$ for the effect of soot on snow and ice albedos in the Northern Hemisphere. They estimate a climate forcing of $1\,\mathrm{W/m^2}$ at middle- and high-latitude land areas in the Northern Hemisphere and over the Arctic Ocean. Furthermore, the IPCC (2007b), Jacobson (2001), and Ramanathan (2007) estimate climate forcings of $0.1 \pm 0.1\,\mathrm{W/m^2}$, $0.06\,\mathrm{W/m^2}$ and $0.1 - 0.3\,\mathrm{W/m^2}$, respectively.
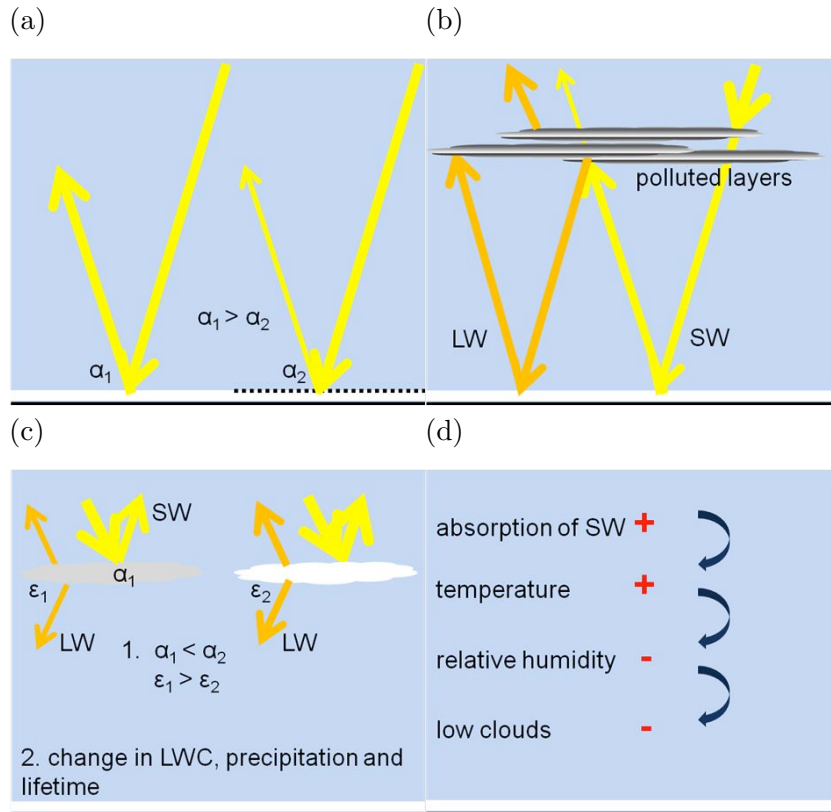
Figure 2.1: Schematic illustration of effects on the Earth's radiation budget by BC: (a) BC snow/ice albedo effect, (b) aerosol direct effect, (c) aerosol indirect effects and (d) semi-direct effect.

The aerosol direct effect (Fig. 2.1b) describes the absorption or scattering of shortwave radiation by aerosols. As mentioned before, BC has a strong ability to absorb light and absorbs both incoming and outgoing radiation (*U.S. EPA*, 2012). That leads to a warming at altitudes above and within the haze layer and in turn, it increases the amount of longwave radiation emitted by the pollution layers to the surface. It results, for highly reflective surfaces like snow or ice covered ground in the Arctic spring, in surface warming (AMAP, 2011). Estimates of BC climate radiative forcing by aerosol direct effect are $0.34 \pm 0.25\,\mathrm{W/m^2}$ (IPCC, 2007*b*), $0.55\,\mathrm{W/m^2}$ (Jacobson, 2001), $0.2 - 0.6\,\mathrm{W/m^2}$ (Hansen, 2002) and $0.9\,\mathrm{W/m^2}$ (Ramanathan, 2007).

Aerosols interact with clouds and perturb the Earth's radiation budget by altering cloud properties (Righi et al., 2011). These processes are called "aerosol indirect effect" (Fig. 2.1c). A distinction is made between the first indirect effect and the second indirect effect. Aerosols act as CCN and increase the cloud droplet number concentration, which leads to a decrease in droplet size, assuming a fixed liquid water content (IPCC, 2007*b*). If an aerosol is able to activate and form a cloud droplet depends on the

aerosol size and the supersaturation inside the cloud. Freshly emitted, small particles are not able to act as a CCN in Arctic stratiform clouds with relatively low supersaturation, but the ability increases with increasing particle size which in turn increases with particle age. BC particles emitted outside and transported to the Arctic may be able to activate and form cloud droplets, even if the cloud's supersaturations are low. This leads to two responses, one in the short-wave range, the other in the long-wave range. In the short-wave range smaller droplets and higher number concentrations lead to higher cloud albedos. Globally, that results in cooling, because higher albedos lead to higher reflection of short-wave radiation. Relating to polar regions, the effect is small if not negligible small, since either the solar zenith angles are high or there is no incoming short-wave radiation or the surface albedo is already high, during months with high pollution (Garrett and Zhao, 2006). For the long-wave range, Garrett and Zhao (2006) show an increase in cloud long-wave emissivity, which leads to a warming effect.

The second indirect effect describes the impact of aerosols on cloud liquid water content, precipitation and cloud lifetime (Righi et al., 2011). The impact of both, first and second indirect effect, on global and Arctic climate is not yet fully understood. Neither the magnitude nor the value is known. Estimates of annual-mean net anthropogenic surface forcing ranging between $-0.98 \pm 0.12 \, \mathrm{W/m^2}$ are mentioned by AMAP (2011). At least, the impact on the Arctic's radiation budget is assumed to be less negative compared to the global impact or may be positive (AMAP, 2011). Since the knowledge of the impact of these effects is poor in general, it is not better known for BC in particular.

Another implification of aerosols and especially of BC is the semi-direct effect (Fig. 2.1d). Absorption of short-wave radiation leads to warming and a decrease in relative humidity, which in turn result in reduction of low cloud cover. On the one hand, this reduction leads to warming, since low clouds have a high albedo and imply no significant reduction of outgoing long-wave radiation. On the other hand, less cloud cover leads to less wet deposition and therefore, an increase in atmospheric life time of BC containing aerosols. The processes described by the semi-direct effect result in an amplification of BC forcing (AMAP, 2011).

Finally, there is one more impact of BC on Arctic climate but in contrast to the effects mentioned before, its processes do not take place in the Arctic. BC affect the radiation budget outside the Arctic, and its impact may affect the Arctic climate due to energy transport via atmosphere and ocean. That leads to an amplification or a reduction of local impacts.

2.4 Black carbon sources and published black carbon concentrations

Ramanathan and Carmichael (2008) mention global annual BC emissions of about 8 Tg/y with an uncertainty of ±50 % in 1996. Biofuels are the origin of 20 % of these emissions, fossil fuels and open biomass burning are responsible for 40 % of these emissions each (Ramanathan and Carmichael, 2008). Bond (2007) found similar ratios for the year 2000. The main source regions changed in the 1950s (Ramanathan and Carmichael, 2008). Northern America and Western Europe are not responsible for the major emissions anymore currently the East Asian and tropical emerging countries are the main emitters of soot (Bond, 2007; Ramanathan and Carmichael, 2008). Another source, especially important for the Arctic, are Inner Arctic coal piles. For instance in Svea, Spitsbergen, wind-driven BC-containing particles may have a localised but not negligible effect on the local radiation budget.

Selected atmospheric BC concentrations of ground measurements published in the last years are mentioned for comparing reasons. Liu et al. (2011) published monthly mean values of EBC concentration measured from 2002 to 2007. Their results are around $90 \, \text{ng/m}^3$ at Alert in both, March and April, aorund $60 \, \text{ng/m}^3$ and $50 \, \text{ng/m}^3$ at Barrow in March and April, respectively, and around $100 \, \text{ng/m}^3$ and $90 \, \text{ng/m}^3$ at Zeppelin, Svalbard in March and April, respectively. Eleftheriadis et al. (2009) report EBC concentrations of about $70 \, \text{ng/m}^3$ and $60 \, \text{ng/m}^3$ at the latter station but averaged from 1998 to 2007 in March and April, respectively. Outside the Arctic, distinct higher values were detected. Annual averaged BC concentrations measured in Indonesian cities are around $2200 \, \text{ng/m}^3$ up to $3370 \, \text{ng/m}^3$ in 2011 (Santoso et al., 2013), while monthly averaged BC concentrations measured at Finish stations varies between $114 \, \text{ng/m}^3$ and $445 \, \text{ng/m}^3$ at a suburban station and between $225 \, \text{ng/m}^3$ and $707 \, \text{ng/m}^3$ at a rural station after 2004 (Hienola et al., 2013). Laborde et al. (2013) item typical values for European cities are $1700 \, \text{ng/m}^3$, $900 \pm 700 \, \text{ng/m}^3$, $2000 \, \text{ng/m}^3$, $3000 \, \text{ng/m}^3$ for Barcelona, Paris, London and Milano, respectively.

3 Airborne measurements

3.1 Black carbon measurement instruments

Black carbon (BC) can be measured in different ways in the atmosphere. Basically, the different techniques are divided into two main groups, namely filter-based techniques and direct techniques. In both cases, the absorption coefficient is determined, except for the difference method. It is important to mention that there are no specific BC instruments. The instruments introduced in the following, are detecting all aerosol which absorb light at the given wavelengths. As mentioned before, BC is not well defined and therefore in the following, it is only mentioned what the authors purport to measure.

3.1.1 Filter-based methods

For measuring BC in the Arctic atmosphere, there are different methods possible. The most common technique is to measure the absorption of BC with a filter-based absorption photometer, like a Particle Soot / Absorption Photometer (PSAP) or an aethalometer, or with a Photoacoustic Spectrometer (PAS) (AMAP, 2011). Additionally, there is one more filter-based technique described in this thesis, namely the Continuous Light Absorption Photometer (CLAP). Basically, the concept is similar for all filter-based instruments. While air is filtered, BC is deposited on a filter and the optical attenuation of transmitted light is measured. The related mass absorption coefficient of the deposited particles, σ_{ap}, is calculated by using Beer's law:

$$I = I_0 e^{-\sigma_{ap} z}, \text{ (Weingartner et al., 2003).} \tag{3.1}$$

where I_0 and I are the average intensities before and after traversing a medium with the thickness z, respectively. The quotient of $\frac{I_0}{I}$ is then the averaged transmittance of the filter of the two time periods. That leads to the equation for the absorption

coefficient:

$$\sigma_{ap} = \frac{1}{x} \ln\left(\frac{I_0}{I}\right) = \frac{a}{v} \ln\left(\frac{I_0}{I}\right). \tag{3.2}$$

where a is the area of the sampling spot, and v is the volume of air sampled in one period. With the absorbance

$$A = \ln\left(\frac{I_0}{I}\right), \text{ the equation for the absorption coefficient } \sigma_{ap} \text{ reads} \tag{3.3}$$

$$\sigma_{ap} = \frac{a}{v} A. \tag{3.4}$$

It is important to mention that the measured quantity is not the absorption coefficient of the deposited particles, σ_{ap}, which is measured by filter-based instruments, but it is the attenuation coefficient, σ_{atn} (Weingartner et al., 2003). InWeingartner et al. (2003), an empirical approach is used to calculate σ_{ap} with the aid of σ_{atn} and two calibration factors C and $R(ATN)$. This approach reads

$$\sigma_{atn} = \sigma_{ap} \frac{1}{C \cdot R(ATN)}, \tag{3.5}$$

where C describes the multiple scattering of the light beam due to the filter material. Its value mainly depends on the filter and the apparatus used. $R(ATN)$ stands for any other effect caused by deposited particles. It varies with changing amount of particles and their optical properties. The target quantity is the aerosol black carbon mass concentration M_{BC} with the unit g/m^3 (Weingartner et al., 2003), which is called equivalent BC in Eleftheriadis et al. (2009). This quantity is derived using σ_{ap} and the mass absorption cross section (MAC) with the unit m^2/g, described by Knox et al. (2009). M_{BC} is then defined by the relationship

$$M_{BC} = \frac{\sigma_{ap}}{\text{MAC}}. \tag{3.6}$$

The MAC is a site specific and instrument specific quantity, which strongly depends on the aerosol type and aerosol age(Weingartner et al., 2003). Two features act sophisticating on the absorption measurement. First, particulate light scattering and multiple scattering caused by the filter matrix (Petzold et al., 2005) are able to reduce the transmission through the loaded filter and creates an artefact absorption, which leads to an increase in the measured absorption. Second, particles which absorbe water enhance the measured light absorption as well (Bond et al., 2013). However, the Arctic air is relatively dry and therefore, the latter feature plays a minor role in the investigated area. The instruments incorporate different methods to compensate these features as effectively as possible. Calibration and correction terms are needed due to filter loading (Bond et al., 1999; *ESRL NOAA*, 2013). Filter-based instruments detect all optically-absorbing material, regardless of whether it is BC or not.

Aethalometer

Named after the Greek word $\alpha\iota\theta\alpha\lambda o\nu\nu$, which means "to blacken with soot", aethalometers are filter-based real-time BC instruments (Hansen et al., 1984), which are measuring the mass concentration of BC particles in the air. Particles are collected on a quarz fiber tape, which is automatically advanced 1 cm, if the chosen loading threshold is reached (*Magee Scientific Corporation*, 2013). Depending on concentration and flow rate, it needs months to years to deplete a roll of tape with 1000 sampling spots (*Magee Scientific Corporation*, 2013). Aethalometers perform a continuous optical analysis on two wavelengths at 370 nm and 880 nm (AE22) and on seven wavelengths from 370 nm to 950 nm (AE31 and AE33). They derive aerosol size distribution, physical properties and allow deductions about primary component identification (*Magee Scientific Corporation*, 2013). With an accuracy of 30 % (Schmid et al., 2005), this technique delivers a rough estimate of BC conditions. As mentioned by Hansen et al. (1984), the aethalometer is a fully automatic instrument, which requires no monitoring or calibration other than periodic checks of the air flow meter response.

Particle Soot / Absorption Photometer (PSAP)

With the Particle Soot / Absorption Photometer (PSAP), a continuous detection of the absorption coefficient is possible (Bond et al., 1999). Light emitted from a light-emitting diode (LED) with one wavelength $\lambda = 565$ nm or with three wavelengths $\lambda_1 = 467$ nm, $\lambda_2 = 530$ nm and $\lambda_3 = 660$ nm (*ESRL NOAA*, 2013) passes an opal glass diffuser before reaching the Pallflex filter attached on a filter holder (Bond et al., 1999). The filter has to be manually replaced, once a loading threshold is reached. Two detectors are installed on the opposite site. One to detect the transmittance of the exposed filter, the other one to detect the transmittance of the non-exposed filter for reference measurements. The instrument requires an external vacuum source supplying a sample flow of $1 - 2\,\text{l/min}$. The precision of the PSAP is reported at about $\sim 25\,\%$ (Magi et al., 2003); Bond et al. (1999) reported an accuracy of $20 - 30\,\%$. At high ratios of organic aerosol to light absorbing carbon ($15 - 20\,\%$), the bias of the absorption coefficient can be around $50 - 80\,\%$ (AMAP, 2011). An empirical method to determine the absorption coefficient actually measured by the PSAP, σ_{psap}, is calculated as follows

$$\sigma_{psap} = \sigma_{ap} \frac{1}{2(0.5398\tau + 0.355)} \tag{3.7}$$

where τ is the filter transmission, with $\tau = 1$ for an unloaded filter (Bond et al., 1999).

Continuous Light Absorption Photometer (CLAP)

In principle, the measuring technique of the Continuous Light Absorption Photometer (CLAP) is similar to that of the PSAP but there are some differences. The sampling time for one filter is eight times longer, because there is not only one, but the CLAP has eight sampling spots. Solenoid valves are used to switch the sampling spot, if the transmittance reaches a threshold of 0.7 (*ESRL NOAA*, 2012). Furthermore, an internal heater is enclosed to reduce the relative humidity inside the instrument. A cellulose fiber layer is additionally absorbing the water in high relative humidity cases (*ESRL NOAA*, 2012). Typically, the CLAP is mounted in combination with a nephelometer, and the sampled air reaches the CLAP after passing a modified TSI nephelometer blower bypass block (*ESRL NOAA*, 2012).The utilized filter, a Pallflex type E70-2075W, is a glass filter cellulose backing, and the same as used for the PSAP except for the size (Walsh, 2012). The CLAP needs an external computer for data logging and to control the instrument (*ESRL NOAA*, 2012).

3.1.2 Direct methods

In this section, three different direct methods are introduced. The Photoacoustic Spectrometer (PAS) and the Single Particle Soot Photometer (SP2) are used to measure the BC content of the atmosphere, detecting energy from absorbed light converted to pressure and laser-induced incandescence, respectively. Another common technique is the so-called difference method (Lack et al., 2006), which uses the assumption that absorption equals the difference of extinction σ_{ep} and scattering σ_{sp}:

$$\sigma_{ap} = \sigma_{ep} - \sigma_{sp}. \tag{3.8}$$

This technique requires two instruments, one for the extinction measurements and one to measure the scattering.

Photoacoustic Spectrometer (PAS)

The Photoacoustic Spectrometer (PAS) uses the direct, photoacoustic method (Lack et al., 2006): A laser induces power modulated light at the acoustic resonance frequency of the PAS, which is absorbed by an aerosol particle. The converted energy is released as heat to the surrounding gas subsequently. The volume expands or the pressure increases, which leads to a pressure wave propagating away from the particle

(Lack et al., 2006). Because of the modulation at the resonance frequency, the wave is amplified, and the acoustic signal is detected by sensitive microphones (Arnott et al., 1999). This signal is related to the absorption coefficient. For a more detailed description of the PAS's mode of operation, see Arnott et al. (1999). The accuracy of photoacoustic instruments is around $5 - 10\,\%$ (Lack et al., 2006). As mentioned before for the filter-based instruments, humidity influences the measured values of the PAS as well. But, as explained before, it is probably not that considerable in the Arctic. This relatively new and advanced instrument is too expensive to use it at several measuring sites (AMAP, 2011).

Single Particle Soot Photometer (SP2)

The Single Particle Soot Photometer (SP2) utilizes real-time, laser-induced incandescence technique, which is a direct method, to quantify the refractory mass of BC (rBC). An aerosol particle is heated by a Nd:YAG, intra-cavity, continuous laser beam with a wavelength of $\lambda = 1064\,\mathrm{nm}$ and is raised to its vaporization temperature. Due to that, thermal radiation is emitted. Four avalanche photodiode detectors (APDs) sense specific wavelength bands with a time resolution of $5\,\mathrm{MHz}$ (Schwarz et al., 2006). One APD detects the scattering signal for all particles, since its filter passes only the wavelength of $\lambda = 1064\,\mathrm{nm}$. Two APDs sense the incandescence signal in the range of visible light. The corresponding filters are a broadband and a narrowband filter passing wavelength of $400 - 800\,\mathrm{nm}$ and $600 - 800\,\mathrm{nm}$, respectively. The ratio of broadband signal to narrowband signal allows the calculation of the colour temperature. Moreover, there is one APD detecting the leading edge of the scattering signal, which allows conclusions about the amount of coating and the mixing state of the particle (*Droplet Measurement Technologies*, 2012). From a specific temperature signal, the rBC mass can be extrapolated, while the intensity of the thermal radiation delivers the BC core mass. The last two quantities are linearly related to each other. Additionally, the light scattered by the particle is linked to the internal mixtures of BC (AMAP, 2011). The reported uncertainties lie in between $25\,\%$ (Schwarz et al., 2008) and $40\,\%$ (Langridge et al., 2012). Minimum BC detections limits are a BC density of $\rho = 10\,\mathrm{ng/m^3}$ and a particle density of $\rho_p = 0.3\,\mathrm{fg/particle}$. The SP2 detects particles of a size range of $70 - 500\,\mathrm{nm}$ mass-equivalent diameter assuming a BC density of $\rho = 1.8\,\mathrm{g/cm^3}$ (*Droplet Measurement Technologies*, 2012).

The SP2 requires an external pump and an external monitor to operate the instrument. This technique is inappropriate for measuring longer time series. The instrument has to be continuously monitored. The data storage has a capacity of around 56 hours of continuous data, which depends on particle concentration and flow rate.

Difference method

The so-called difference method is not one instrument, but a method to calculate the absorption from the difference of extinction and scattering. For measuring aerosol extinction cavity ring down spectroscopy is used; the technique is described in (Strawa et al., 2003). An integrating nephelometer supplies the scattering data. Anderson et al. (1996) provide a detailed description of a total scatter/backscatter integrating (TSI) nephelometer. The accuracies are 2 % or better and around 7 % for extinction and scattering, respectively (Lack et al., 2006). The weakness of this method is the propagation of uncertainty due to the differences in measuring the two quantities. The uncertainty for the absorption coefficient is supposed to be much higher than the ones for extinction and scattering alone.

3.2 Field campaigns

The Polar Airborne Measurements and Arctic Regional Model Simulation Project (PA-MARCMiP) is an airborne research project. Its incentive is to aquire knowledge about physical processes due to current environmental changes in the Inner Arctic, thus the reduction of uncertainties in regional and global model simulations. Measurements of sea-ice thickness, aerosol concentration and meteorological parameters are conducted on board the Polar 5 in the Western Arctic north of $65°N$, whereby the focus is on sea-ice thickness measurements. So far, four PAMARCMiP campaigns were implemented in the spring of 2009, 2011, 2012 and 2013, however the PAMARCMiP13 campaign was discontinued, since technical problems with the sea-ice thickness instrument occured. Therefore, only data of the first three campaigns are available and analysed in this thesis. The campaigns are organized by the Alfred Wegener Istitute Helmholtz Centre for Polar and Marine Research (former: Alfred Wegener Institute for Polar and Marine Research) in cooperation with several other institutes and companies.

In this study, in principal, three locations are used as starting points for the flight

tracks, namely Longyearbyen, Station Nord and Alert. Longyearbyen is located at $78°13'N$, $15°38'E$ on Spitsbergen, the biggest island of the Svalbard archipelago. Station Nord ($81°36'N$, $16°40'W$) is the northernmost military base of the Danish Defence. It is located in the flat terrain of Kap Prins Knud in Kronprins Christian Land, north-eastern Greenland at a height of $25\,m$ above sea level (AMAP, 2011). Alert ($82°27'N$, $62°31'W$) is located in Nunavut, Canada or more specifically on the northernmost end of Ellesmere Island at a height of $210\,m$ above sea level (AMAP, 2011). Furthermore, Eureka, Resolute Bay, Sachs Harbour, Inuvik and Barrow are used as starting points. Barrow, Alaska ($71°19'N$, $156°36'W$) is the easternmost measuring site used and the northernmost city in the United States of America. The measuring site is placed at a height of $11\,m$ above sea level (AMAP, 2011). The Russian drifting stations NP36, NP38 and NP40 were meant to be used for intermediate landing, but only NP36 was approached. An overview of these starting points is given in Table 3.1.

Table 3.1: The used starting points with their location and the information in which years they have been used. * means planned but not used.

starting point	location	2009	2011	2012	2013
Barrow	$71°19'N$, $156°36'W$	x	x		
Inuvik	$68°19'N$, $133°37'W$	x	x		
Sachs Harbour	$71°59'N$, $125°15'W$	x			
Resolute Bay	$74°142'N$, $94°50'W$	x	x	x	
Eureka	$79°59'N$, $85°49'W$	x	x	x	
Alert	$82°27'N$, $62°31'W$	x	x	x	*
NP36	*drifting*	x			
Station Nord	$81°36'N$, $16°40'W$	x	x	x	*
Longyearbyen	$78°13'N$, $15°38'E$	x	x	x	x

3.2.1 Aircraft and instrumentation

During all PAMARCMiP campaigns, the research aircraft, Polar 5, is used for the measurements. The aerosol instruments are integrated in a so-called aerosol rack (Fig. 3.1), which in turn is intergrated inside the cabin of the aeroplane. The aerosol rack contains four instruments, which are measuring atmospheric aerosols, namely a NOAA Continuous Light Absorption Photometer (CLAP), a Model 3563 Integrating Nephelometer (TSI Incorporated), an Ultra-High Sensitivity Aerosol Spectrometer (UHSAS, Droplet Measurement Technologies) and the SP2.
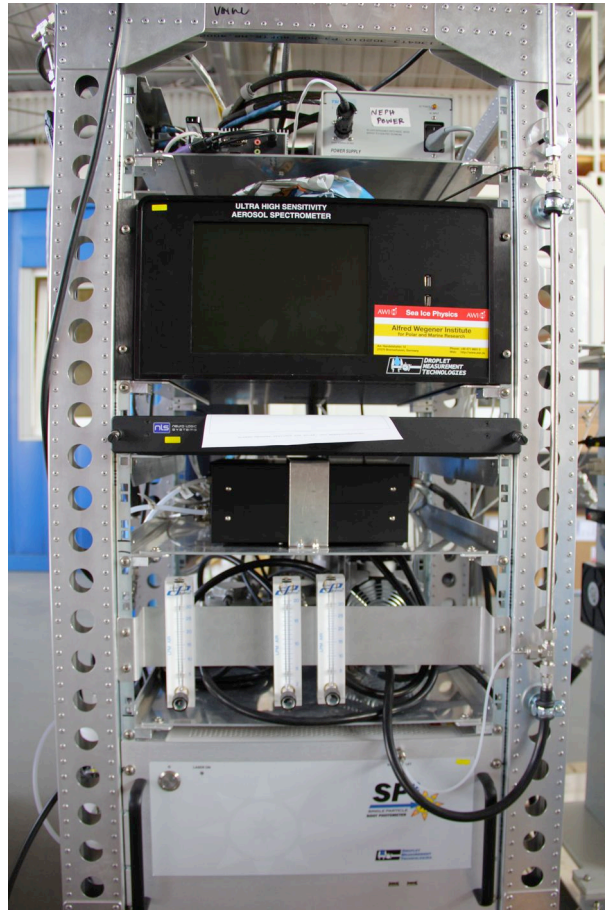
Figure 3.1: Aerosol rack with the integrated Model 3563 Integrating Nephelometer (top and to the right of the aerosol rack), CLAP (top, behind the Model 3563 Integrating Nephelometer), UHSAS (middle) and SP2 (bottom).

Polar 5 is a Basler BT-67 (Basler Turbo Conversion LLC), based on a Douglas DC-3, formally used as a "Raisin Bomber" (Fig. 3.2). It has the Canadian registration "C-GAWI" and is part of the AWI research fleet. The span of the plane is 29.00 m and the length is 20.66 m. The minimum operation height is at 105 ft, the maximum operation height is at 25000 ft.

Figure 3.2: Polar 5 in the hangar at the regional airport of Bremerhaven.

The sampled air enters the aerosol rack's tubing via a heated airborne low turbulence aerosol inlet (Huebert et al., 2004) located outside the plane. The inlet is heated to prevent freezing, thus plugging of the pipes and tubes. Two modes are feasible, the measuring mode and the zero flow mode. At the measuring mode, the sampled air enters the tubing outside the plane and is supplied to the instruments. At the zero flow mode, the inlet valve is closed and the air inside the tubing is flowing around in a circuit, passing a filter and the instruments. The latter mode is used for calibration.

In preparation for the measurements, the instruments are switched on, before take-off. The measurements start with opening the inlet valve and closing the zero flow valve, after take-off. Immediately afterwards, the inlet heater has to be switched on. Once during the flight, the calibration mode runs for calibration reasons. The flow rates have to be monitored and adjusted, and the Nd:YAG laser temperature and its power requires observation. Shortly before landing, the inlet heater is switched off. The measurements end with opening the zero flow valve and closing the inlet valve after touch down. The data records are stored and processed afterwards.

3.2.2 Flight tracks

The flight tracks begin at the already described starting points (Tab. 3.1) and head in the direction where the sea ice is located. In most cases, they head in a northward

direction (Fig. 3.4). In Table 3.2 the time periods in which the campaigns take place is listed and the spatial expansion of each PAMARCMiP campaign is declared, as well. PAMARCMiP09 is the widest campaign of the three and the Polar 5 reaches not only the northernmost measuring point of all three campaigns but also the westernmost and easternmost measuring point. It has to be considered that not every day measurements were conducted during the campaign, but on some days more than one flight took place.

Table 3.2: Overview of the duration and the spatial expansion of Polar 5 flights during PAMARCMiP09, -11 and -12.

year	period of time	latitude		longitude	
		min	max	min	max
2009	01.04.–25.04.	$70°45'N$	$88°43'N$	$168°22'W$	$23°11'E$
2011	30.03.–05.05.	$63°28'N$	$86°02'N$	$161°58'W$	$19°05'E$
2012	20.03.–05.04.	$77°27'N$	$85°28'N$	$107°23'W$	$15°22'E$

The aim of the aerosol measurements is to collect data in the atmospheric boundary layer and in the free troposphere. With only one aeroplane and without a tow vehicle, which is equipped with measuring instruments, it is not possible to measure in two hights at the same time. Therefore, an ideal flight pattern includes a low-level flight and a high-level flight, which are only distinguished in measuring height. However, that is barely possible. Additionally, the vertical distributions of aerosols are of peculiar interest. For this purpose, profile flights are performed. The Polar 5 accomplishes vertical helical patterns, upwards as well as downwards. Ideally, each flight contains at least one low-level and one high-level segment and one vertical profile segment (Fig. 3.3).
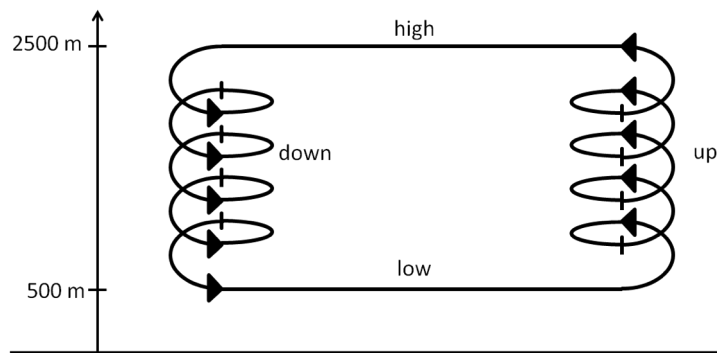
Figure 3.3: Schematic illustration of a measuring flight with all four segments.

3.3 Data analysis

To analyse the data, the area where the campaigns took place, is seperated into different regions. Different areas are identified based on the distribution of detected cyclones during April for the years 1979-2000 by Affeld (2003), Fig. 4.11. The five regions are the following ones. Every location northwards of or at $83°N$ belongs to Region 5, locations eastwards of or at $5°W$ summarized to Region 4 (note that there were no measurements eastwards of $23°11'W$). The region between $5°W$ and $70°W$ is called Region 3, while the locations between $70°W$ and $95°W$ are summarized to Region 2. The largest region is Region 1, which covers the region westwards of $95°W$. The regions and the associated geographic coordinates are listed in Table 3.3 and are shown in Figure 3.4.

Table 3.3: Geographic coordinates of the defined regions.

region	location	
	latitude	longitude
1	$< 83°N$	$< 95°W$
2	$< 83°N$	$70°W > lon \geq 95°W$
3	$< 83°N$	$5°W > lon \geq 70°W$
4	$< 83°N$	$\geq 5°W$
5	$\geq 83°N$	$-180°$ - $+180°$

3.3.1 Available data

The datasets used in this thesis are collected on three PAMARCMiP campaigns in the years 2009, 2011 and 2012. These campaigns took place during the Arctic spring, using varying starting points listed in Table 3.1. Apart from rBC, other particle measurements are conducted and meteorological parameters are measured. Furthermore, the sea ice thickness is measured. In this thesis, mainly rBC concentration data is used. In order to compare it or place it in context with other parameters, data of all meteorological parameters and all aerosol data is processed to a certain level. The flight tracks splitted in flight segments are listed in Table A.1, A.2 and A.3. However, not for every flight or flight segment, rBC concentration data is available.
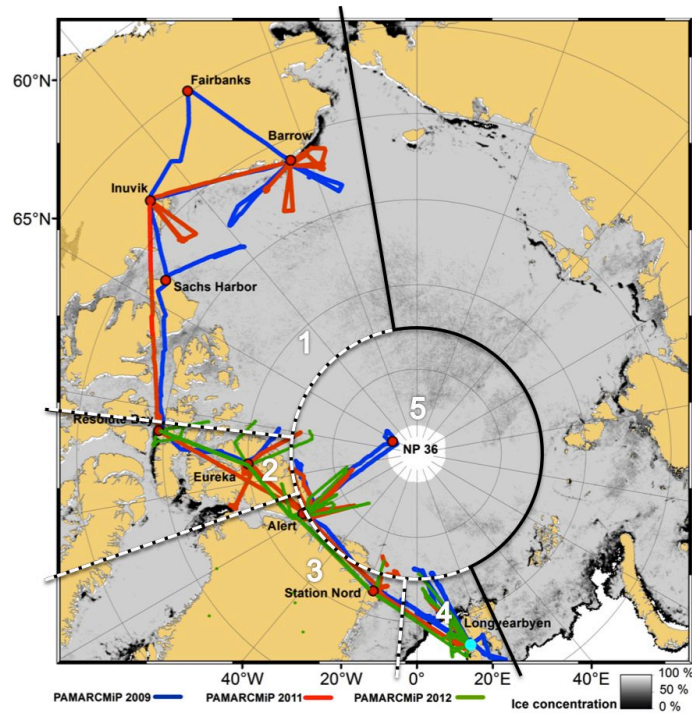
Figure 3.4: Separation of the five regions and flight tracks of the PAMARCMiP campaigns in 2009, 2011 and 2012 (courtesy of Thomas Krumpen, modified).

There exist several difficulties concernig the rBC measurements and the data. Beginning with the rBC instrument, the SP2 is not designed for airborne measurements. Variing measuring hight, thus variing air pressure, movements as well as changes in ambient air temperature may disturb the measurements. Heating of the cabin is complicated and to keep the cabin temperature constant is nearly impossible. An additional problem are the low air temperatures in the measuring area and the scarce insulation of the aeroplane. Despite preheating efforts, it leads to cooling of the instrument and temperature changes during the measurements. Furthermore, BC measurements with aeroplanes bear the potential risk that exhaust gases may enter the inlet and reach the instrument, thus bias the measurements. The measuring instrument and the method, and therefore the diputable quality of the recorded data is not the only problem. The manner of collecting data reveals additionally difficulties concerning data analysis. The spatial data coverage is low in the measuring area and the Russian part of the Arctic is not included in data collection at all. Moreover, data is only available for three years and only for few weeks within the year. The problem with that data is, there are no measurements at one place for different times and vice versa, there are no measurements at different places at the same time. Therefore, direct comparisons for different locations or different times are not possible. Summarising, the data analysis is difficult and its significance is expected to be moderate.

3.3.2 Data processing

The available data exist in the form of four datasets for each day of measurement. Depending on the parameter, the data may already be processed. To facilitate data analysis, one dataset per day is generated in the following way. To receive the whole dataset of one day, five datasets with different parameters are combined. The ABS-dataset includes the rBC concentration data as well as optical parameters of aerosols. Meteorological parameters are contained in both AWI- and ECT-dataset. Additionally, parameters linked to the aerosol optical depth (AOD-dataset) and radiation parameters (RAD-dataset) are part of the complete dataset. The datasets can have different timesteps, since the average time may vary. That must be taken into account in terms of further processing. Parameters, which are assumed to be potentially important for analysis of BC concentrations, are chosen and plotted to identify outliers and systematic errors. In the next step, unphysical or inexplicable values are deleted. That includes for instance negative wind speeds or negative particle concentrations. rBC concentrations $< 10 \, \text{ng/m}^3$ are deleted as well, since they are lower than the lower detection limit of the SP2. Outliers with a difference of four times the standard deviation are deleted as well. The revised data set is then averaged over $30s$ and splitted into four kinds of flight segments, namely low-level segments "low", high-level segements "high" and the profile upwards and downwards segments, "up" and "down", respectively. The last steps are to plot the data of the segments, to double-check them and to delete possibly remaining errors. This procedure is chosen, since the errors vary from case to case and an automated processing is not useful. Nevertheless, the chosen way of data processing is relativ labour-intensive and for larger datasets, a development of a more efficient way is recommended.

4 Distribution of black carbon in the western Arctic

4.1 Vertical distribution of black carbon

In order to analyse the vertical distribution of rBC concentrations, data of the profile segments are used in this section only. Data of up- and downwards segments are not distinguished. An overview of the regions and the number of measurements conducted during the PAMARCMiP campaigns in 2009, 2011 and 2012 are given in Table 4.1. In Section 4.1.1, spatial variations are analysed, whereas temporal variations are studied in Section 4.1.2.

Table 4.1: Numbers of vertical profiles conducted in each region during PAMARCMiP campaigns in the years 2009, 2011 and 2012. Measurements are only listed, if rBC concentration data are included.

year	Region 1	Region 2	Region 3	Region 4	Region 5
2009	9	3	2	15	5
2011	8	6	8	11	13
2012	1	3	2	12	3

4.1.1 Spatial variations

For the analysis of spatial variations, the examined area is divided into five regions, as described in Section 3.3. At first, the regions are compared according to the year the data is collected. For each region, the corresponding vertical profiles of rBC concentration and the associated 200 m-averaged values are shown in Figures 4.1, 4.2 and 4.4. Above altitudes of about 3000 m, data density gets lower, hence data is only plotted up to this altitude. The same holds for altitudes lower than 100 m. To facilitate the analysis within one measuring period, the abscissae are not consistent in these figures,

but vary from year to year.

The vertical distribution of rBC concentrations in 2009 is ordered by region and shown in Figure 4.1. The measurements in Region 1 show no height dependence of rBC concentrations and lower values compared to Region 3 and 4 at most of the altitude levels. In Region 2, slightly higher rBC concentrations, around $50 \, \text{ng/m}^3$, are apparent between altitudes of about $600 \, \text{m}$ and $800 \, \text{m}$ than at the other altitude levels. Mean values around $25 \, \text{ng/m}^3$ exist at the remaining altitude levels. On average, rBC concentrations measured in Region 3 are with values around $30 \, \text{ng/m}^3$ higher than in Region 1 and 2. However, only one to two profiles are recorded and averaged and, therefore, the expressiveness of the averaged profile may be insufficient.

A certain number of non-averaged profiles in Figure 4.1-4 reveal a jump in rBC concentration between $100 \, \text{m}$ and $200 \, \text{m}$. At it, the threshold of $100 \, \text{ng/m}^3$ is exceeded. Up to an altitude of $140 \, \text{m}$, the averaged rBC concentration is decreasing with increasing height. Above that level, the averaged profile reveals no evident dependence of rBC concentration and altitude. All but one of the non-averaged plots of Region 5 reveal no significant changes in rBC concentration with height, except a near-ground jump. The measurement on 10.4.2009 during the second upward segment, shows more than twice as high values compared to the other measurements in this region. That plot additionally reveals two zones with higher rBC concentrations. A lower zone between $200 \, \text{m}$ and $1000 \, \text{m}$ and an upper zone between $1000 \, \text{m}$ and $1500 \, \text{m}$.

As shown in Figure 4.1-6, there cannot be found either a characteristic profile of rBC concentration for one region or a height dependence of rBC concentration in 2009. The spatial variation is realtively low with a standard deviation of about $8 \, \text{ng/m}^3$.
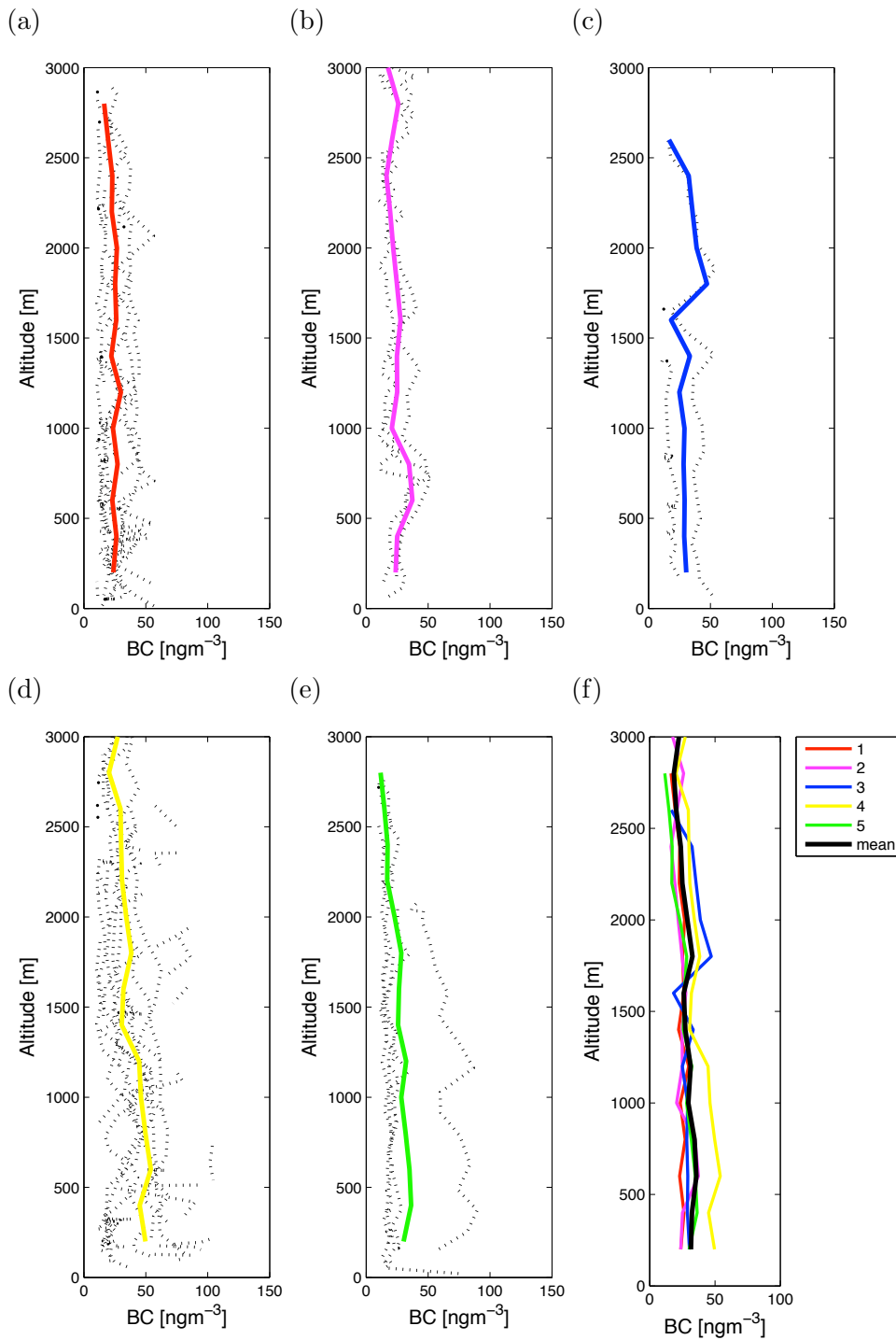
Figure 4.1: rBC concentration as a function of height for all upward and downward segments recorded in (a) Region 1, (b) Region 2, (c) Region 3, (d) Region 4 and (e) Region 5 during the PAMARCMiP09 campaign in 2009 and (f) the associated mean profile with average intervals of 200 m.

In 2011 (Fig. 4.2a), the highest mean values at every altitude level are derived for Region 1. Additionally, high standard deviations reveal a high variability compared to the other regions. Noticeable in this graph is the vertical profile, measured on the 2.4.2011 during an upward segment. High rBC concentrations, especially at altitudes between 1500 m and 2000 m exhibit values up to 170 ng/m^3. This profile ends with a jump at an altitude of 2217 m, however, one of the other measurements reveals values almost up to 200 ng/m^3 at an altitude of about 2760 m. Figure 4.2bshows a region with remarkable high rBC concentrations. Up to 150 ng/m^3 are reached at altitudes between 1600 m and up to 2400 m measured during a downward flight on the 10.4.2011. In contrast, mean values for this region range between 15 ng/m^3 and 60 ng/m^3. Additionally, a slight decrease in rBC concentration with increasing altitude of about 30 ng/m^3 is apparent from the lowest level up to 1600 m.

In Region 3, several peaks with values above 100 ng/m^3 can be found in various heights. The averaged rBC concentration is around 40 ng/m^3 and varies barely with height. The highest values recorded in Region 4 are found in the lowest levels, which holds for the averaged values, as well. Non-averaged profiles reach up to 150 ng/m^3. The averaged profile in Figure 4.2d shows a slight decrease in rBC concentrations with increasing height. One of the non-averaged profiles reveals a jump in rBC concentrations up to 190 ng/m^3 near the ground.

The regional differences in 2011 are greater than in 2009 but again, all in all no characteristic vertical profile of rBC concentrations and no height dependence can be found (Fig. 4.2f). Apart from Region 1, the averaged graphs of each region show similar values. A standard deviation of about 15 ng/m^3 confirms this finding.
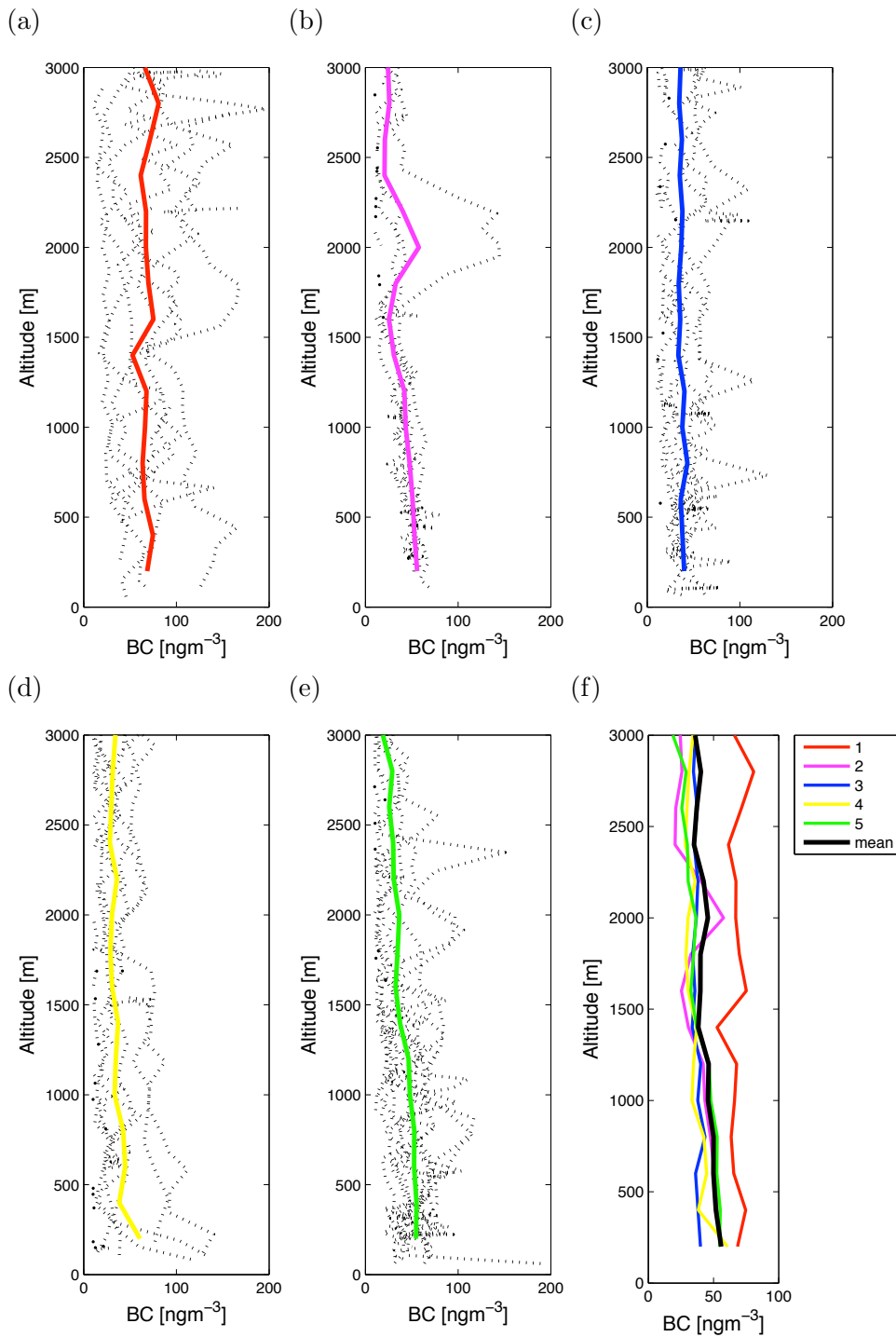
Figure 4.2: rBC concentration as a function of height for all upward and downward segments recorded in (a) Region 1, (b) Region 2, (c) Region 3, (d) Region 4 and (e) Region 5 during the PAMARCMiP11 campaign in 2011 and (f) the associated mean profile with average intervals of 200 m.
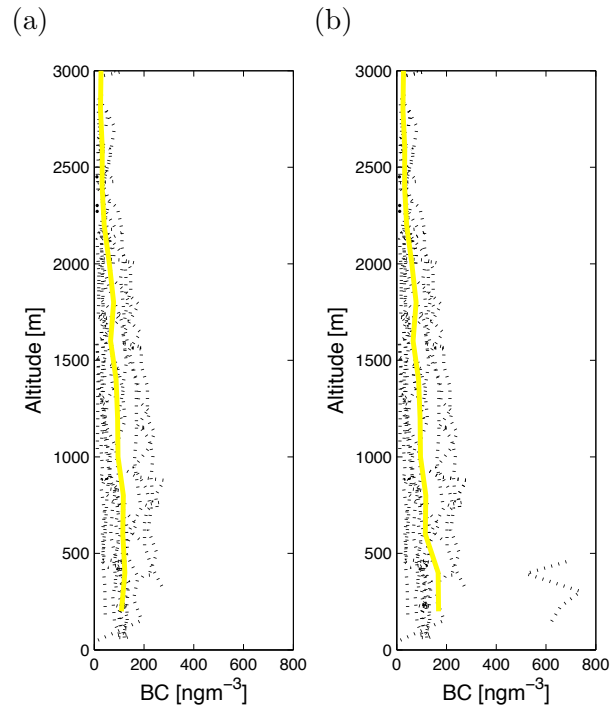
Figure 4.3: rBC concentration as a function of height for (a) all upward and downward segments recorded during the PAMARCMiP12 campaign in Region 4 and (b) the modified dataset without rBC concentrations above $500\,\mathrm{ng/m^3}$. The associated mean profiles with average intervals of $200\,\mathrm{m}$ are also indicated.

Figure 4.4 shows the vertical distribution of rBC concentrations recorded at all upward and downward flights during the PAMARCMiP12 campaign in 2012. An exception is made for Region 4. Not all data is plotted and shown in Figure 4.4d, therefore, it is labeled with an asterisk. The difference between Region 4 and Region 4* is shown in Figure 4.3. Extreme high rBC concentrations up to $739\,\mathrm{ng/m^3}$ were measured on 21.3.2012 during the second downward flight. Because of these anomalous values, two cases are analysed separately, the one including all data of the PAMARCMiP campaign in 2012 is called "Region 4" and the one without the mentioned values is called "Region 4*". In the following analyses, Region 4* is used for spatial and temporal comparisons but analyses of Region 4 are added, if it appears to be useful. This exception is made to keep a possible distortion of the results as low as possible.

For the sake of completeness, the only vertical profile recorded in Region 1 is displayed in Figure 4.4a. It shows neither height dependence nor noticeable values in any height. In comparison to the other regions, the rBC concentrations measured in Region 2 are relative low in all heights, especially in altitudes below $500\,\mathrm{m}$. During the measurements on 5.4.2012 of a downward segment, rBC concentrations decrease down

to $12 \, \text{ng/m}^3$ while the averaged values amount to $80 \, \text{ng/m}^3$. However, these altitudes are covered by one measuring flight only, which reveals relative low values in all heights with a mean of about $45 \, \text{ng/m}^3$, averaged over all altitudes. Nevertheless, the decrease of rBC concentrations in altitudes below $500 \, \text{m}$ is remarkable.

The rBC concentrations measured in Region 3 (Fig. 4.4c), lie close together and vary not much with height, but two features diverge from this uniform appearance. A jump around $250 \, \text{m}$ from about $70 \, \text{ng/m}^3$ up to $200 \, \text{ng/m}^3$ are visible between $400 \, \text{m}$ and $800 \, \text{m}$. In Region 4*, the $200 \, \text{ng/m}^3$ threshold is clearly exceeded several times in altitudes between $300 \, \text{m}$ and $1400 \, \text{m}$. Even so, low rBC concentrations are recorded as well. The averaged profile reveals a decrease in rBC concentration with increasing height. The highest values in almost all altitudes are measured in Region 5 (Fig. 4.4e). In altitudes of around $1750 \, \text{m}$, rBC concentrations up to almost $400 \, \text{ng/m}^3$ are reached during the downward segment on 2.4.2012, while almost the same value is reached after a jump at an altitude of about $2890 \, \text{m}$ on the same day but during the upward segment. Another profile shows values close around $100 \, \text{ng/m}^3$ for every altitude. The derived mean value is around $160 \, \text{ng/m}^3$ with standard deviations around $103 \, \text{ng/m}^3$. Thus, the vertical distribution of rBC concentrations for Region 5 is highly dependend on the analysed vertical profile. Even for 2012, no height dependence can be found (Fig. 4.4f). A standard deviation of about $50 \, \text{ng/m}^3$ reveals a higher variation between the regions compared to 2009 and 2011.
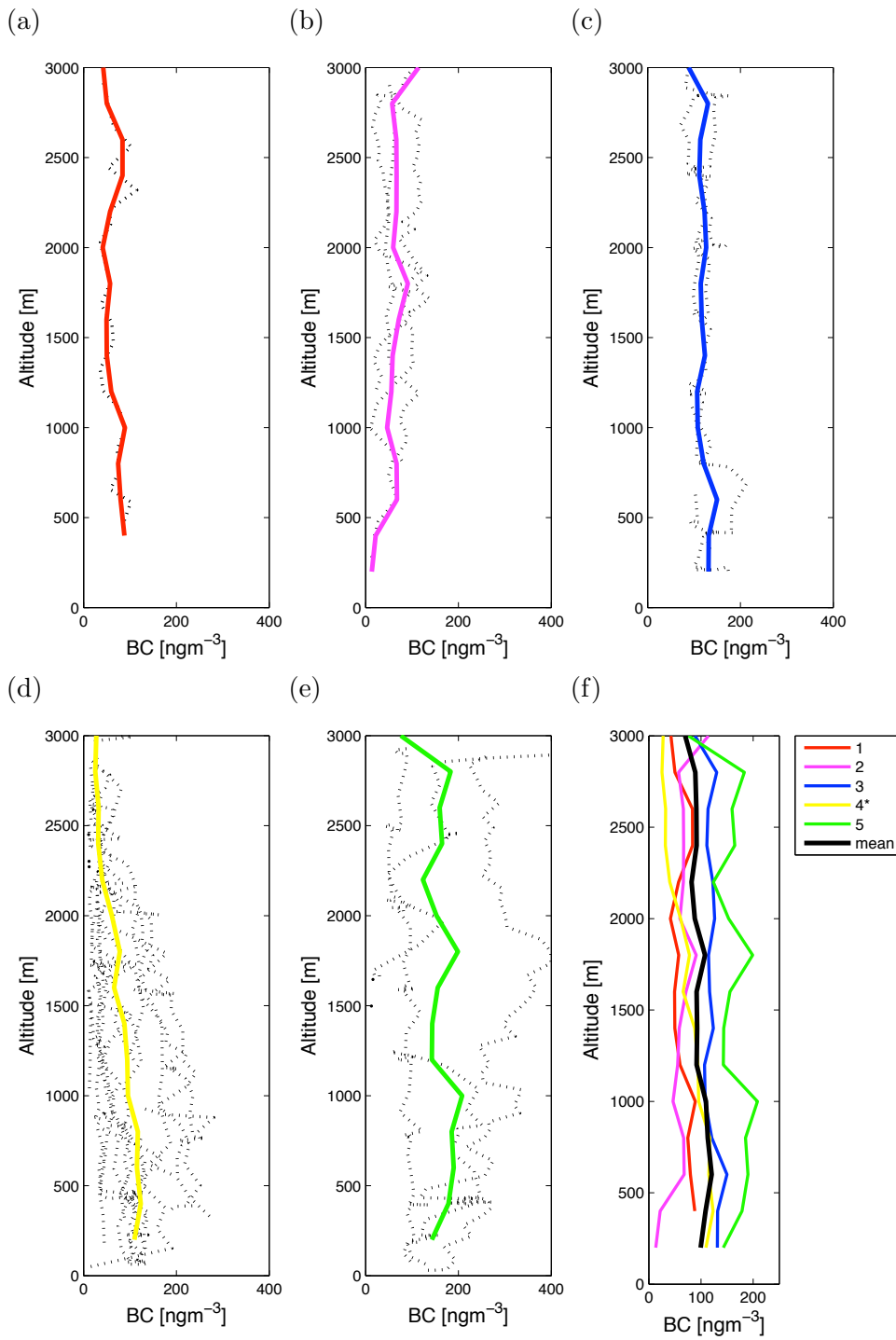
Figure 4.4: rBC concentration as a function of height for all upward and downward segments recorded in (a) Region 1, (b) Region 2, (c) Region 3, (d) Region 4* and (e) Region 5 during the PAMARCMiP12 campaign in 2012 and (f) the associated mean profile with average intervals of 200 m.

4.1.2 Temporal variations

In this section, the averaged vertical profiles of all PAMARCMiP campaigns are ordered by region. These profiles are compared in order to analyse the temporal variations of vertical distribution of rBC concentrations. The plottet profiles are the same as shown in Figures 4.1 - 4.4 plus the associated standard deviations

$$\sigma_{\text{rBC}} = \sqrt{\frac{1}{N} \sum_{i=1}^{N} (\text{rBC}_i - \overline{\text{rBC}})^2} \tag{4.1}$$

indicated by bars.

Figure 4.5a exhibits huge differences between average rBC concentrations measured in 2009 and 2011. While the mean value is around $24\,\text{ng/m}^3$ and the standard deviation around $10\,\text{ng/m}^3$ in 2009, averaged rBC concentrations lie around $66\,\text{ng/m}^3$ with standard deviations of about $36\,\text{ng/m}^3$ in 2011. Therefore, not only the averaged rBC concentrations are higher in 2011 than in 2009, but they vary much more in 2011 than the values do in 2009. The mean values fluctuate only slightly in both profiles, particularly in 2009, they are nearly constant with height. For 2012 unfortunately only one profile exist for Region 1, hence its representativeness is relatively poor. Nevertheless, it might support the 2011 average values, which are in a similar range. For 2012 the mean values are around $65\,\text{ng/m}^3$. In Region 2 (Fig. 4.5b), the averaged profiles are not far apart from each other. Averaged over all heights, the mean rBC concentrations are $24\,\text{ng/m}^3$, $37\,\text{ng/m}^3$ and $81\,\text{ng/m}^3$ for 2009, 2011 and 2012, respectively. Despite these large differences in the averaged profiles, standard deviations up to $55\,\text{ng/m}^3$ in 2011 and $51\,\text{ng/m}^3$ in 2012 reduce this gap, especially between rBC concentrations measured in 2012 and both other years.

Figure 4.5c shows for Region 3 rather similar mean values for 2009 and 2011, $30\,\text{ng/m}^3$ and $35\,\text{ng/m}^3$, respectively. The mean values vary only slightly with height in 2011, while variations of medium strength can be found in altitudes above $1600\,\text{m}$ in 2009. Note that altitudes above $1800\,\text{m}$ are only covered by one vertical measurement. Compared to the results of these two years, mean values are much higher in 2012. With mean values around $121\,\text{ng/m}^3$, they even are in another order of magnitude. Mean values of 2012 differ from those of the other years, and the most in altitudes below $1000\,\text{m}$.

(a)

(b)

(c)

(d)

(e)
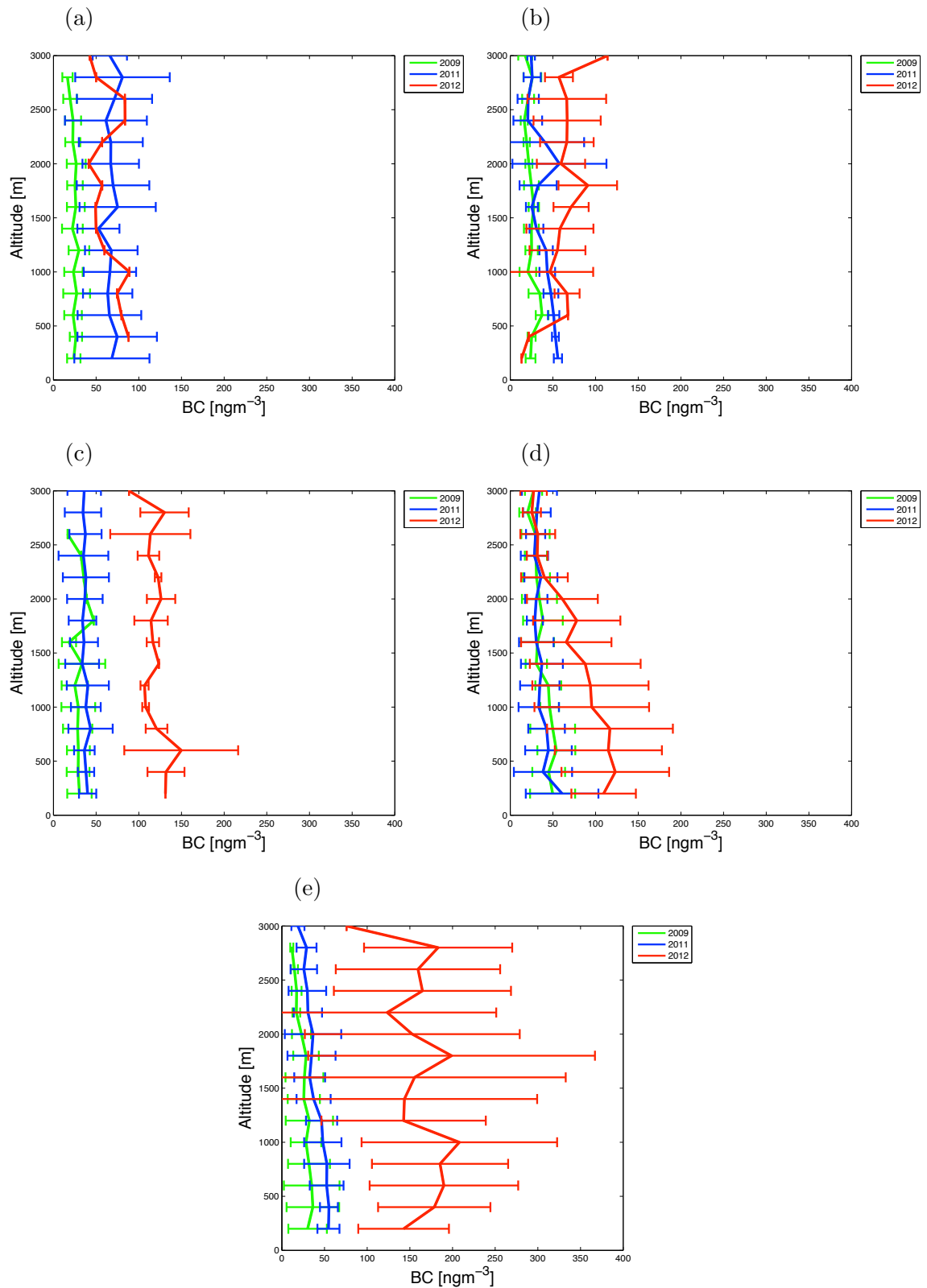
Figure 4.5: Mean rBC concentration as a function of height in (a) Region 1, (b) Region 2, (c) Region 3, (d) Region 4* and (e) Region 5. All upward and downward segments recorded during the PAMARCMiP09- (2009), PAMARCMiP11- (2011) and PAMARCMiP12 campaign (2012) are averaged over intervals of 200 m. Standard deviations, σ, of measured data are indicated by bars.

In Region 4*, as well as in Region 4, the mean values are close together above 2200 m for all years and the standard deviations of around $17 \, \text{ng/m}^3$ reveal relative small variations (Figure 4.5d). In contrast to that, mean values and standard deviations remain in the same range in altitudes below 2200 m in 2009 and 2011, but the mean values of 2012 increase from $40 \, \text{ng/m}^3$ at a height of about 2200 m to $168 \, \text{ng/m}^3$ at a height of about 200 m, or in Region 4* to $123 \, \text{ng/m}^3$ at a height of about 400 m. Coincidently, the standard deviation increases from $27 \, \text{ng/m}^3$ at a height of about 2200 m to $180 \, \text{ng/m}^3$ at a height of about 200 m. In Region 4*, the standard deviation increases up to $74 \, \text{ng/m}^3$ at an altitude of about 800 m and decreases again to $38 \, \text{ng/m}^3$ at a height of about 200 m.

The results of Region 5 (Fig. 4.5e) reveal mean values around $26 \, \text{ng/m}^3$ in 2009 and $35 \, \text{ng/m}^3$ in 2011, which slightly decrease with height. As shown by standard deviations around $103 \, \text{ng/m}^3$, the values of 2012 are highly variable. Additionally, mean values vary around $160 \, \text{ng/m}^3$ in 2012, which is one order of magnitude higher than in 2009 and 2011. As mentioned before, three vertical profiles of rBC concentration of three extremely different values are recorded in Region 5 in 2012. Hence, the standard deviations are high.

An increase of rBC concentrations in all altitudes covered by the measurements is visible since 2009. Especially, the difference between the results of 2012 and both, 2009 and 2011, are evident. This is particularly apparent in Region 3 and 5, and in Region 4 except for altitudes above 2200 m. In Region 2 this feature is not as obvious as in the regions already mentioned, nevertheless, the highest rBC concentrations of Region 2 are measured in 2012, except at the two lowermost altitude levels. A particular case is Region 1. The huge gap between the averaged rBC concentrations in 2009 and 2011 is obvious, but then the averaged rBC concentration is almost the same in 2012. However, the 2012-profile consists of only one vertical measurement and it cannot be verified, whether it is representative of rBC concentrations in Region 1 in 2012.

4.2 Horizontal distribution of black carbon

Inhomogeneous distribution of BC sources in the western Arctic, thus in the analysed area, might lead to an inhomogeneous distribution of BC within this area. Additionally, long-range transport of BC into this area may spatially and temporally vary. The

resulting spatial variations of rBC concentrations are described and analysed in Section 4.2.1. In Section 4.2.2, temporal variations are examined.

4.2.1 Spatial variations

Table 4.2 gives an overview of the mean rBC concentration ordered by year and region. Mean rBC concentrations for each region averaged over the three years and for each year averaged over the five regions are additionally listed.

Table 4.2: Mean rBC concentration in ng/m^3 ordered by region, year and altitude, as well as, the mean rBC concentration for all years and for all regions.

year	altitude	Region 1	Region 2	Region 3	Region 4	Region 5	all
2009	$\leq 500\,\mathrm{m}$	23	20	21	37	22	27
	$500 - 2500\,\mathrm{m}$	25	23	23	32	24	27
	$\geq 2500\,\mathrm{m}$	26	17	15	25	15	22
	all	24	19	20	32	23	26
2011	$\leq 500\,\mathrm{m}$	54	52	44	43	52	50
	$500 - 2500\,\mathrm{m}$	85	42	44	37	45	51
	$\geq 2500\,\mathrm{m}$	96	31	33	48	32	54
	all	78	39	41	45	47	52
2012	$\leq 500\,\mathrm{m}$	80	- - - -	101	188	99	140
	$500 - 2500\,\mathrm{m}$	64	57	110	72	120	83
	$\geq 2500\,\mathrm{m}$	43	78	109	31	217	65
	all	67	76	105	103	119	102
all	all	51	39	48	64	61	55

In 2009, rBC concentrations detected in the five regions, differ not much from each other. Mean rBC concentrations averaged over altitudes of $h \leq 500\,\mathrm{m}$ range between $20\,\mathrm{ng/m^3}$ in Region 2 and $37\,\mathrm{ng/m^3}$ in Region 4, while the mean values for altitudes of $h \geq 2500\,\mathrm{m}$ range between $15\,\mathrm{ng/m^3}$ in Region 3 and $26\,\mathrm{ng/m^3}$ in Region 1. The overall average is around $26\,\mathrm{ng/m^3}$ in 2009. Few higher values, up to $106\,\mathrm{ng/m^3}$, are measured around Svalbard, west of Resolute Bay and northwest of Barrow (Fig. 4.6a).

(a)

(b)

(c)
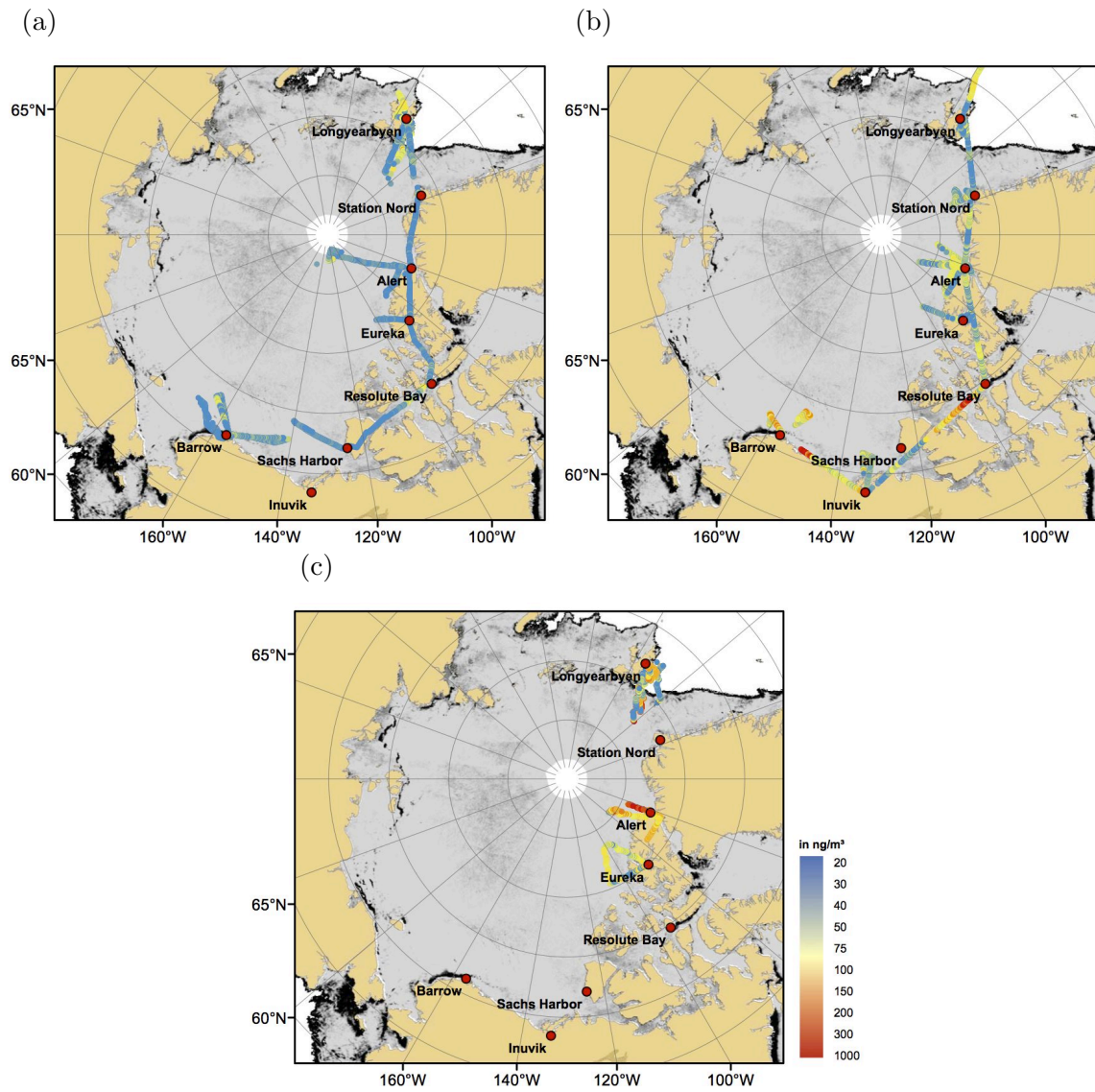
Figure 4.6: Horizontal distribution of rBC concentration measured at all measuring heights during (a) PAMARCMiP09, (b) PAMARCMiP11 and (c) PAMAR-CMiP12.

Compared to the horizontal distribution of rBC in 2009, the pattern is different in 2011. The measuring area is divided into two parts with a dividing line around $100°W$, visible in Figure 4.6b. The area east of this dividing line includes all regions, except the major part of Region 1. These regions are mainly characterized by rBC concentrations $< 100\,\text{ng/m}^3$, mean values between $39\,\text{ng/m}^3$ in Region 2 and $47\,\text{ng/m}^3$ in Region 5 (Tab. 4.2), and relative low variations. The area west of the dividing line, namely the major part of Region 1, shows high variations and relative high rBC concentrations. The rBC concentration averaged over all altitudes is about $78\,\text{ng/m}^3$, with the lowest mean value in altitudes of $h \leq 500\,\text{m}$ and the highest in altitudes of $h \geq 2500\,\text{m}$. The maxima are located west of Resolute Bay and on the way from Innuvik to Barrow.

The highest mean rBC concentration is derived for Region 5 in 2012, which reaches a mean value averaged over all altitudes of $119\,\text{ng/m}^3$ (Tab. 4.2). That is caused by the high rBC concentrations in the upper levels north of Alert, namely up to $217\,\text{ng/m}^3$. As shown in Figure 4.6c, the lowest values are measured on the flights starting at Eureka, namely Region 1 and 2. Around Spitsbergen, rBC concentrations ranging between $10\,\text{ng/m}^3$ and $805\,\text{ng/m}^3$ are detected and result in a mean value of around $103\,\text{ng/m}^3$. rBC concentrations averaged over the three years identify Region 2 with the lowest and Region 4 with the highest mean value.

As mentioned in Section 4.1 and shown in Table 4.2, a height dependency of rBC concentration that is consistent for all years cannot be found. Therefore, the horizontal distribution of rBC concentration is examplarily shown for the data of 2011 (Fig. 4.7). The results of 2009 and 2012 are only described briefely.

As described above, the measuring area can be divided in two parts in 2011. The same holds for comparing the two altitude levels (Fig. 4.7). The dividing line is again around $100°W$. West of the dividing line, rBC concentrations are higher in the upper level than in the lower level. However, they are partly recorded during ferry flights between Resolute Bay and Inuvik and between Inuvik and Barrow, where no low-level flight took place. Therefore, in those cases a direct comparison is not possible. East of $100°W$, higher values are recorded in the lower altitudes than in the upper ones. That is especially visible northwest of Eureka and for the flights starting in Alert.

(a)　　　　　　　　　　　　　　　(b)
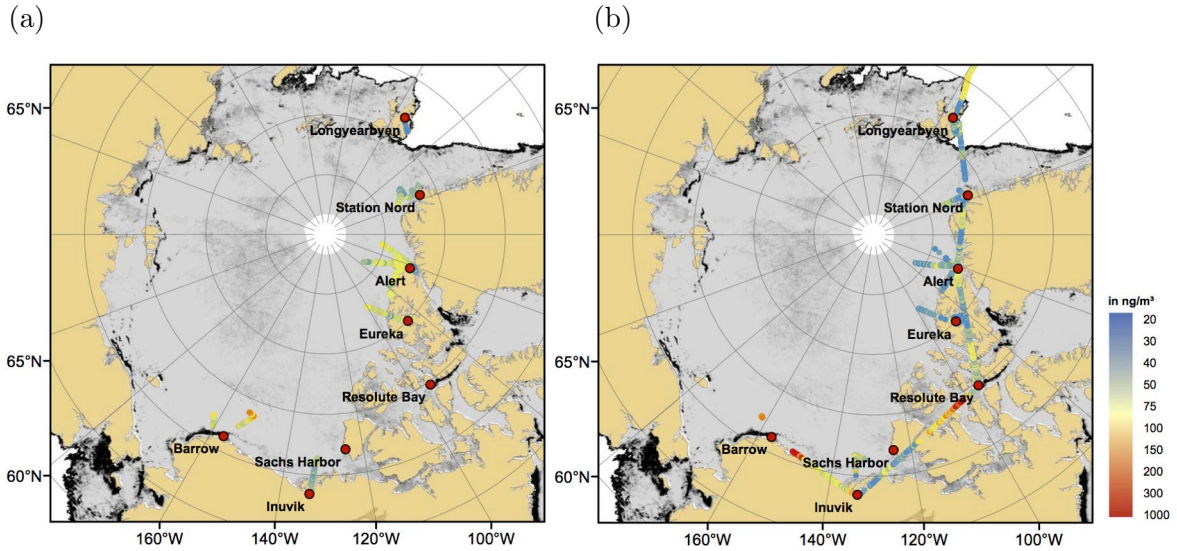
Figure 4.7: Horizontal distribution of rBC concentration measured at altitudes (a) $h \leq$ 500 m and (b) $h \geq 2500$ m during PAMARCMiP11.

The separate analyses of altitudes $h \leq 500$ m and $h \geq 2500$ m reveal no significant differences in the data collected in 2009. In 2012, the only remarkable feature is located north and west of Spitsbergen. rBC concentrations up to 614 ng/m^3 are detected in altitudes $h \leq 500$ m, while rBC concentrations up to 130 ng/m^3 are detected in altitudes $h \geq 2500$ m. The associated mean values are 185 ng/m^3 and 30 ng/m^3, respectively.

Spatial variations of the horizontal distribution of rBC concentration are not consistent in 2009, 2011 and 2012. Therefore, reasons for the results are separately made for each year. If local sources are neglected because of the presence of sea-ice in the area during the measurements, some explanatory approaches for the described results can be made. The homogeneous horizontal distribution and the absence of regional differences in the horizontal distribution of rBC concentration in 2009, might be a result of transport of air masses originate in the same source areas or from source areas with similar amounts of BC emissions. This explanation might hold for the measuring area east of $100°W$ in 2011, as well. West of $100°W$, the measured rBC might be emitted by sources of different intensities. Another possible reason for the regional differences might be that the emissions originate in one source area, but underwent different processes during transport, namely dry and wet deposition. Therefore, potential differences in transport velocity, might lead to different amounts of rBC. The results of 2012 show a heterogeneous horizontal distribution. Similar reasons as described for the measuring area west of $100°W$ in 2011, might be applicable for the results of 2012. However, the data density is compared to the other years low and the measuring area is only partly covered by measurements. Thus, conclusions of the results of 2012 are rather vague.

4.2.2 Temporal variations

For Region 1, an insufficient amount of data is available for 2012, therefore, only the data of 2009 and 2011 are compared. As visible in Figures 4.8a and 4.8c, the detected rBC concentrations are higher and more variable in 2011 than in 2009. The derived mean values (Tab. 4.2) support that rBC concentrations increase from 2009 to 2011. An increase in rBC concentration in Region 2 is visible in Figures 4.8b, d, e. The mean values about double from $20\,\mathrm{ng/m^3}$ in 2009 to $39\,\mathrm{ng/m^3}$ in 2011, and again to $76\,\mathrm{ng/m^3}$ in 2012.
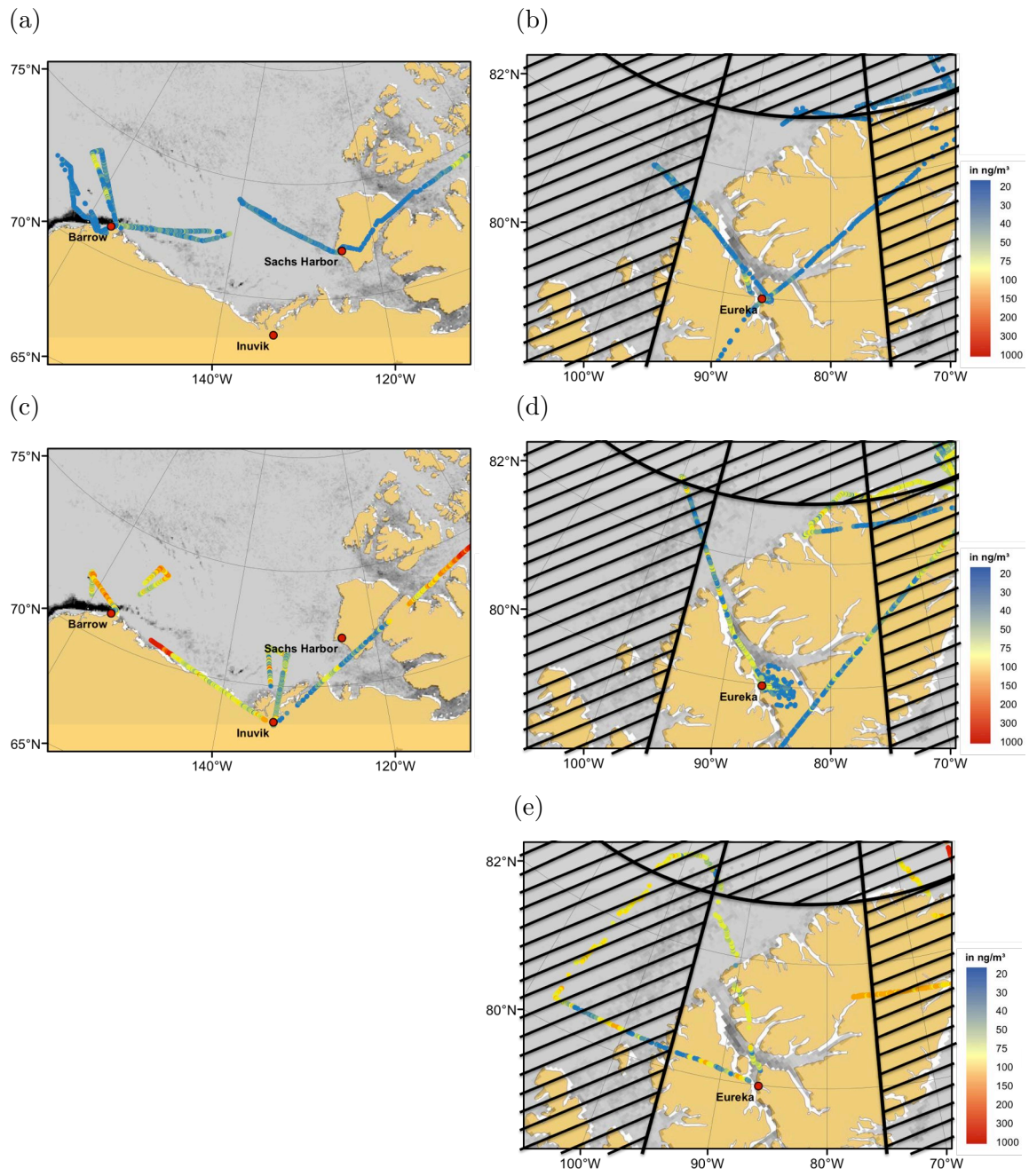
Figure 4.8: Horizontal distribution of rBC concentration in Region 1 in (a) 2009 and (c) 2011, and in Region 2 in (b) 2009, (d) 2011 and (e) 2012.

An increase in rBC concentration is visible in Region 3, too (Fig. 4.9a, c, e). From 2009 to 2011, the mean value doubles roughly from $20 \, \text{ng/m}^3$ to $41 \, \text{ng/m}^3$ and increases up to $105 \, \text{ng/m}^3$ in 2012. This development is manly seen in the measurements around Alert. The way in which the data is plotted may suggest a decrease of rBC concentration in Region 4 from 2009 to 2011 (Fig. 4.9b, d). However, there is a slight increase in the mean rBC concentrations (Tab. 4.2). The increase of rBC concentration is clearly visible in this region from 2011 to 2012 in Figure 4.9d and Figure 4.9f. The mean rBC concentrations rise from $37.5 \, \text{ng/m}^3$ up to $103.4 \, \text{ng/m}^3$ in this case.
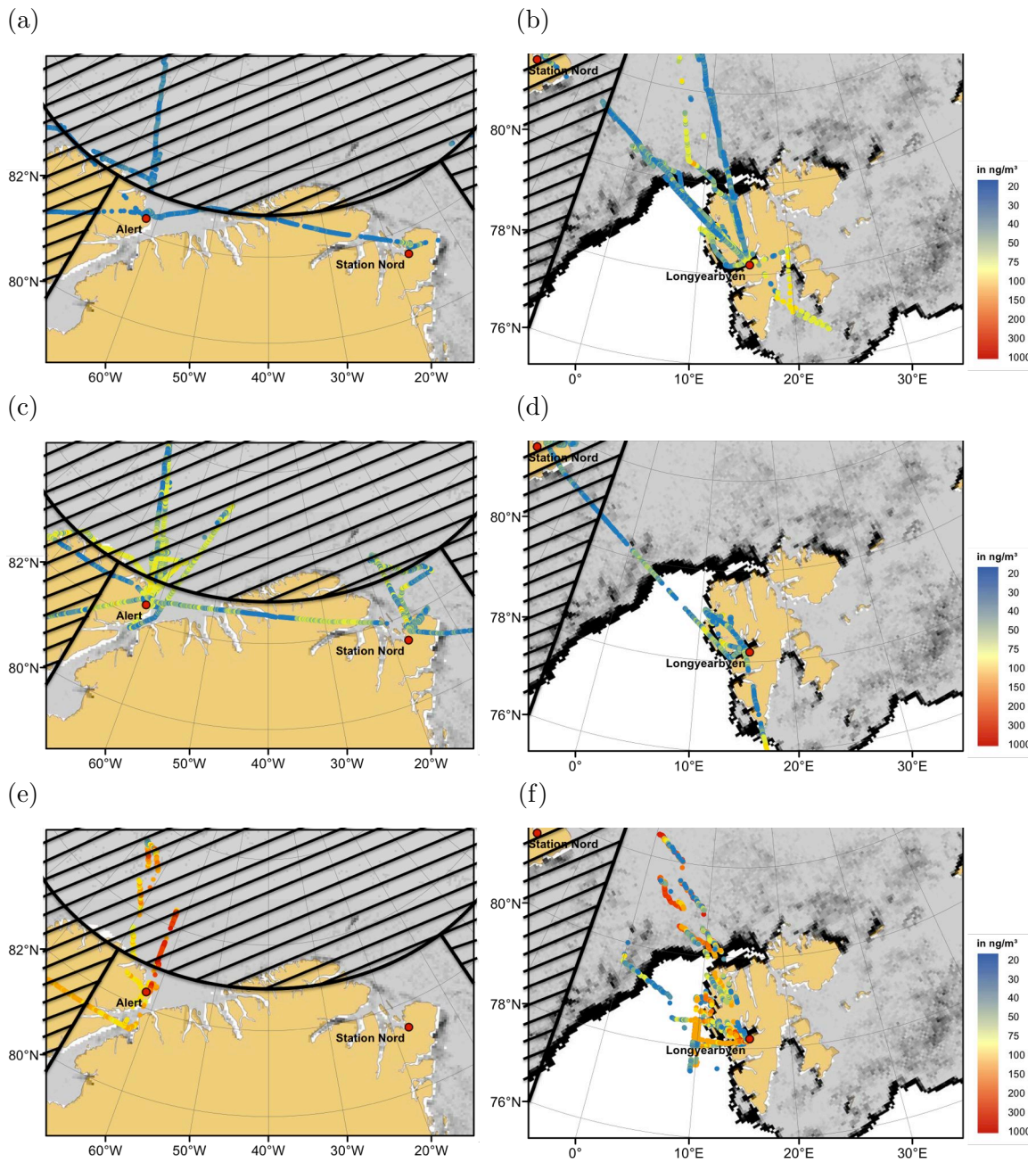
Figure 4.9: Horizontal distribution of rBC concentration in Region 3 in (a) 2009, (c) 2011 and (e) 2012, and in Region 4 in (b) 2009, (d) 2011 and (f) 2012.

Roughly, one track is conducted in all of the three years, namely the one starting in Alert and heading in a northwesterly direction (Fig. 4.10a-c). Up to a certain point, the measured rBC concentrations of the different years can almost directly be compared with each other and a distinct increase with time can be seen. In this region, the mean rBC concentration derived for 2011 is approximately twice as much as the one derived for 2009 and the value for 2012 is more than two times the value of 2011.

(a)

(b)

(c)
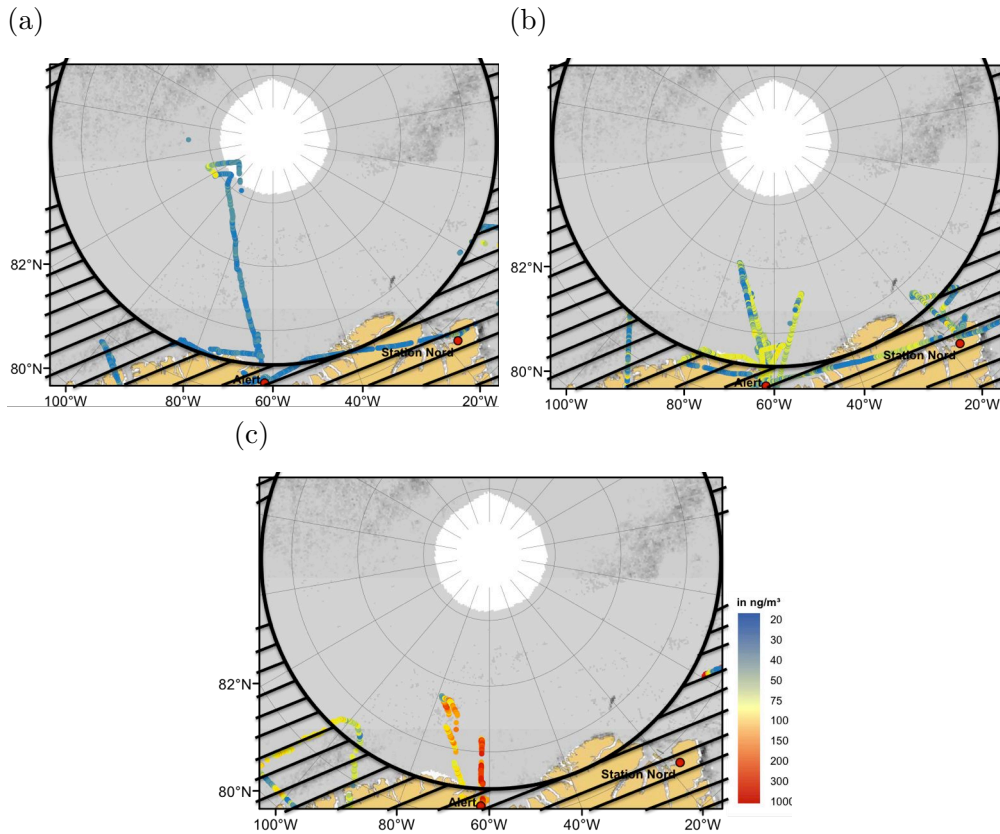
Figure 4.10: Horizontal distribution of rBC concentration in Region 5 in (a) 2009, (b) 2011 and (c) 2012.

The analyses of the horizontal distribution of rBC reveal larger temporal differences than spatial differences. The annual mean rBC concentrations approximately double from about $26 \, \text{ng/m}^3$ to about $52 \, \text{ng/m}^3$ in 2009 and 2011, respectively (Tab. 4.2). From 2011 to 2012, the mean rBC concentration almost doubles again to $102 \, \text{ng/m}^3$. A similar increase reveal the analyses for the different regions, except Region 1. The spatial differences increase from 2009 to 2011 and again, from 2011 to 2012. However, the regional mean rBC concentrations range between $39 \, \text{ng/m}^3$ in Region 2 and $64 \, \text{ng/m}^3$ in Region 4. Possible reasons for these results might be interannual differences in the amount of rBC emissions and/or differences in the transport mechanisms influencing the amount of rBC transported to the Arctic, like changes in wind patterns or deposition processes.

4.3 Source area identification

Using the example of three vertical rBC concentration profiles (Fig. 4.11), a trajectory analysis is made to identify possible source areas.

Two models are used, namely FLEXPART (Stohl et al., 2007), which is a backward-running Lagrangian particle dispersion model and the HYbrid Single-Particle Lagrangian Integrated Trajectory (HYSPLIT) model of the Air Resources Laboratory (ARL) of the U.S. National Oceanic and Atmospheric Administration (NOAA) (Draxler and Hess, 1997). Two FLEXPART products are used, the column-integrated potential emission sensitivity (PES) and the footprint PES. The first product delivers the PES integrated over the entire atmospheric column, while the latter delivers the PES averaged over the lowest model layer, which is $0 - 100\,\mathrm{m}$. Both outputs are derived with a total backward run time of 30 days. Two HYSPLIT products are used as well. A single backward trajectory and an ensemble of backward trajectories with slightly different starting points, shifted in latitude, longitude and altitude. The total backward run time of the model is 10 days. For the HYSPLIT model results, only plots of ensemble backward trajectories are shown.

The FLEXPART results are provided by Sabine Eckhardt from the Norwegian Institute for Air Research (NILU). They are driven with meteorological input data from the European Centre for Medium Range Weather Forecasts (ECMWF). The HYSPLIT model is run using the Real-time Environmental Applications and Display sYstem (READY) website (http://www.ready.noaa.gov) provided by the NOAA Air Resources Laboratory. The meteorological input data is the Global Data Assimilation System's (GDAS) 3-hourly archive data provided by the National Weather Service's National Centers for Environmental Prediction (NCEP) with a horizontal resolution of one degree.

The chosen vertical profiles show either a typical profile without any height dependency of rBC concentrations (Figs. 4.11a) or reveal higher rBC concentrations in one altitude range than in other altitudes (Figs. 4.11b, c).
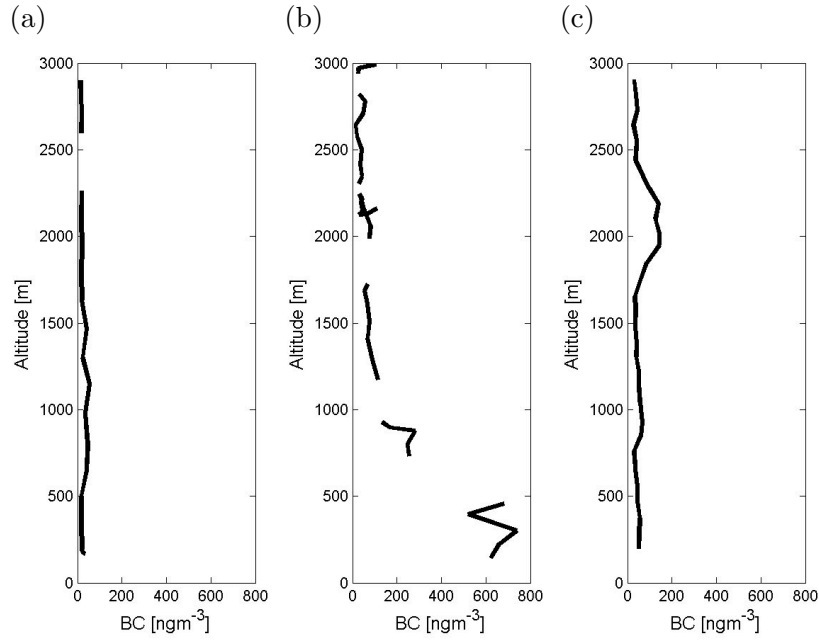
Figure 4.11: rBC concentration as a function of height for profiles recorded on a) at $80°N, 8°E$ 5.4.2009 on the upward flight, b) at $79°N, 11°E$ 21.3.2012 on the downward flight and c) at $75°N, 95°W$ 10.4.2011 on the upward flight.

As mentioned in Section 4.1.1, a height dependency of rBC cannot be verified. Figure 4.11a shows such a typical profile recorded near the northwest coast of Spitsbergen on 5.4.2009. The ensemble trajectories and the single trajectories of the runs with the starting points at an altitude of $h = 500\,\text{m}$ (Fig. 4.12a) and at an altitude of $h = 2000\,\text{m}$ (Fig. 4.12b) show a similar behaviour: both reveal a high probability for the measured air masses originating from the central Arctic. Since the Arctic Ocean is covered by sea-ice in the Arctic spring, and other rBC sources are assumed to be rare in the peripheral regions of the Arctic, the relative low rBC concentrations are reasonable.

On 21.3.2012 (Fig. 4.11b), the distinct difference of the amount of rBC concentrations measured at altitudes between $200\,\text{m}$ and $500\,\text{m}$, and those measured at altitudes above $1500\,\text{m}$ might be explained by the modelled backward trajectories. The ensemble trajectories and the single trajectory of the run with the starting point at an altitude of $h = 500\,\text{m}$ (Fig. 4.13a) show that these air masses originate in Eurasian regions, where they most likely pass BC sources. Air masses in an altitude of $2500\,\text{m}$ (Fig. 4.13b) show relative low rBC concentrations, which is probably caused by the fact that these air masses originate in Arctic regions, with mainly sea ice covered surfaces, in the North Atlantic or in Canada. In these regions, the probability of BC sources is rather small compared to the Eurasian regions.
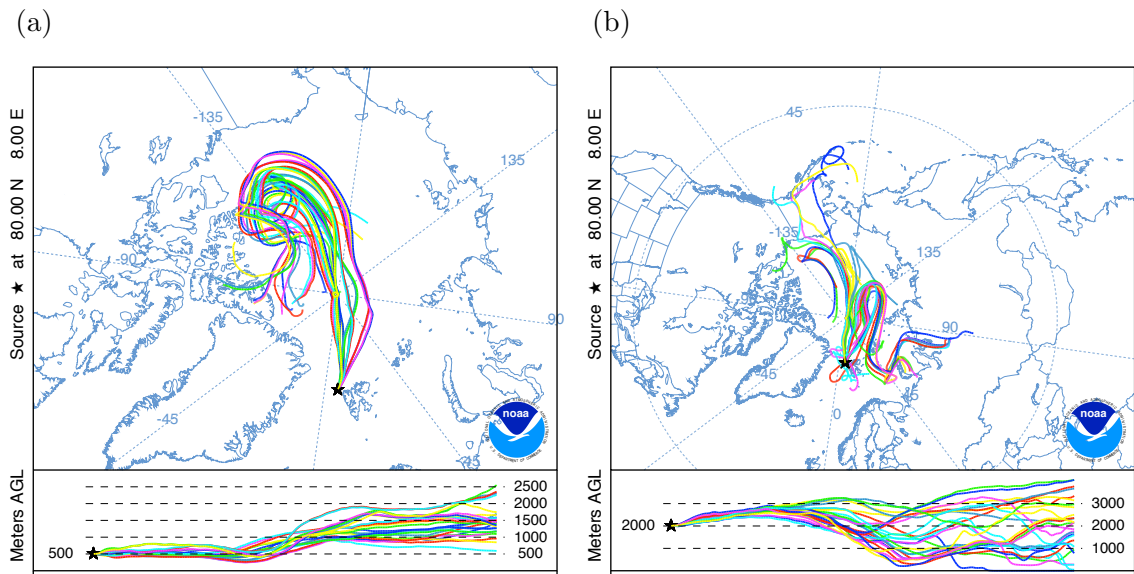
Figure 4.12: Ensemble backward trajectories modelled with HYSPLIT ending at (a) $h = 500\,\text{m}$ and at (b) $h = 2000\,\text{m}$ at $80°N, 8°E$ on 5.4.2009.
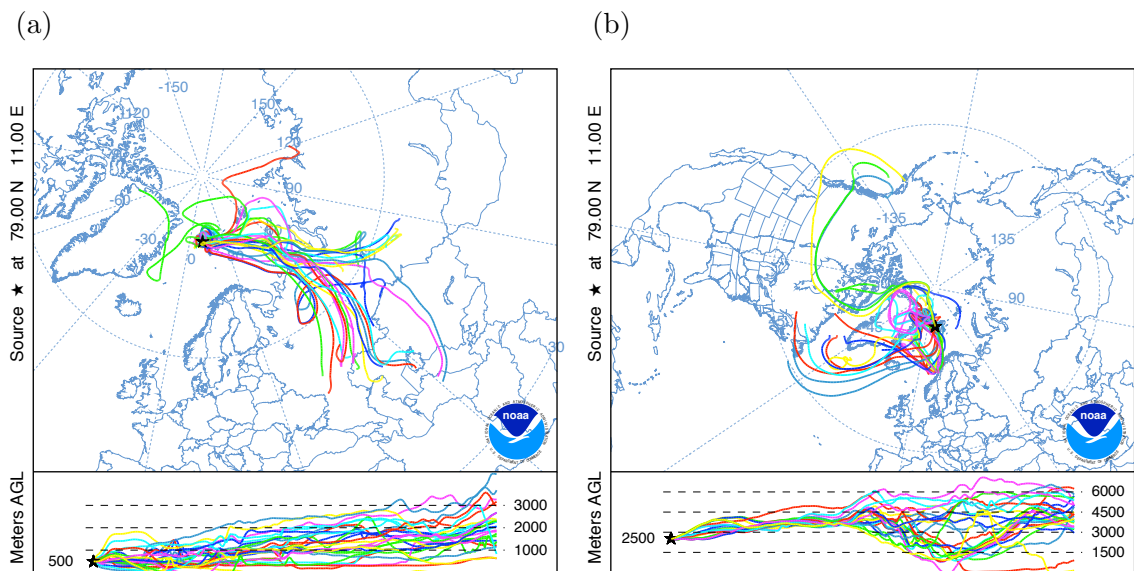
Figure 4.13: Ensemble backward trajectories modelled with HYSPLIT ending at (a) $h = 500\,\text{m}$ and at (b) $h = 2500\,\text{m}$ at $79°N, 11°E$ on 21.3.2012.

These findings are supported by the FLEXPART results. In Figure 4.14a, the column-integrated PES reveals probable source areas in Greenland, the Arctic Ocean and the North Atlantic, while the footprint PES (Fig. 4.14b) shows that the origin of the air mass measured in altitudes below $100\,\text{m}$ is mainly located in Eurasian regions.

(a)   (b)
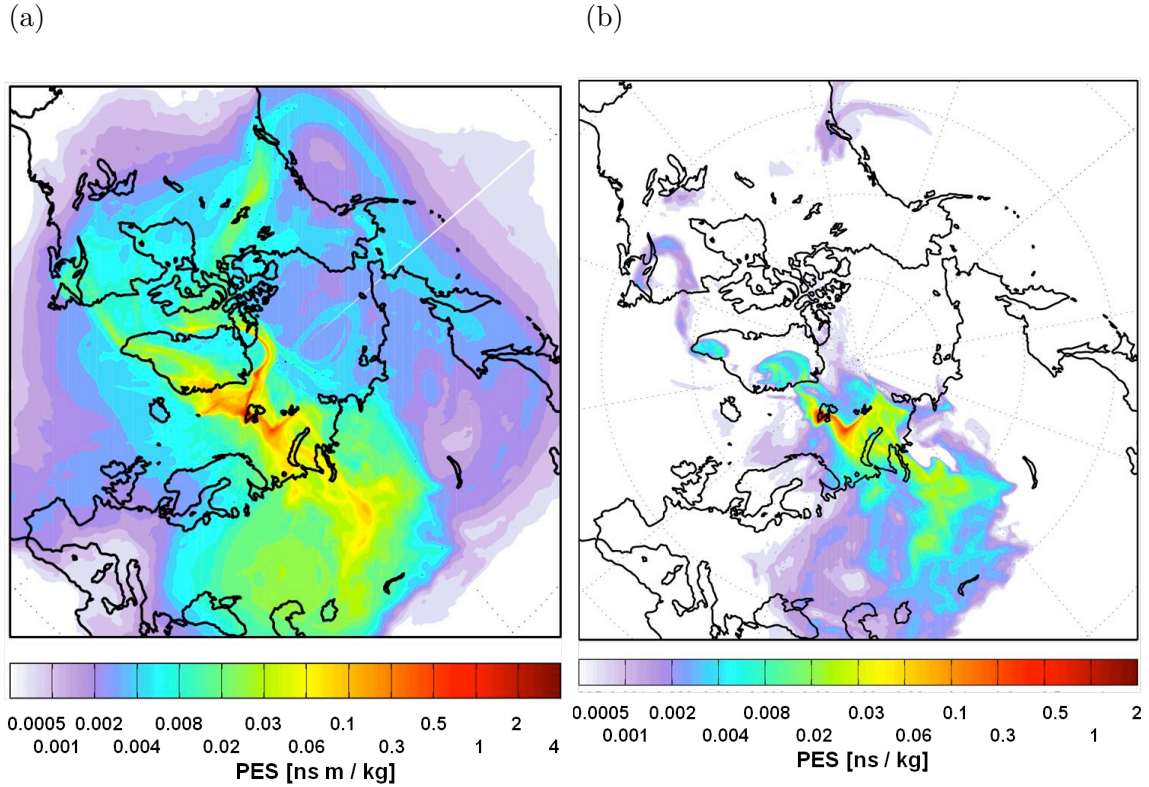
Figure 4.14: Column-integrated (a) and footprint potential emission sensitivity (PES) (b) for a backward FLEXPART simulation ending at $79°N, 11°E$ on 21.3.2012 (courtesy of Sabine Eckhardt, NILU).

The general synopsis of the weather on 21.3.2012 (Fig. 4.15) support these findings, too. The pattern of the surface pressure reveals a weak low west of Svalbard and a distinctive low pressure area further south, above the Ural Mountains. Southwest of the Ural Mountains, the Siberian High is located. These circumstances promote air masses from South East Europe and South West Asia to penetrate northward. The pattern of wind at 700 hPa reveals air masses reaching the measuring point from northwesterly and westerly directions. That corresponds with the backward trajectories in Figure 4.13b and the column-integrated PES in Figure 4.14a. For the HYSPLIT results, this finding is not astonishing, because the model is driven with meteorological data provided by NCEP. Also, the FLEXPART results match also, despite using meteorological input data from the ECMWF.
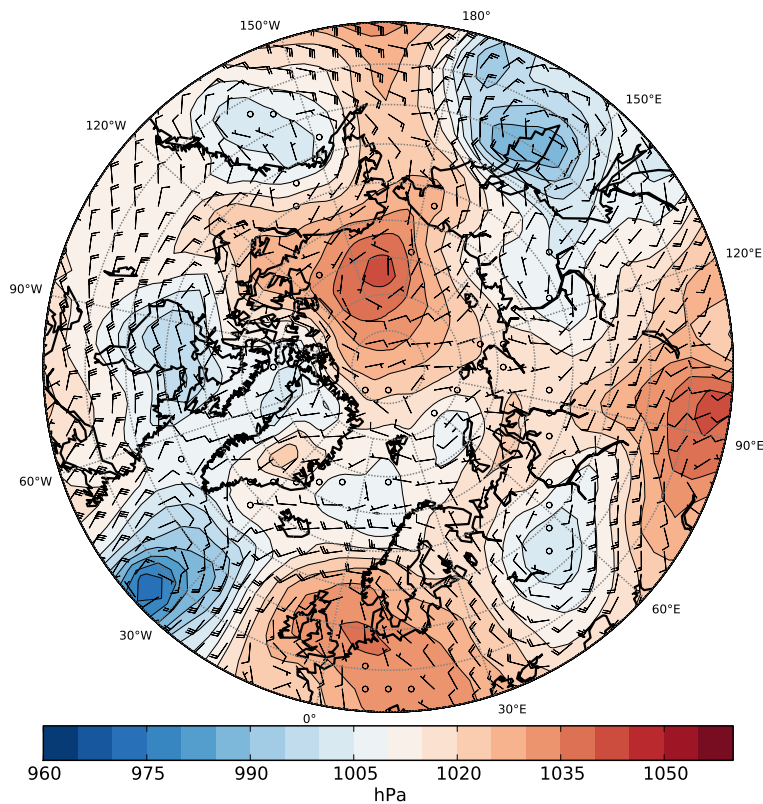
Figure 4.15: NCEP/NCAR 3-hourly mean sea level pressure and wind in 700 hPa on 21.3.2012 (courtesy of Hannes Schulz).

The same analysis is done for the vertical profile recorded on 10.4.2011 (Fig. 4.11c). A slight bimodal peak in rBC concentration is located in altitudes around 2100 m. HYSPLIT is run with one starting point at an altitude of 750 m and with another at an altitude of 2000 m. The ensemble of backward trajectories, as well as, the single backward trajectories, reach further south for the run with $h = 2000$ m (Fig. 4.16a) than the trajectories for the run with $h = 750$ m (Fig. 4.16b). Additionally, some of

the ensemble trajectories of the run with the higher starting altitude reach the area around Svalbard. The FLEXPART outputs reveal partly similar results. The plot of footprint PES shows that the origin of the measured air mass is mainly located in the central Arctic, while the plot of column-integrated PES reveals additionally probable source areas in the North of the Eurasian continent. Since sources near the measuring site can be neglected, the origin of the relatively high rBC concentrations might be in Northern Russia or around Svalbard.

(a)   (b)
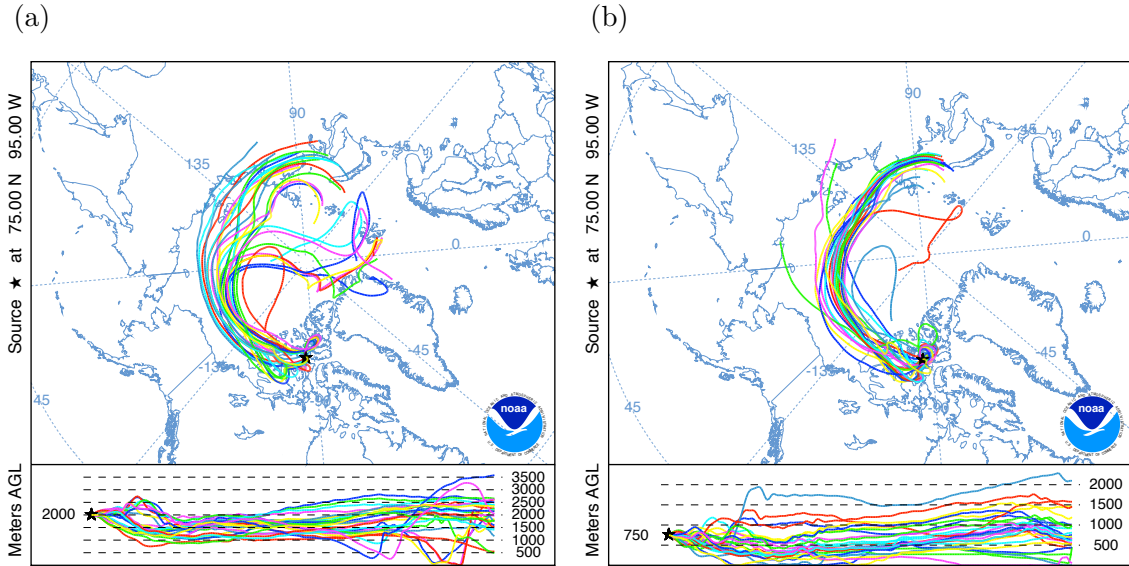
Figure 4.16: Ensemble backward trajectories modelled with HYSPLIT starting at (a) $h = 2000\,\mathrm{m}$ and at (b) $h = 750\,\mathrm{m}$ at $75°N, 95°W$ on 10.4.2011.

Currently, local sources play a minor role in the Arctic spring, since the sea-ice covered Arctic Ocean prevents almost all shipping activity and other utilisations which includes the production of rBC. Thus, the measured vertical distributions of rBC concentration are mainly dependent on long-range transport of rBC into the Arctic. Therefore, the area the air masses originate and the type, intensity and amount of sources in the area of origin are decisive for the amount of BC in the Arctic atmosphere. Additionally, the advection velocity plays a certain role. The faster the advection of BC containing air masses, the higher the probability for not being deposited but transported into the Arctic.

Results of the trajectory calculations are closely related to the meteorological situation occurring during and before the in-situ measurements. Thus, model runs using the same input except the meteorological data and/or spatial resolution, may deliver different backward trajectories and probably lead to different possible source areas. As mentioned in Section 2.2, wet and dry deposition act as sinks for atmospheric

BC. These processes taking place during transport are not taken into account. If the atmospheric lifetime is reduced because of dry or wet deposition, it may lead to misinterpretations concerning the amount of BC transported into the Arctic. Furthermore, the mere backward trajectory analysis delivers no information at which location of the trajectory the sources really are and what kind of sources the rBC originate from.

5 Correlation with other parameters

Data of BC concentration or other parameters related to the amount of BC in the atmosphere is rare, especially in the Arctic. Therefore, it would be helpful to find a surrogate parameter, which allows inferences about atmospheric BC. Carbon monoxide (CO) is such a surrogate parameter (Baumgardner et al., 2002) but it is not measured during the PAMARCMiP campaigns. In addition, potential relationships between BC and the analysed parameters may help making processes during emission and transmission more understandable. In the following sections, correlations between rBC and atmospheric ozone, particle concentration, aerosol optical depth and surface albedo recorded during the PAMARCMiP campaigns are analysed.

The correlation analysis is individually made for each year. At first, all data pairs are analysed, afterwards data pairs measured at altitudes $h \leq 500\,\mathrm{m}$ and $h \geq 2500\,\mathrm{m}$ are analysed separately. These two altitude ranges are chosen in order to analyse data from the free troposphere and the atmospheric boundary layer (ABL) seperately. In several cases, the height of the ABL might be lower than $500\,\mathrm{m}$ and data measured outside the ABL. However, it is a feasible approach and a compromise between the actual ABL height and the lowest levels the airborne measurements are realisable. Above a certain flight level, albedo measurements are not useful, since the pyranometer detects the back scattered solar irradiance of the whole half space. Thus, for the albedo data the analysed altitude range is restricted to $h \leq 500\,\mathrm{m}$. Furthermore, data recorded in altitudes $h \leq 500\,\mathrm{m}$ and $h \geq 2500\,\mathrm{m}$ are ordered and analysed by region. To complete this investigation, the individual high- and low-level segments are analysed, as well. If a parameter is not dependent on exactly one other parameter, an analysis of specific groups of data may reveal correlations, while an analysis of the entire data pairs may show no correlation or vice versa. "Specific groups of data" means data with at least one common characteristic, like time, altitude, region or the day the measurement took place. Effects of several parameters on rBC concentration are conceivable and,

therefore, the described procedure is chosen. The used statistical tools are Pearson's correlation coefficient

$$r = \frac{cov(x, y)}{\sigma_x \sigma_y} \tag{5.1}$$

with the covariance

$$cov(x, y) = \frac{1}{N} \sum_{i=1}^{N} (x_i - \overline{x})(y_i - \overline{y}) \tag{5.2}$$

and the standard deviations σ_x and σ_y as well as, the squared Pearson's correlation coefficient, the coefficient of determination, R^2. In order to compare the derived correlation coefficients with each other, a classification is introduced. The determined values of r are interpreted as listed in Table 5.1.

Table 5.1: Intervals of correlation coefficients and their corresponding degree of correlation.

r	degree of correlation
$\pm 0.7 - \pm 1.0$	strong positively or negatively correlated
$\pm 0.5 - \pm 0.69$	medium positively or negatively correlated
$\pm 0.3 - \pm 0.49$	weak positively or negatively correlated
$-0.3 - 0.3$	negligible

In Section 5.1, the correlation analysis for rBC and O_3 concentrations is exemplary for the correlation analyses for rBC concentration and three other parameters. Several plots include a sum of results to give an overview and to facilitate the comparison between specific groups of data. In addition, B.1-B.9 in the Appendix B offer a more detailed illustration of these results. The other correlation analyses are shown in less detail in Section 5.2.

5.1 Correlations between black carbon and ozone

Ozone concentration data are available for 2009 and 2011 but not for 2012. It is detected by a TECO 49C UV photometer (Thermo Electron Inc., Franklin, MA). As described in Latha and Badarinath (2004), the ratio between rBC and O_3 concentrations indicates if the probed air contains fresh emissions, emissions changed by chemical reactions or if stratospheric O_3 is measured because of downwelling. High rBC concentrations and low O_3 concentrations indicate fresh emissions, high rBC concentrations

and high O_3 concentrations indicate that chemical reactions have taken place and low rBC concentrations and high O_3 concentrations indicate downwelling of stratospheric O_3. They conclude this from measurements over a tropical urban site and not for an Arctic environment as analysed in this thesis. It is questionable whether an analogy can be drawn between these two cases. Kaleschke et al. (2004) describe a O_3 destruction by bromine, which originates from frost flowers located on the sea ice surface. They describe the O_3 destruction as "... very efficiently in two interlinked catalytic cycles ...". This process is observed in the beginning of the polar day and may cause a lower correlation between O_3 and rBC in lower altitudes.

The correlation coefficient of all rBC and O_3 concentrations recorded in 2009 is $r_{all} = 0.02$ which reveals a negligible degree of correlation. The analyses in which two altitude ranges are distinguished, reveal slightly higher correlation coefficients of $r_{h \leq 500\,m} = 0.34$ and $r_{h \geq 2500\,m} = 0.13$, which is visualised in a scatter plot shown in Figure 5.1a. Figure 5.1b shows the dependencies between all rBC and O_3 concentrations recorded in 2011, as well as the results for altitudes $h \leq 500\,m$ and $h \geq 2500\,m$. The determined correlations coefficients are $r_{all} = 0.07$, $r_{h \leq 500\,m} = -0.02$ and $r_{h \geq 2500\,m} = 0.25$.

(a) (b)
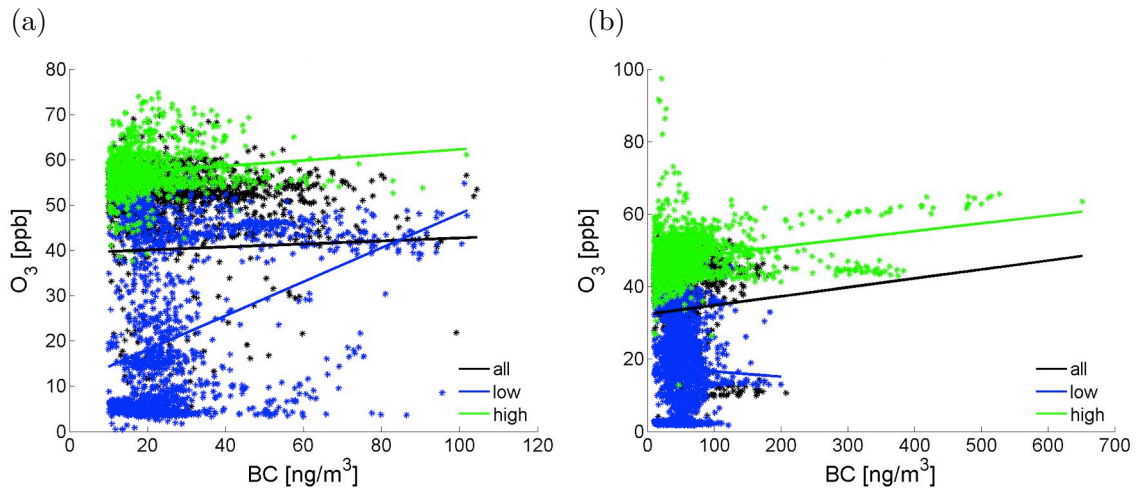
Figure 5.1: Scatter plots of rBC and O_3 concentrations recorded at all altitudes (black), altitudes $h \leq 500\,m$ (blue) and altitudes $h \geq 2500\,m$ (green) during a) PA-MARCMiP09 and b) PAMARCMiP11 with the associated linear regression line (note the different scaling).

The correlations analysed by region, shown in Figure 5.2 and 5.3, are highly variable for 2009 and 2011. In 2009 (Figs. 5.2a and 5.3a), the highest dependencies are found in altitudes $h \leq 500\,m$ in Region 1 and 2, and in $h \geq 2500\,m$ in Region 3 with values between 0.53 and 0.54. In comparison to all data and the data distinguished between the two altitude ranges (Fig. 5.1b), Figures 5.2b and 5.3b show partly higher

dependencies between the two parameters. While the highest value for altitudes $h \leq 500\,\text{m}$ is found to be 0.42 and located in Region 4, the highest value for altitudes $h \geq 2500\,\text{m}$ is found to be 0.59 and is located in Region 4, as well.
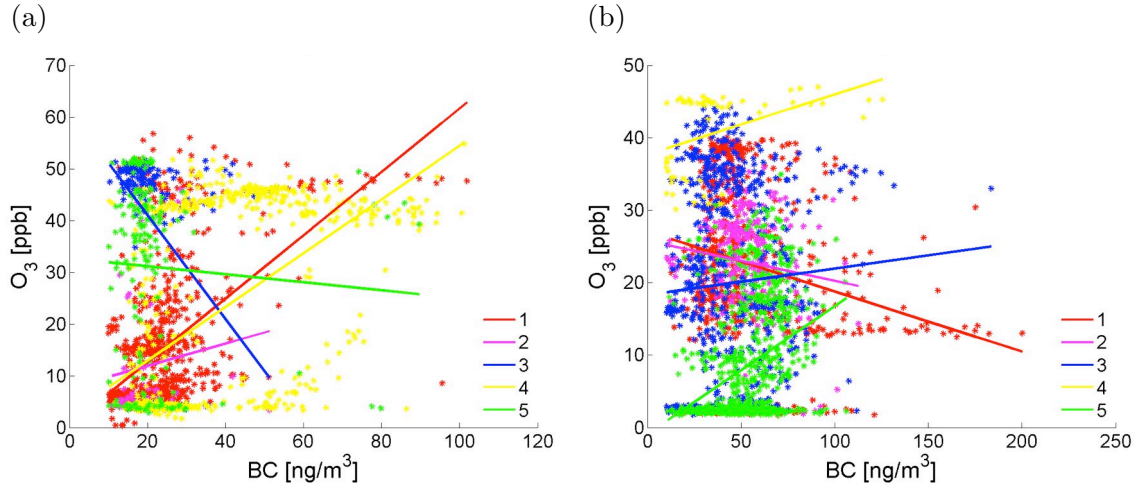
Figure 5.2: Scatter plots of rBC and O_3 concentrations recorded at altitudes $h \leq 500\,\text{m}$ in Region 1 (red), 2 (magenta), 3 (blue), 4 (yellow) and 5 (green) during (a) PAMARCMiP09 and (b) PAMARCMiP11 with the associated linear regression line (note the different scaling).

In 2009, correlation coefficients for the individual low-level flights vary between -0.18 and 0.77 with the highest values on 4.4.2009 (Fig. 5.4a). That is the only low-level segment on which strongly positive linear correlations are found. Apart from that only negligible small correlation coefficients are derived. Values for high-level flights range between -0.72 on 5.4.2009 and 0.94 on 3.4.2009, which are visualised in Figure 5.4b and 5.4c. In total, there are three high-level flights which show a strong positive or negative linear correlation between rBC and O_3 concentrations and eleven which show weak or negligible correlations between these two parameters.

Figure 5.5a shows the low-level flight with the strongest correlation in 2011. A correlation coefficient of 0.72 is derived for 15.4.2011. Apart from that, for approximately two thirds of the flight segments negligible correlations are derived, for one third weak or medium correlations are derived. Notwithstanding that the strongest correlation coefficient of all low-level segments is positive, the averaged correlation coefficient and the median of all correlation coefficients are both < 0 in 2011. That indicates, that emissions from local sources are detected or down-welling of stratospheric O_3 took place.

(a) (b)
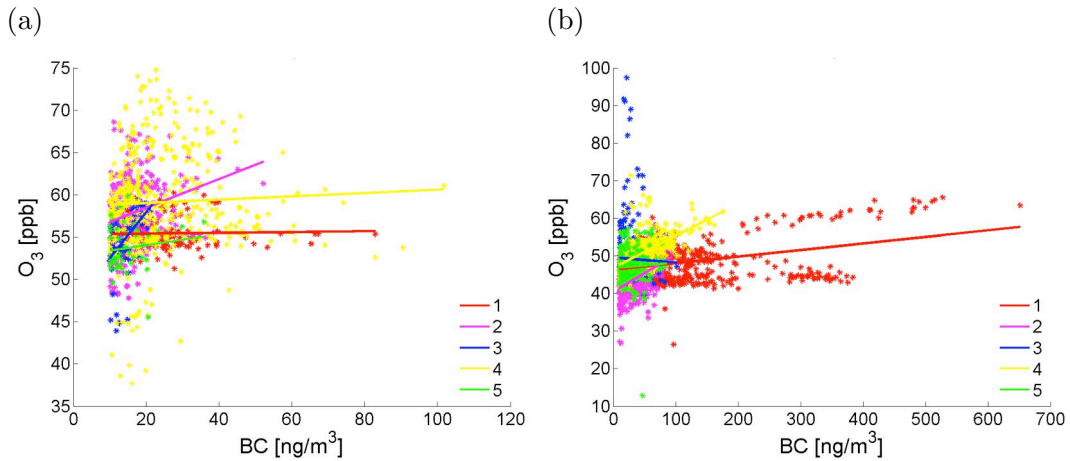
Figure 5.3: Scatter plots of rBC and O_3 concentrations recorded at altitudes $h \geq$ 2500 m in Region 1 (red), 2 (magenta), 3 (blue), 4 (yellow) and 5 (green) during (a) PAMARCMiP09 and (b) PAMARCMiP11 with the associated linear regression line (note the different scaling).

Correlation coefficients derived for the high-level segments are higher than the ones for the low-level segments. The analysis reveals strong correlations for 20 % of the segments and medium correlations for another 20 % of the segments. The determined correlations are positive except the one derived for 2.4.2011. Figure 5.5b and c show scatter plots for the segments with strong dependencies between rBC and O_3 concentrations, with values of 0.95 and 0.78.

A general statement about the correlation between rBC and O_3 concentrations based on the available data is not possible. Nevertheless, the results allow some conclusions. In both years, stronger positive correlations are found in the higher level. That can be caused by the fact, that O_3 concentrations are usually higher in higher altitudes than in lower altitudes and the assumption that higher O_3 concentrations leads to higher correlations with rBC concentrations. Another reason may be an unknown difference in the two air masses, hence a difference in origin, path of transmission and/or processes during transmission. For instance, air masses in the higher altitude levels are more likely affected by long range transport than air masses inside the ABL. A process can be the already mentioned O_3 destuction by bromine near the sea ice covered surface. In case of strong correlations, the parameters are always positive correlated, which holds for medium correlations as well, except the high-level segment on 5.4.2009 (Fig. 5.4b). These results lead to the assumption, that chemically altered air masses are mainly detected, which are transported into the measuring sites. That is reasonable, because rBC sources are barely located in the Arctic and shipborne emissions are not probable during the present ice conditions in the Arctic spring.
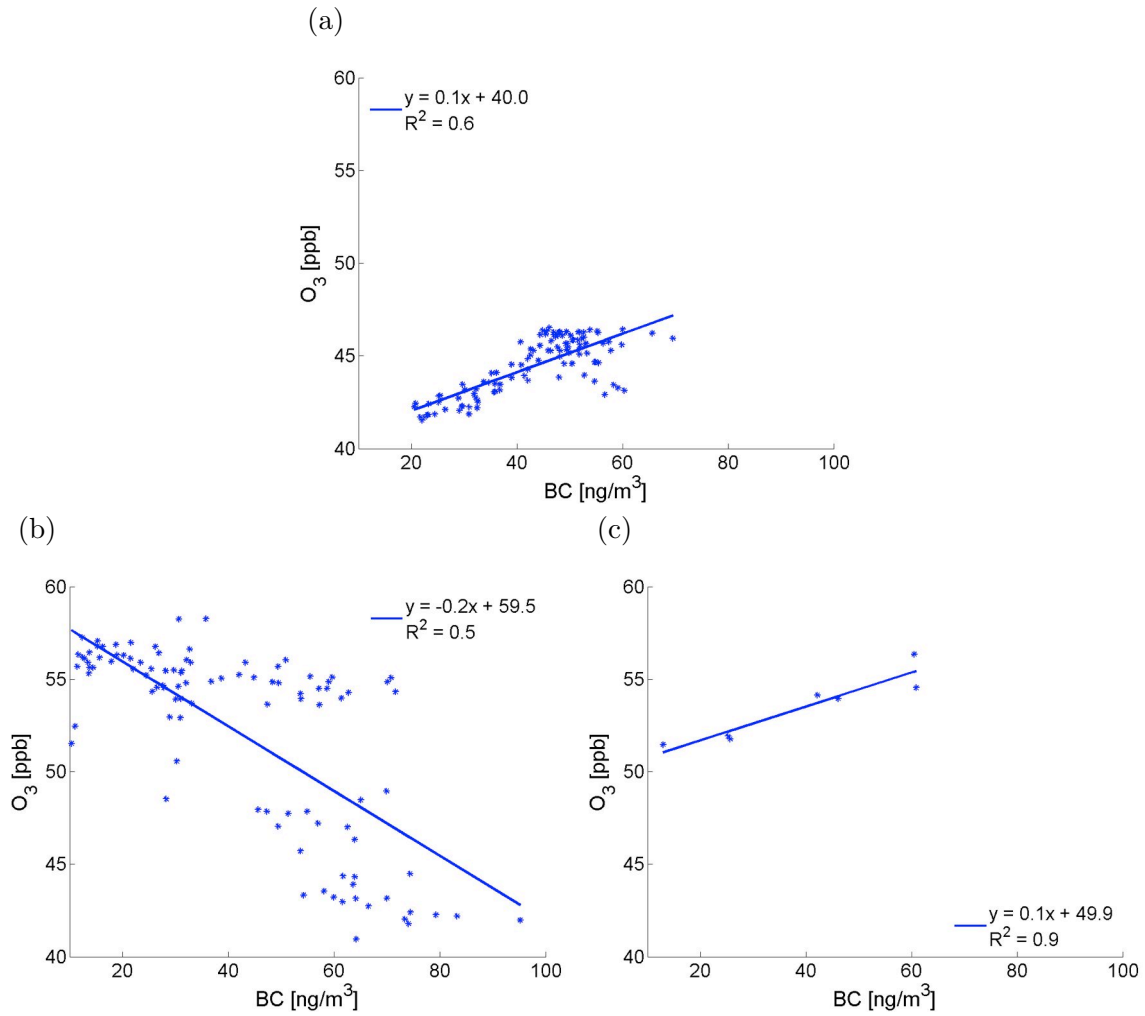
Figure 5.4: Scatter plots of rBC and O$_3$ concentrations recorded on (a) 4.4.2009 at low-level, (b) 5.4.2009 and (c) 3.4.2009 both at high-level with the associated linear regression line and the coefficient of determination R^2.

(a)

(b)

(c)
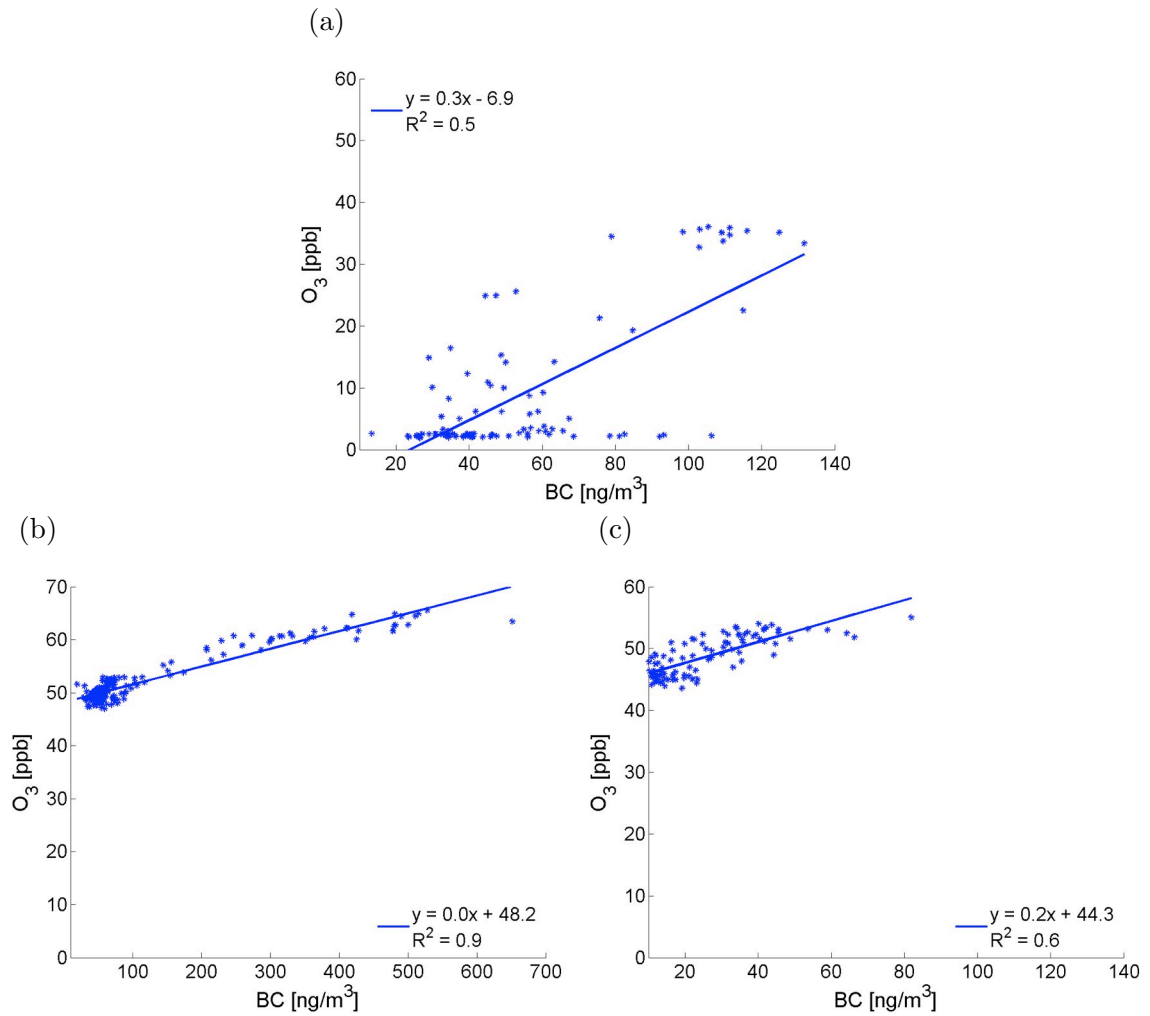
Figure 5.5: Scatter plots of rBC and O_3 concentrations recorded on (a) 15.4.2011 at low-level, (b) 3.4.2011 (note the different scaling) and (c) 29.4.2011 both at high-level with the associated linear regression line and the coefficient of determination R^2.

5.2 Correlations between black carbon and particle concentration, AOD and albedo

The following correlation analyses for rBC concentration and particle concentration, AOD and albedo are conducted the way it is made for rBC and O_3 concentrations in Section 5.1. An overview is given by one table per year (Tab. 5.2 - 5.4) and the main points are described and discussed in this section. The corresponding scatter plots can be found in the appendix.

Table 5.2: Correlation coefficients of rBC concentration and particle concentration, AOD and albedo ordered by altitude range and region are listed for individual segments in 2009. Colours indicate the degree of correlation: strong (dark blue), medium (mid-blue), weak (light blue). Uncoloured table cells indicate negligible degree of correlation.

2009	particle concentration		AOD		albedo
	low	high	low	high	low
all	0.29		0.02		- - - -
	0.45	0.23	-0.10	0.01	0.19
Region 1	0.53	0.11	0.10	0.64	0.28
Region 2	0.39	0.46	-0.75	-0.50	-0.30
Region 3	-0.28	0.61	0.66	-0.05	-0.02
Region 4	0.53	0.41	0.68	0.26	-0.29
Region 5	-0.07	0.03	0.27	0.12	-0.51
01.04.2009	- - - -	0.18	- - - -	- - - -	- - - -
02.04.2009	0.00	- - - -	- - - -	- - - -	0.25
03.04.2009	0.23	0.86	-0.97	- - - -	-0.19
04.04.2009	0.90	-0.02	- - - -	0.68	-0.23
05.04.2009	0.08	0.55	0.15	0.28	0.29
05.04.2009	- - - -	0.44	- - - -	- - - -	- - - -
06.04.2009	0.25	0.72	-0.56	- - - -	-0.05
06.04.2009	- - - -	0.14	- - - -	- - - -	- - - -
08.04.2009	- - - -	0.68	- - - -	0.11	- - - -
09.04.2009	-0.13	0.71	-0.34	0.28	-0.17
10.04.2009	- - - -	0.60	- - - -	- - - -	- - - -
11.04.2009	- - - -	0.44	- - - -	-0.04	- - - -
13.04.2009	- - - -	0.11	- - - -	0.08	- - - -
14.04.2009	- - - -	0.21	- - - -	0.28	- - - -
15.04.2009	- - - -	0.20	- - - -	0.87	- - - -
16.04.2009	0.03	- - - -	0.17	- - - -	0.08
24.04.2009	0.35	-0.24	-0.05	- - - -	-0.04
25.04.2009	0.38	0.77	- - - -	- - - -	- - - -

Table 5.3: Correlation coefficients of rBC concentration and particle concentration, AOD and albedo ordered by altitude range and region are listed for individual segments in 2011. Colours indicate the degree of correlation as described for Table 5.2.

2011	particle concentration		AOD		albedo
	low	high	low	high	low
all	0.42		0.40		- - - -
	0.24	0.49	0.35	0.51	0.05
Region 1	-0.24	0.75	0.36	0.51	-0.03
Region 2	-0.05	0.67	-0.42	- - - -	0.01
Region 3	0.60	0.11	- - - -	- - - -	-0.06
Region 4	0.44	0.71	- - - -	- - - -	- - - -
Region 5	0.48	0.22	- - - -	- - - -	-0.08
01.04.2011	-0.35	- - - -	0.10	- - - -	0.06
02.04.2011	-0.07	0.22	0.56	-0.25	-0.62
03.04.2011	- - - -	0.96	- - - -	0.73	- - - -
04.04.2011	0.75	-0.06	-0.32	-0.27	- - - -
05.04.2011	-0.08	- - - -	-0.85	- - - -	- - - -
06.04.2011	- - - -	0.72	- - - -	0.57	- - - -
10.04.2011	- - - -	0.38	- - - -	- - - -	- - - -
14.04.2011	0.13	- - - -	- - - -	- - - -	0.01
15.04.2011	0.76	- - - -	- - - -	- - - -	- - - -
16.04.2011	0.41	- - - -	- - - -	- - - -	-0.13
17.04.2011	0.37	0.61	- - - -	- - - -	-0.07
18.04.2011	0.2123	- - - -	- - - -	- - - -	0.06
21.04.2011	- - - -	0.16	- - - -	- - - -	- - - -
22.04.2011	-0.16	- - - -	- - - -	- - - -	0.02
27.04.2011	- - - -	0.08	- - - -	- - - -	- - - -
28.04.2011	0.29	- - - -	- - - -	- - - -	- - - -
29.04.2011	- - - -	0.90	- - - -	- - - -	- - - -
05.05.2011	- - - -	0.60	- - - -	- - - -	- - - -
05.05.2011	- - - -	0.92	- - - -	- - - -	- - - -

Particle concentration

Particles with diameters between 60 nm and 1000 nm are detected by an Ultra-High Sensitivity Aerosol Spectrometer (UHSAS) and the data are available for 2009 and 2011, but not for 2012. Correlations between rBC concentration and particle concentration are analysed in order to investigate possible dependencies between these parameters. Note that rBC concentration is not a subset of particle concentration. rBC particles may be smaller than the lower detection limit of the UHSAS. Additionally, a direct comparison is difficult because of different units ng/m^3 and ppb for rBC concentration and particle concentration, respectively.

Table 5.4: Correlation coefficients of rBC concentration and particle concentration ordered by altitude range and region are listed for individual days in 2012. Colours indicate the degree of correlation as described for Table 5.2.

2012	AOD	
	low	high
all		0.20
	-0.23	0.41
Region 1	0.09	0.13
Region 2	- - - -	-0.70
Region 3	-0.12	-0.45
Region 4	0.36	0.33
Region 5	-0.11	0.06
20.03.2012	- - - -	-0.34
21.03.2012	- - - -	0.44
22.03.2012	- - - -	-0.06
24.03.2012	-0.05	0.15
04.04.2012	-0.25	- - - -
05.04.2012	0.00	-0.03

As concluded for the correlation between rBC and O_3 concentrations, a general statement about the correlation between rBC and particle concentrations based on the available data is not possible. However, the correlation coefficients of rBC and particle concentrations are higher in almost all cases. These correlation analyses expose two main features: 1) the data recorded in 2011 reveal stronger correlations than the data recorded in 2009 and 2) the data detected in altitudes $h \geq 2500\,\text{m}$ reveal stronger correlations than the data detected in altitudes $h \leq 500\,\text{m}$. A reason for 1) may be a higher rBC concentration and a lower particle concentration in 2011 compared to 2009, which leads to a higher fraction of rBC in the particle concentration and in turn a stronger correlation. This explanation do not hold for 2), though. The ratio of rBC to particle concentration is about the same in both altitude ranges. One reason might be the discrepancy between the measured rBC concentration and the actual amount of rBC particles.

For the same rBC concentration the amount of rBC particles can be higher at higher altitudes than at lower altitudes, if the mass of rBC particles is lower. Thus, the amount of particles can be higher at higher altitudes and in turn, the ratio of rBC to particle concentration can be higher. Investigations of the processes the particles are involved may deliver further answers. The correlation coefficients reveal a negligible degree of correlation for 50 % of all low- and high-level segments, nevertheless the other 50 % show a positive correlation of rBC and particle concentrations.

Aerosol optical depth (AOD)

The aerosol optical depth (AOD) is a measure of aerosol induced weakening of the atmospheric transparency. In 2009, it is measured with a 8-channel Sun photometer system (U.S. National Oceanic and Atmospheric Administration (NOAA) and the Institute of Atmospheric Sciences Climate National Research Council (ISAC-CNR), Italy). The measuring device is located inside a quartz dome on the roof of the Polar 5. Further information about the instrument can be found in Stone et al. (2010). For the other campaigns, a Sun photometer tracking active (SPTA) is used (Dr. Schulz & Partner GmbH). The following analysis is made to examine the presumption that AOD is increasing with increasing rBC concentration.

The correlation analyses of rBC concentration and AOD deliver no unambiguous statement about their correlation. Among a distinct number of correlations of negligible degree, both positive and negative correlation coefficients, reveal correlations of weak up to strong degrees. A reason for this ambiguous result may be the fact, that the rBC concentration measured in an air parcel at flight altitude, while the AOD is a quantity integrated from atop the aeroplane to the top of the atmosphere (TOA). Since the measured rBC concentration is presumably not representative for the rBC concentration in the whole air column above the aeroplane, the used method may lead to discrepancies.

Albedo

The albedo of snow and ice covered surfaces in the Arctic spring is usually high but BC deposited on these surfaces decreases their albedo (Warren, 2013). The aim of the following correlation analysis is to make a statement how the surface albedo is influenced by atmospheric rBC concentration. The albedo is measured by two Kipp and Zonen CMP22 pyranometer and the data is available for 2009 and 2011.

Two correlation coefficients indicating non-negligible degree of correlation are derived. The first is derived for the data recorded at Region 5 in 2009 and the second on 2.4.2011 (Tabs. 5.2, 5.3). Both of them are of medium degress of correlation and negative. If the fact, that the data basis may be too poor to get reliable results out of these analyses is neglected, the used method will probably not succeed anyway. rBC concentrations are detected in a parcel of air directly above the surface of which the measured albedo is related to. Presumably, the rBC particles will not deposit on the surface straight below the location they are detected. Depending on wind direction and wind speed,

the rBC particles will deposit in the vicinity of the measuring site or far away of it. For more convincing results, the correlation between rBC concentrations and the albedo of the surface the rBC particles deposit should be analysed. The data basis for this kind of analysis is not delivered by the PAMARCMiP campaigns.

In some cases, relative high correlation coefficients result, and indicate strong correlations between rBC concentration and the other analysed parameters, however, the correlation analyses reveal in other cases that a negligible degree of correlation is not exceeded. Different reasons are feasible for these contradictory results. Assuming the cases with strong degree of correlation not to be coincidental, methods of measurements or the analysis of two mismatching parameters may lead to these contradiction. As already mentioned, the first point holds for the correlation analysis of rBC concentration and AOD. A rBC concentration integrated over the same air column, the AOD is derived for, might be more suitable than a point measurement. The second point holds for the analysis of rBC and the other three parameters. Since a linear dependency between the particle mass and the particle number cannot be assumed, the significance of the results of a correlation analysis of rBC concentration, measured in ng/m^3, and O_3, measured in ppb, or the particle concentration, measured in cm^{-3}, are questionable. As mentioned before, correlation coefficients derived for rBC concentration and albedo are of negligible degree of correlation, except two cases with medium degree of correlation. Surface albedo is not correlated to rBC concentration measured in altitudes above that surface (Warren, 2013), but it is shown for BC concentrations on that surface.

6   Conclusions

6.1   Discussion of results

The vertical and horizontal distribution of atmospheric rBC concentration is investigated for the western Arctic using data of three PAMARCMiP campaigns in 2009, 2011 and 2012. Spatial and temporal differences of these distributions are analysed and source areas are identified for rBC concentrations of three exemplary vertical profiles. Additionally, correlation analyses are used in order to identify probable proxy parameters for rBC.

Two main challenges go along with all mentioned analyses. The first one is the not unambiguous defined term "black carbon" and the distinction against the term "soot", which is not unambiguous, as well. Therefore, a characterisation of BC based on information published in previous and current literature, is problematic. Additionally, there exist different kinds of BC, dependent on the used measuring technique, namely rBC and EBC. To what extent the two parameters are comparable is not known. Thus, comparison of the investigated rBC concentrations with previously published values of BC concentrations is challenging.

The second challenge concerning the investigations is the low data density. Beside the data of the PAMARCMiP campaigns, there exist not many other data sets of BC concentrations in the Arctic. Continuous BC measurements are conducted at some stations, but they deliver only data of ground measurements, and no analyses of vertical distributions of BC concentration are possible. The PAMARCMiP data allow such analyses, but only for few weeks in the spring of 2009, 2011 and 2012. However, the measuring area, as well as the flight tracks vary from campaign to campaign. Thus, only few measurements are conducted at exact the same location, but in different years. Therefore, a conclusion of the temporal evolution of rBC concentration is problematic and decreases its validity. Clear statements about differences in rBC concentrations in

two altitude ranges might be vague, if the difference in time between two measurements is two large. Probably, measurements during up- and downward segments deliver more reliable results, since the time difference is smaller.

The following conclusions should be regarded in consideration of the above mentioned difficulties.

Temporal differences

An increase in rBC concentration is found from 2009 to 2011 and from 2011 to 2012. The mean value approximately doubles from about $26\,\mathrm{ng/m^3}$ to about $52\,\mathrm{ng/m^3}$ in 2009 and 2011, respectively. From 2011 to 2012, the mean rBC concentration almost doubles again to $102\,\mathrm{ng/m^3}$. This evolution reveals an increase in rBC concentration increasing with time, since the first doubling proceeds in two years, the second in one year.

In comparison with previous data collected in the Arctic spring (Fig. 6.1), the measured rBC concentrations of all three PAMARCMiP campaigns are relatively low. However, the decreasing trend from 1986 to 2009 is not merely discontinued, but rather shows a reversed behaviour. A prediction of the future evolution based on these analyses is vague. Anyhow, the increase in rBC concentration during the years 2009 to 2012 is almost three times faster than the decrease from 1986 to 2009.

Vertical distribution

In comparison to previous measurements (Fig. 6.1), the vertical profiles of rBC concentration reveal no height dependency. Neither on regional average, nor for the single profiles. Only Region 4 constitutes an exception. Especially in 2011 and 2012, the averaged vertical profiles show higher values in near-surface altitudes and a decrease in rBC concentration with increasing altitude. The same holds for some individual vertical profiles. That leads to the assumption that long-range transport of BC is the main component during all three PAMARCMiP campaigns and local sources are an important factor in Region 4. Since the altitude range in which the BC particles are located is important concerning its effect on the Arctic climate, the knowledge of the vertical distribution of BC is of particular importance.
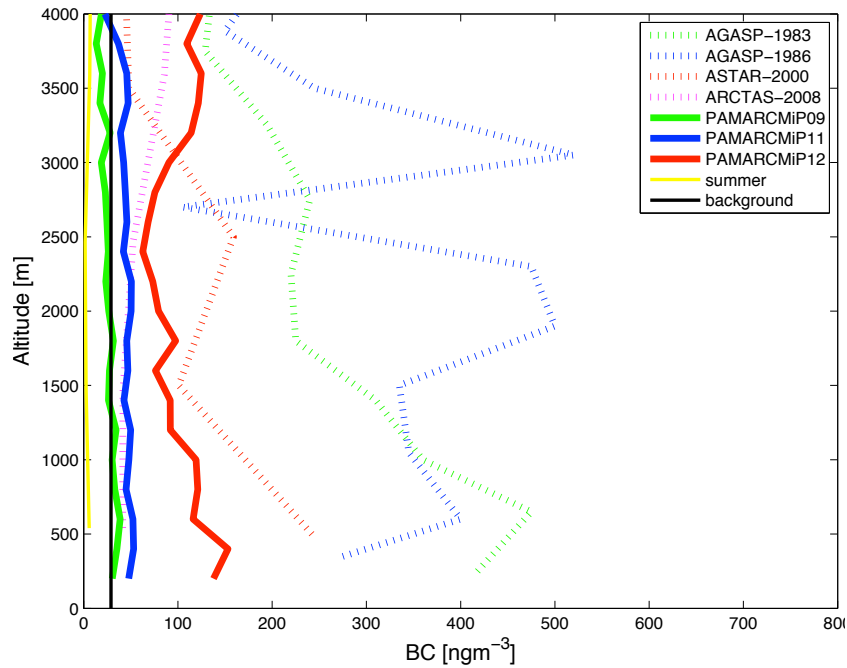
Figure 6.1: Averaged Vertical distribution of EBC and rBC concentrations measured during several aircraft campaigns in the Arctic (based on Figure 5 of Stone et al. (2010)).

Horizontal distribution

The analyses of the horizontal distributions of rBC concentration in the five regions reveal the lowest spatial differences in 2009 and increased differences with time. While differences between the regions are barely found in 2009, distinct regional differences exist in 2011. In 2011, the horizontal distribution of rBC concentration is characterised by a boundary at approximately $100°W$, which divides the measuring area in two parts. The eastern part is similar in the horizontal distribution in 2009 and 2011, but with higher values. The western part is more heterogeneous than the one east of $100°W$. In 2012, spatial differences exist, but low data density limits the validity of the results.

Source area identification

For three exemplary vertical profiles trajectory analyses are conducted in order to identify possible source areas of the measured rBC concentrations. Transport from different areas may lead to different amounts of rBC concentration. Air masses including high rBC concentrations are identified to originate from Eurasia and transported into the Arctic, while transport mainly within the Arctic leads to low rBC concentrations in

general. Air masses originated from the North Atlantic, Greenland and the North of Canada reveal low rBC concentrations in the Arctic, as well. The results are closely related to the meteorological situation occurring during the measurements and, therefore, differences in the meteorological data used by the model or differences in the spatial resolution of the model, may lead to distinct diffrences in the calculation of the trajectories. Atmospheric lifetime influencing processes, including wet and dry deposition during transport are not taken into account. Furthermore, these kind of analysis delivers neither information about the location of the sources, nor the type of sources, which lead to the measured rBC concentration.

Potential proxy parameters

The quest of proxy parameters for rBC concentrations failed. Thus, neither the ozone concentration, nor the particle concentration, nor aerosol optical depth, nor albedo measured during the PAMARCMiP campaigns are useful parameters to draw conclusions for rBC concentration. Partly, the used measurement methods deliver parameters which are not suitable for the comparison with the measured rBC concentration. This leads to negligible correlations and is the case for the analysed AOD data. Another reason is the mismatch of the compared parameters. Ozone data are given as particle number and particle concentrations have the unit of a volume concentration, while rBC concentration data are given as mass concentrations. To stick to carbon monoxide (CO) as a surrogate parameter (Baumgardner et al., 2002) appears to be much more useful.

6.2 Outlook

This far, the investigations of BC in the Arctic are rare and this thesis is an approach to supply an overview of the current rBC concentrations in the western Arctic. During the analyses, several questions arise as a by-product. Since a master thesis is limited in its extent, some of these questions are still unanswered. The main questions are related to lacking knowledge about BC sources and transport mechanisms. The increase in rBC concentration in the western Arctic from 2009 to 2012 cannot be explained and the probable reasons can only be assumed. An increase in the number of BC sources, an increase in BC emissions and changes in transport mechanisms of BC into the Arctic may lead to the revealed increase. These factors may also cause changes in the vertical

and horizontal distribution of BC.

This thesis reveals some difficulties which demand for improvements. First of all, it is essential to agree on an unambiguous definition of the terms "black carbon" and "soot". At least inside the community dealing with BC and BC related topics it would help to prevent misunderstandings and misinterpretations. Additionally, a convention on the terms "refractory black carbon" and "equivalent black carbon" should be agreed upon. Secondly, there should be found another way to clean the data.

Last not least, if there is more data to process, the used method is too time-consuming and too labour-intensive.

However, a higher data density is needed in order to increase the reliability of the results. Thus, more extensive measurements should be conducted. Future measurements are needed to observe the evolution of rBC concentrations in the Arctic. The impact of the different effects of BC on the Arctic climate should be investigated more precisely. The two latter items may then lead to an assessment of future developments concerning BC and its impact on the Arctic climate. In future measurements, CO and CO_2 should also be measured in order to facilitate source area identification. Since currently, the long-range transport is the dominant factor and the amount of measured concentrations depend mainly on the source area, it is necessary to investigate the potential BC sources in the future.

Acknowledgements

I would like to thank many people who have helped me through the completion of this thesis.

First of all, I would like to thank my first supervisor Prof. Dr. K. Heinke Schlünzen who enabled me to write this thesis externally. I thank her for encouraging me and I appreciated her advice.

I would like to express my gratitude to my second supervisor Andreas Herber from the Alfred Wegener Institute, Helmholtz Centre for Polar and Marine Research for the support to make this thesis possible.

I am indebted to the MeMi group, especially, for taking the time to peruse my presentation and for giving me constructive feedback.

I also would like to thank the section of sea-ice physics of the Alfred Wegener Institute, Helmholtz Centre for Polar and Marine Research. I owe special thanks to Thomas Krumpen, who assisted me with the Figures in Section 4.2, and to my colleague Martin Schiller. It was a pleasure to share the office with you.

Thanks to Sabine Eckhardt from NILU Norwegian Institut for Air Research for providing the FLEXPART results. Additionally, I acknowledge the NOAA Air Resources Laboratory (ARL) for the provision of the HYSPLIT transport and dispersion model and READY website used in this thesis.

Lastly, I would like to thank my family and friends for all their support and sympathy, for their love and patience, particularly, in hard times. Thank you. Dankeschön. Tusen takk.

Appendix A

Table A.1: Conducted flight tracks of PAMARCMiP09 in 2009.

flight no.	date	location			
		low	high	up	down
1	01.04.	– – – – – –	78°N/14°E–79°N/11°E	78°N/15°E	79°N/12°E
2	02.04.	77°N/20°E–79°N/20°E	– – – – – –	78°N/15°E	77°N/18°E
3	02.04.	– – – – – –	– – – – – –	78°N/18°E	78°N/15°E
4	03.04.	80°N/8°E–83°N/3°E	83°N/1°E–81°N/10°E	83°N/11°E	80°N/9°E
5	04.04.	79°N/10°E–78°N/13°E	79°N/14°E–79°N/13°E	78°N/15°E	79°N/11°E
6	04.04.	– – – – – –	– – – – – –	– – – – – –	79°N/11°E
7	05.04.	80°N/3°E–81°N/3°W	78°N/15°E–80°N/6°E	80°N/8°E	79°N/11°E
8	05.04.	– – – – – –	81°N/4°W–81°N/0°E	– – – – – –	– – – – – –
9	06.04.	81°N/12°E–83°N/8°E	79°N/15°E–80°N/13°E	78°N/15°E	80°N/13°E
10	06.04.	– – – – – –	82°N/11°E–80°N/13°E	– – – – – –	– – – – – –
11	08.04.	– – – – – –	79°N/14°E–81°N/12°W	78°N/15°E	82°N/16°E
12	09.04.	83°N/50°W–82°N/60°W	82°N/19°W–83°N/41°W	82°N/18°W	83°N/46°W
13	10.04.	– – – – – –	84°N/65°W–88°N/103°W	83°N/62°W	88°N/116°W
14	10.04.	– – – – – –	– – – – – –	88°N/122°W	89°N/110°W
15	11.04.	83°N/86°W–83°N/63°W	82°N/63°W–83°N/84°W	82°N/62°W	83°N/85°W
16	13.04.	– – – – – –	82°N/64°W–80°N/83°W	82°N/62°W	80°N/85°W
17	14.04.	– – – – – –	79°N/88°W–76°N/91°W	80°N/87°W	76°N/91°W
18	15.04.	– – – – – –	75°N/97°W–72°N/122°W	75°N/96°W	70°N/124°W
19	16.04.	72°N/128°W–73°N/139°W	– – – – – –	74°N/140°W	72°N/127°W
20	24.04.	– – – – – –	71°N/155°W–72°N/146°W	71°N/156°W	71°N/156°W
21	24.04.	71°N/161°W–73°N/167°W	– – – – – –	71°N/157°W	– – – – – –
22	24.04.	– – – – – –	– – – – – –	73°N/168°W	– – – – – –
23	25.04.	72°N/156°W–74°N/163°W	73°N/164°W–71°N/156°W	74°N/164°W	71°N/157°W

Table A.2: Conducted flight tracks of PAMARCMiP11 in 2011.

flight no.	date	location			
		low	high	up	down
24	30.03.	$71°N/158°W$–$71°N/161°W$	$72°N/162°W$–$71°N/157°W$	$72°N/162°W$	$71°N/157°W$
25	31.03.	$72°N/151°W$–$71°N/156°W$	– – – – –	$72°N/150°W$	$72°N/150°W$
26	01.04.	$71°N/156°W$–$72°N/162°W$	– – – – –	$72°N/161°W$	$72°N/157°W$
27	02.04.	$72°N/161°W$–$73°N/153°W$	$72°N/157°W$–$71°N/157°W$	$74°N/153°W$	$71°N/157°W$
28	03.04.	– – – – –	$71°N/154°W$–$69°N/135°W$	– – – – –	$69°N/134°W$
29	04.04.	$69°N/133°W$–$71°N/132°W$	$72°N/134°W$–$70°N/134°W$	$71°N/133°W$	$69°N/134°W$
30	05.04.	$68°N/134°W$–$71°N/133°W$	– – – – –	$71°N/132°W$	$71°N/132°W$
31	06.04.	– – – – –	$69°N/132°W$–$74°N/100°W$	– – – – –	$75°N/97°W$
32	10.04.	– – – – –	$79°N/86°W$–$82°N/68°W$	$75°N/95°W$	$82°N/65°W$
33	11.04.	– – – – –	– – – – –	$82°N/62°W$	$82°N/62°W$
34	14.04.	$82°N/63°W$–$85°N/50°W$	– – – – –	$85°N/52°W$	$83°N/61°W$
35	14.04.	– – – – –	– – – – –	$82°N/63°W$	– – – – –
36	15.04.	$83°N/62°W$–$85°N/68°W$	– – – – –	$85°N/71°W$	$83°N/61°W$
37	16.04.	$83°N/62°W$–$84°N/63°W$	– – – – –	$84°N/64°W$	– – – – –
38	17.04.	$83°N/62°W$–$86°N/75°W$	$86°N/73°W$–$84°N/65°W$	$86°N/75°W$	$83°N/62°W$
39	18.04.	$83°N/62°W$–$83°N/79°W$	– – – – –	$83°N/81°W$	$83°N/65°W$
40	18.04.	– – – – –	– – – – –	$84°N/58°W$	$84°N/58°W$
41	20.04.	$80°N/86°W$–$80°N/86°W$	– – – – –	– – – – –	– – – – –
42	21.04.	– – – – –	$80°N/86°W$–$80°N/85°W$	$80°N/85°W$	$80°N/86°W$
43	22.04.	$80°N/86°W$–$83°N/100°W$	– – – – –	$83°N/99°W$	$80°N/87°W$
44	22.04.	– – – – –	– – – – –	$80°N/86°W$	$80°N/86°W$
45	23.04.	– – – – –	$80°N/83°W$–$79°N/74°W$	$79°N/75°W$	$79°N/74°W$
46	27.04.	– – – – –	$83°N/58°W$–$82°N/21°W$	$83°N/62°W$	$82°N/17°W$
47	28.04.	$82°N/17°W$–$84°N/18°W$	– – – – –	$84°N/18°W$	$83°N/17°W$
48	28.04.	– – – – –	– – – – –	$82°N/13°W$	$82°N/15°W$
49	29.04.	– – – – –	$81°N/-8°E$–$79°N/11°E$	$81°N/10°W$	$78°N/13°E$
50	30.04.	– – – – –	– – – – –	$78°N/15°E$	$78°N/13°E$
51	04.05.	– – – – –	– – – – –	$81°N/5°E$	$79°N/15°E$
52	04.05.	– – – – –	– – – – –	$78°N/15°E$	$79°N/11°E$
53	04.05.	– – – – –	– – – – –	$79°N/12°E$	$79°N/13°E$
54	05.05.	– – – – –	$78°N/16°E$–$71°N/19°E$	$78°N/15°E$	$70°N/19°E$
55	05.05.	– – – – –	$69°N/18°E$–$64°N/12°E$	$70°N/19°E$	$64°N/12°E$

Table A.3: Conducted flight tracks of PAMARCMiP12 in 2012

flight no.	date	location low	location high	up	down
56	20.03.	$80°N/10°E$–$81°N/3°E$	$81°N/3°E$–$80°N/1°E$	$83°N/1°E$	– – – – – –
57	21.03.	– – – – – – –	$78°N/15°E$–$79°N/6°E$	$78°N/15°E$	$78°N/8°E$
58	21.03.	– – – – – – –	– – – – – – –	$79°N/10°E$	$79°N/11°E$
59	22.03.	– – – – – – –	$78°N/10°E$–$79°N/11°E$	$78°N/9°E$	$78°N/11°E$
60	22.03.	– – – – – –	– – – – – –	$78°N/11°E$	$79°N/9°E$
61	24.03.	$81°N/7°E$–$83°N/1°E$	$82°N/3°E$–$79°N/11°E$	$78°N/15°E$	$80°N/12°E$
62	24.03.	– – – – – –	– – – – – –	$82°N/1°E$	$79°N/10°E$
63	28.03.	– – – – – –	– – – – – –	$82°N/61°W$	$83°N/61°W$
64	29.03.	– – – – – –	– – – – – –	$81°N/62°W$	$81°N/77°W$
65	02.04.	– – – – – –	– – – – – –	$84°N/62°W$	$83°N/62°W$
66	04.04.	$83°N/68°W$–$85°N/76°W$	– – – – – –	$85°N/74°W$	$83°N/64°W$
67	05.04.	$83°N/102°W$–$81°N/107°W$	$80°N/86°W$–$83°N/93°W$	$79°N/85°W$	$82°N/94°W$
68	05.04.	– – – – – –	– – – – – –	$80°N/107°W$	$82°N/94°W$

Appendix B

Black carbon and particle concentration
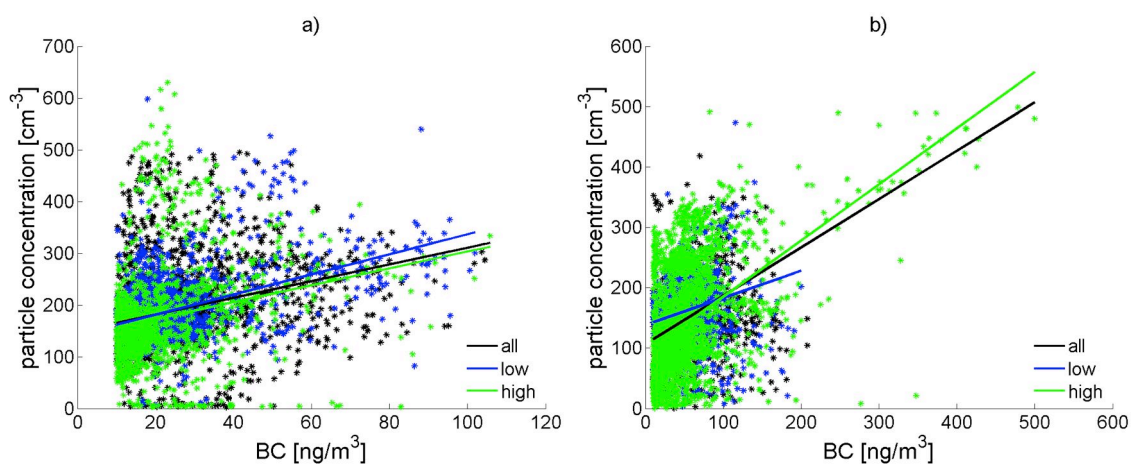
Figure B.1: Scatter plots of rBC and particle concentrations recorded at all altitudes (black), altitudes $h \leq 500\,\mathrm{m}$ (blue) and altitudes $h \geq 2500\,\mathrm{m}$ (green) during a) PAMARCMiP09 and b) PAMARCMiP11 with the associated linear regression line.
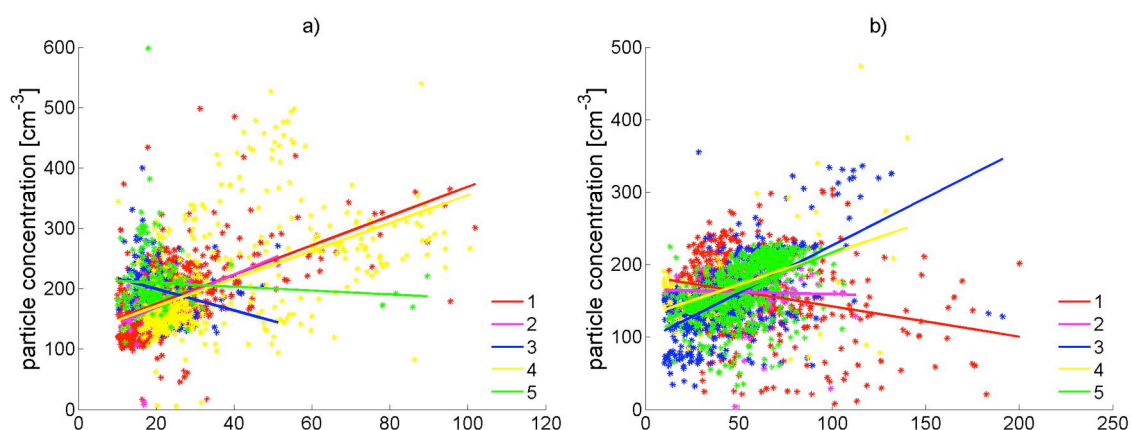
Figure B.2: Scatter plots of rBC and particle concentrations recorded at altitudes $h \leq$ 500 m in Region 1 (red), 2 (magenta), 3 (blue), 4 (yellow) and 5 (green) during a) PAMARCMiP09 and b) PAMARCMiP11 with the associated linear regression line.
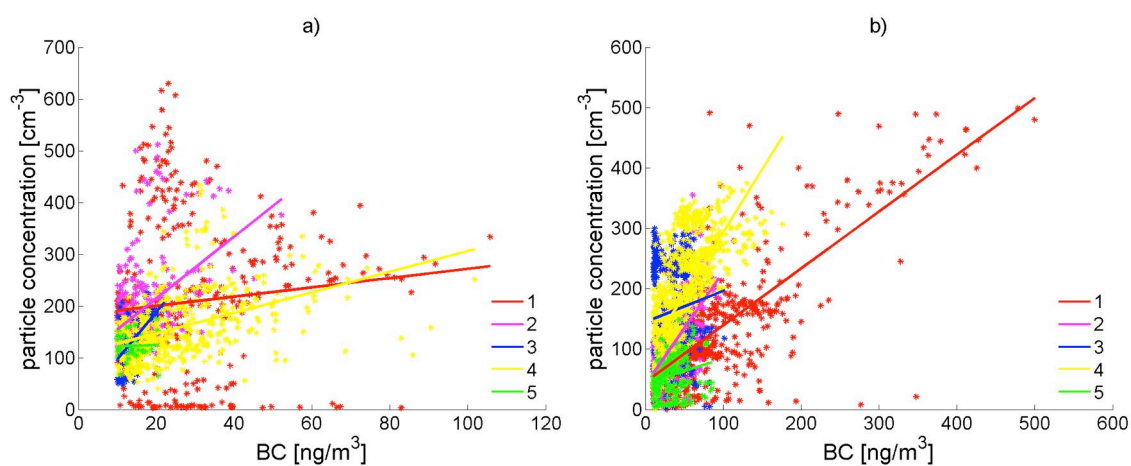
Figure B.3: Scatter plots of rBC and particle concentrations recorded at altitudes $h \geq$ 2500 m in Region 1 (red), 2 (magenta), 3 (blue), 4 (yellow) and 5 (green) during a) PAMARCMiP09 and b) PAMARCMiP11 with the associated linear regression line.

Black carbon and aerosol optical depth
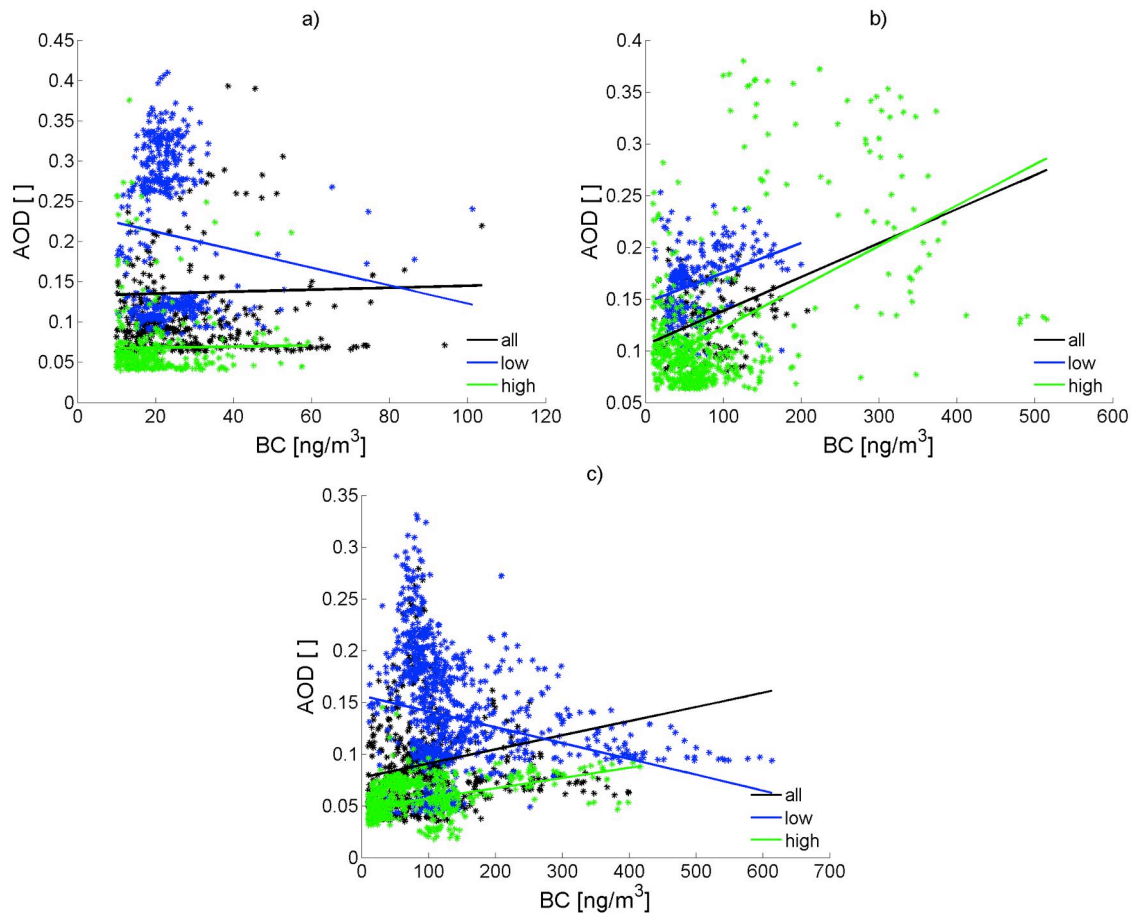
Figure B.4: Scatter plots of rBC concentrations and AOD recorded at all altitudes (black), altitudes $h \leq 500\,\mathrm{m}$ (blue) and altitudes $h \geq 2500\,\mathrm{m}$ (green) during a) PAMARCMiP09, b) PAMARCMiP11 and c) PAMARCMiP12 with the associated linear regression line.
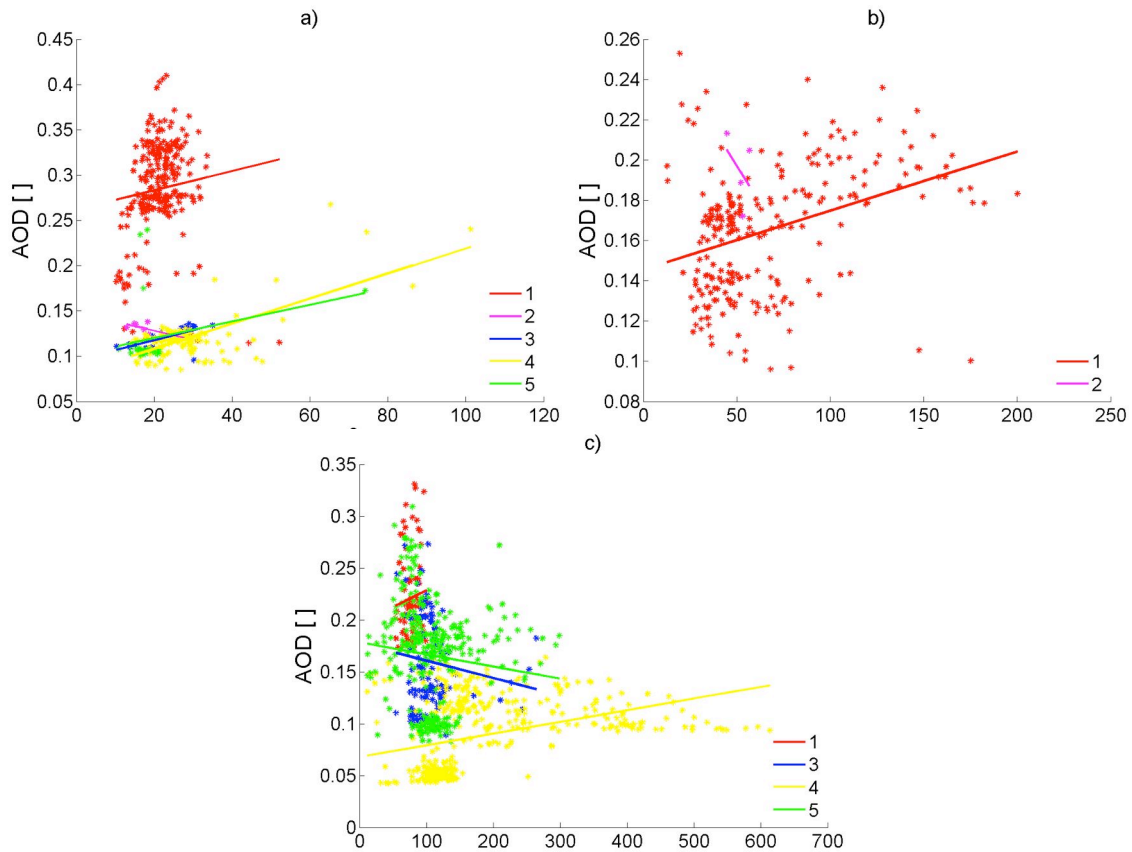
Figure B.5: Scatter plots of rBC concentrations and AOD recorded at altitudes $h \leq$ 500 m in Region 1 (red), 2 (magenta), 3 (blue), 4 (yellow) and 5 (green) during a) PAMARCMiP09, b) PAMARCMiP11 and c) PAMARCMiP12 with the associated linear regression line.
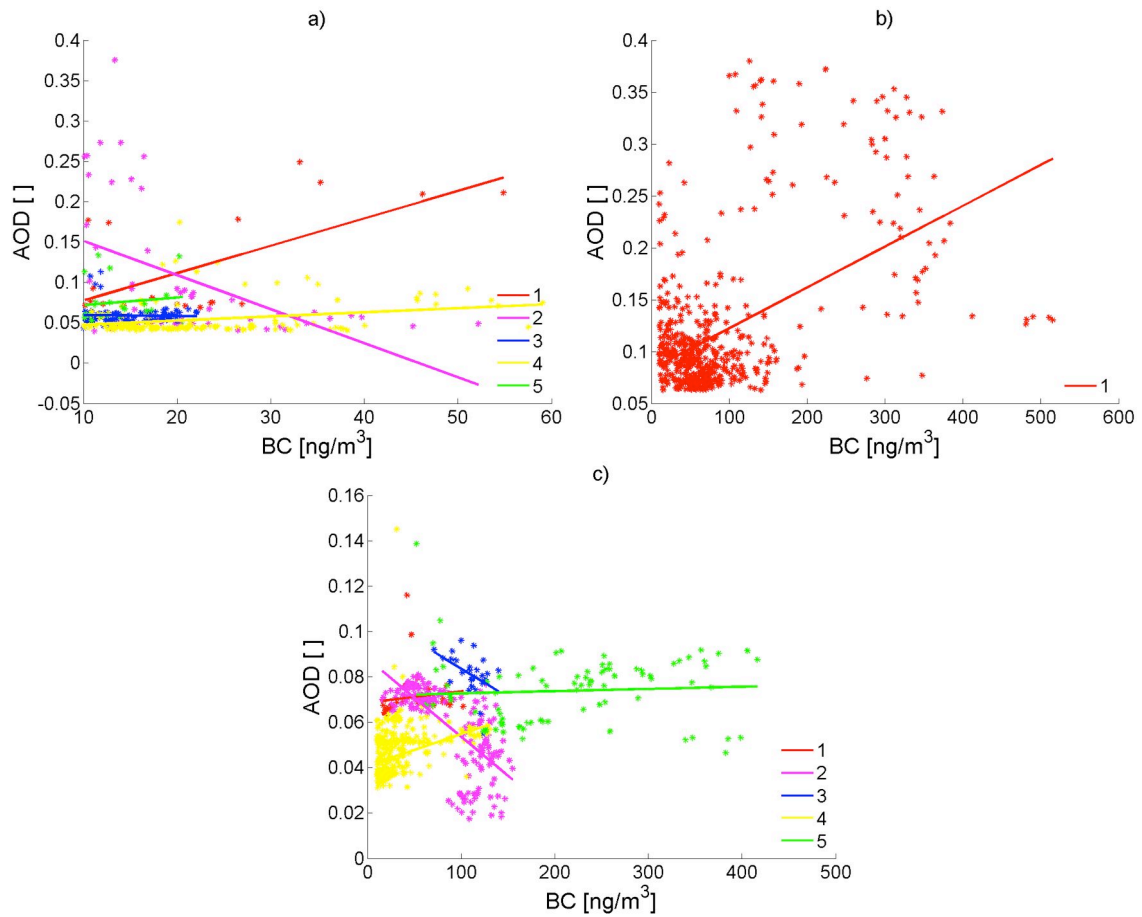
Figure B.6: Scatter plots of rBC concentrations and AOD recorded at altitudes $h \geq$ 2500 m in Region 1 (red), 2 (magenta), 3 (blue), 4 (yellow) and 5 (green) during a) PAMARCMiP09, b) PAMARCMiP11 and c) PAMARCMiP12 with the associated linear regression line.

Black carbon and albedo
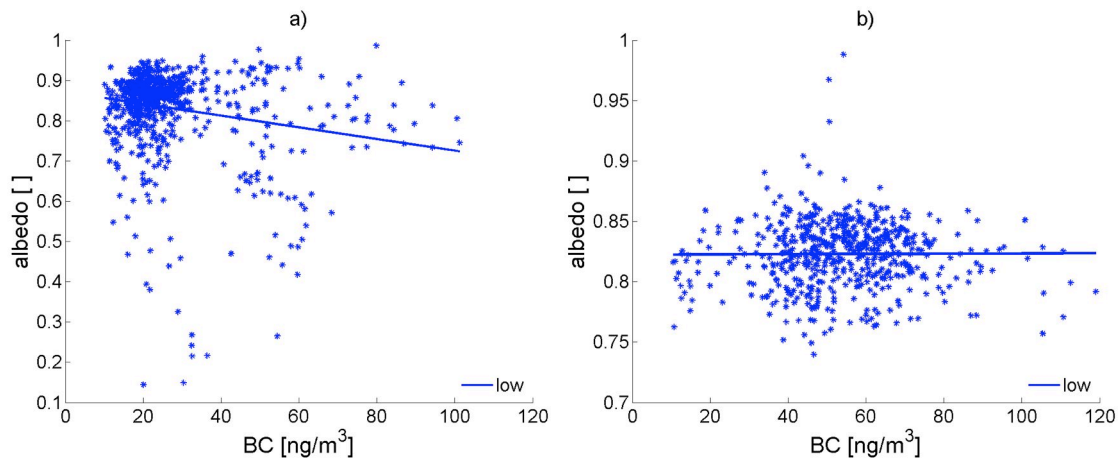
Figure B.7: Scatter plots of rBC concentrations and surface albedo recorded at altitudes $h \leq 500\,\mathrm{m}$ during a) PAMARCMiP09 and b) PAMARCMiP11 with the associated linear regression line.
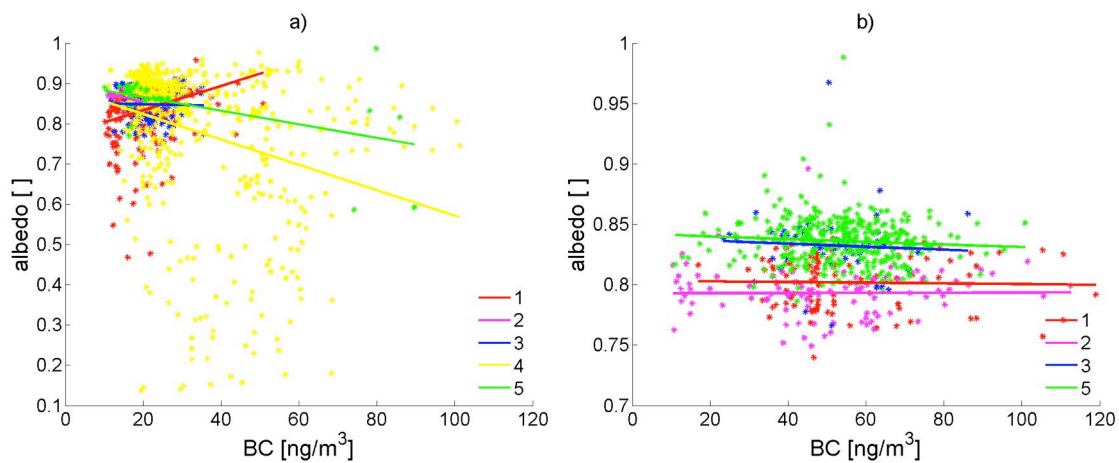
Figure B.8: Scatter plots of rBC concentrations and surface albedo recorded at altitudes $h \leq 500\,\mathrm{m}$ in Region 1 (red), 2 (magenta), 3 (blue), 4 (yellow) and 5 (green) during a) PAMARCMiP09 and b) PAMARCMiP11 with the associated linear regression line.
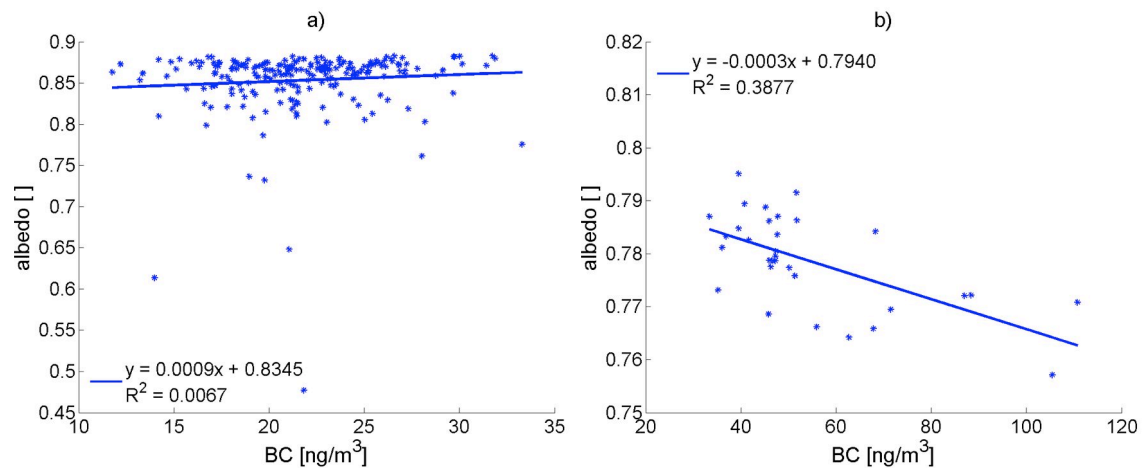
Figure B.9: Scatter plots of rBC concentration and albedo recorded on a) 16.4.2009 and b) 2.4.2011 both at low-level with the associated linear regression line and the coefficient of determination R^2.

List of Symbols

a	-	area of the sampling spot
A	-	absorbance
ABL	-	atmospheric boundary layer
AOD	-	aerosol optical depth
APD	-	avalanche photodiode detector
ARL	-	Air Resources Laboratory
BC	-	black carbon
BrC	-	brown carbon
C	-	calibration factor, describes the multiple scattering of the light beam due to filter material
CCN	-	cloud concensation nuclei
CFCs	-	chlorofluorocarbons
CH_4	-	methane
CLAP	-	Continuous Light Absorption Photometer
CO	-	carbon monoxide
CO_2	-	carbon dioxide
$cov(x, y)$	-	covariance of x and y
d	-	diameter
EBC	-	equivalent black carbon
h	-	height
HYSPLIT	-	HYbrid Single-Particle Lagrangian Integrated Trajectory
I	-	average intensity after traversing a medium
I_0	-	average intensity before traversing a medium
LED	-	light-emitting diode
λ	-	wavelength
M_{BC}	-	aerosol black carbon mass concentration

MAC	-	mass specific absorption coefficient / mass absorption cross section
N	-	sample size
N_2O	-	dinitrogen monoxide
O_3	-	ozone
OC	-	organic carbon
PAMARCMiP	-	Polar Airborne Measurements and Arctic Regional Model Simulation Project
PAS	-	Photoacoustic Spectrometer
PES	-	potential emission sensitivity
PSAP	-	Particle Soot / Absorption Photometer
r	-	Pearson's correlation coefficient
rBC	-	refractory black carbon
$R(ATN)$	-	calibration factor, stands for any other effect caused by deposited particles
R^2	-	coefficient of determination
SO_2	-	sulphur dioxide
SP2	-	Single Particle Soot Photometer
SPTA	-	Sun photometer tracking active
σ_{ap}	-	mass absorption coefficient
σ_{atn}	-	attenuation coefficient
σ_{rBC}	-	standard deviation of rBC
σ_{ep}	-	extinction coefficient
σ_{psap}	-	absorption coefficient actually measured by the PSAP
σ_{sp}	-	scattering coefficient
σ_x	-	standard deviation of x
σ_y	-	standard deviation of y
TOA	-	top of the atmosphere
τ	-	filter transmission
UHSAS	-	Ultra-High Sensitivity Aerosol Spectrometer
v	-	volume of air sampled
x	-	parameter x
$\overline{x}$	-	mean of x
y	-	parameter y

$\overline{y}$ -   mean of y

z -   thickness

$\overline{y}$ -   mean of y

z -   thickness

List of Figures

List of Tables

Bibliography

Affeld, B. (2003), Zyklonen in der Arktis und ihre Bedeutung für den Eistransport durch die Framstraße, PhD thesis, Universität Hamburg, Von-Melle-Park 3, 20146 Hamburg.

AMAP (2011), *The Impact of Black Carbon on Arctic Climate.* By: P.K. Quinn, A. Stohl, A. Arneth, T. Berntsen, J. F. Burkhart, J. Christensen, M. Flanner, K. Kupiainen, H. Lihavainen, M. Shepherd, V. Shevchenko, H. Skov, and V. Vestreng. Arctic Monitoring and Assessment Programme (AMAP), Oslo, 72 pp.

Anderson, T., Covert, D., Marshall, S., Laucks, M., Charlson, R., Waggoner, A., Ogren, J., Caldow, R., Holm, R., Quant, F., Sem, G., Wiedensohler, A., Ahlquist, N. and Bates, T. (1996), 'Performance Characteristics of a High-Sensitivity, Three-Wavelength, Total Scatter/Backscatter Nephelometer', *Journal of Atmospheric and Oceanic Technology* **17**(5), 967–986.

Arnott, W. P., Moosmüller, H., Rogers, C. F., Jin, T. and Bruch, R. (1999), 'Photoacoustic spectrometer for measuring light absorption by aerosol: instrument description', *Atmospheric Environment* **33**(17), 2845–2852.

Baumgardner, D., Raga, G., Peralta, O., Rosas, I., Castro, T., Kuhlbusch, T., John, A. and Petzold, A. (2002), 'Diagnosing black carbon trends in large urban areas using carbon monoxide measurements', *Journal of Geophysical Research: Atmospheres* **107**(D21), ICC 4–1–ICC 4–9.

Bond, T. (2007), 'Testimony for the Hearing on Black Carbon and Climate Change', *Testimony to the House Committee on Oversight and Government Reform, October 18, 2007, 16 pp* .

Bond, T. C., Anderson, T. L. and Campbell, D. (1999), 'Calibration and Intercomparison of Filter-Based Measurements of Visible Light Absorption by Aerosols', *Aerosol Science and Technology* **30**(6), 582–600.

References

Bond, T. C., Doherty, S. J., Fahey, D. W., Forster, P. M., Berntsen, T., DeAngelo, B. J., Flanner, M. G., Ghan, S., Kärcher, B., Koch, D., Kinne, S., Kondo, Y., Quinn, P. K., Sarofim, M. C., Schultz, M. G., Schulz, M., Venkataraman, C., Zhang, H., Zhang, S., Bellouin, N., Guttikunda, S. K., Hopke, P. K., Jacobson, M. Z., Kaiser, J. W., Klimont, Z., Lohmann, U., Schwarz, J. P., Shindell, D., Storelvmo, T., Warren, S. G. and Zender, C. S. (2013), 'Bounding the role of black carbon in the climate system: A scientific assessment', *Journal of Geophysical Research: Atmospheres* **118**(11), 5380–5552.

Buseck, P. R., Adachi, K., Gelencsér, A., Tompa, E. and Pósfai, M. (2012), 'Are black carbon and soot the same?', *Atmospheric Chemistry and Physics Discussions* **12**(9), 24821–24846.

Cape, J., Coyle, M. and Dumitrean, P. (2012), 'The atmospheric lifetime of black carbon', *Atmospheric Environment* **59**(0), 256–263.

Draxler, R. and Hess, G. (1997), 'Description of the HYSPLIT_4 modeling system', *NOAA Tech. Memo. ERL ARL-224, NOAA Air Resources Laboratory, Silver Spring, MD, 24 pp* .

Droplet Measurement Technologies (2012). Single Particle Soot Photometer (SP2): Operator Manual – DOC-0171 – Revision G-2, 2012.

Eleftheriadis, K., Vratolis, S. and Nyeki, S. (2009), 'Aerosol black carbon in the European Arctic: Measurements at Zeppelin station, Ny-Ålesund, Svalbard from 1998–2007', *Geophysical Research Letters* **36**(2).

ESRL NOAA (2012). online published at ftp://ftp.cmdl.noaa.gov/aerosol/doc/inst/clap/CLAP_User_Manual.pdf, visited on 21.11.2011 at 2pm.

ESRL NOAA (2013). online published at http://www.esrl.noaa.gov/gmd/aero/instrumentation/psap_desc.html, visited on 1.2.2013 at 4pm.

Fuller, K. A., Malm, W. C. and Kreidenweis, S. M. (1999), 'Effects of mixing on extinction by carbonaceous particles', *Journal of Geophysical Research: Atmospheres* **104**(D13), 15941–15954.

Garrett, T. and Zhao, C. (2006), 'Increased Arctic cloud longwave emissivity associated with pollution from mid-latitudes', *Nature* **440**, 787–789.

Hansen, A., Rosen, H. and Novakov, T. (1984), 'The aethalometer - An instrument for the real-time measurement of optical absorption by aerosol particles', *Science of The Total Environment* **36**(0), 191–196.

Hansen, J. (2002), 'A brighter future', *Climatic Change* **52**, 435–440.

Hansen, J. and Nazarenko, L. (2004), 'Soot climate forcing via snow and ice albedos', *Proceedings of the National Academy of Science of the USA* **101**(2), 423–428.

Hienola, A. I., Pietikäinen, J.-P., Jacob, D., Pozdun, R., Petäjä, T., Hyvärinen, A.-P., Sogacheva, L., Kerminen, V.-M., Kulmala, M. and Laaksonen, A. (2013), 'Black carbon concentration and deposition estimations in Finland by the regional aerosol-climate model REMO-HAM', *Atmospheric Chemistry and Physics* **13**(8), 4033–4055.

Horvath, H. (1993), 'Atmospheric light absorption-a review', *Atmospheric Environment. Part A. General Topics* **27**(3), 293–317.

Huebert, B. J., Howell, S. G., Covert, D., Bertram, T., Clarke, A., Anderson, J. R., Lafleur, B. G., Seebaugh, W. R., Wilson, J. C., Gesler, D., Blomquist, B. and Fox, J. (2004), 'PELTI: Measuring the Passing Efficiency of an Airborne Low Turbulence Aerosol Inlet', *Aerosol Science and Technology* **38**(8), 803–.826.

IPCC (2007*a*), *Climate Change 2007: Mitigation.* B. Metz, O.R. Davidson, P.R. Bosch, R. Dave, L.A. Meyer. Contribution of Working Group III to the Fourth Assessment, Report of the Intergovernmental Panel on Climate Change, Cambridge University Press, Cambridge, United Kingdom, 863 pp.

IPCC (2007*b*), *Climate Change 2007: The Physical Science Basis.* S. Solomon, D. Qin, M. Manning, Z. Chen, M. Marquis, K.B. Averyt, M. Tignor, and H.L. Miller. Contribution of Working Group I to the Fourth Assessment, Report of the Intergovernmental Panel on Climate Change, Cambridge University Press, Cambridge, United Kingdom, 996 pp.

Jacobson, M. (2001), 'Strong radiative heating due to the mixing state of black carbon in atmospheric aerosols', *Nature* **409**, 695–697.

Kaleschke, L., Richter, A., Burrows, J., Afe, O., Heygster, G., Notholt, J., Rankin, A. M., Roscoe, H. K., Hollwedel, J., Wagner, T. and Jacobi, H.-W. (2004), 'Frost flowers on sea ice as a source of sea salt and their influence on tropospheric halogen chemistry', *Geophysical Research Letters* **31**(16).

Laborde, M., Crippa, M., Tritscher, T., Jurányi, Z., Decarlo, P. F., Temime-Roussel, B., Marchand, N., Eckhardt, S., Stohl, A., Baltensperger, U., Prévôt, A. S. H., Weingartner, E. and Gysel, M. (2013), 'Black carbon physical properties and mixing state in the European megacity Paris', *Atmospheric Chemistry and Physics* **13**(11), 5831–5856.

Lack, D. A., Lovejoy, E. R., Baynard, T., Pettersson, A. and Ravishankara, A. R. (2006), 'Aerosol Absorption Measurement using Photoacoustic Spectroscopy: Sensitivity, Calibration, and Uncertainty Developments', *Aerosol Science and Technology* **40**(9), 697–708.

Langridge, J. M., Lack, D., Brock, C. A., Bahreini, R., Middlebrook, A. M., Neuman, J. A., Nowak, J. B., Perring, A. E., Schwarz, J. P., Spackman, J. R., Holloway, J. S., Pollack, I. B., Ryerson, T. B., Roberts, J. M., Warneke, C., de Gouw, J. A., Trainer, M. K. and Murphy, D. M. (2012), 'Evolution of aerosol properties impacting visibility and direct climate forcing in an ammonia-rich urban environment', *Journal of Geophysical Research: Atmospheres* **117**(D21).

Latha, K. M. and Badarinath, K. (2004), 'Correlation between black carbon aerosols, carbon monoxide and tropospheric ozone over a tropical urban site', *Atmospheric Research* **71**(4), 265 – 274.

Liu, J., Fan, S., Horowitz, L. W. and Levy, H. (2011), 'Evaluation of factors controlling long-range transport of black carbon to the Arctic', *Journal of Geophysical Research: Atmospheres* **116**(D4).

Magee Scientific Corporation (2013). online published at http://www.mageesci.com/air_sampling_products/aethalometer_overview.html, visited on 31.1.2013 at 11am.

Magi, B. I., Hobbs, P. V., Schmid, B. and Redemann, J. (2003), 'Vertical profiles of light scattering, light absorption, and single scattering albedo during the dry, biomass burning season in southern Africa and comparisons of in situ and remote sensing measurements of aerosol optical depths', *Journal of Geophysical Research* **108**(D13).

Moosmüller, H., Chakrabarty, R. and Arnott, W. (2009), 'Aerosol light absorption and its measurement: A review', *Journal of Quantitative Spectroscopy and Radiative Transfer* **110**(11), 844–878.

Nilsson, E. D. and Rannik, U. (2001), 'Turbulent aerosol fluxes over the Arctic Ocean: 1. Dry deposition over sea and pack ice', *Journal of Geophysical Research: Atmospheres* **106**(D23), 32125–32137.

Petzold, A., Ogren, J. A., Fiebig, M., Laj, P., Li, S.-M., Baltensperger, U., Holzer-Popp, T., Kinne, S., Pappalardo, G., Sugimoto, N., Wehrli, C., Wiedensohler, A. and Zhang, X.-Y. (2013), 'Recommendations for reporting "black carbon" measurements', *Atmospheric Chemistry and Physics* **13**(16), 8365–8379.

Petzold, A., Schloesser, H., Sheridan, P., Arnott, W., Ogren, J. and Virkkula, A. (2005), 'Evaluation of Multiangle Absorption Photometry for Measuring Aerosol Light Absorption', *Aerosol Science and Technology* **1**(4), 40–51.

Ramanathan, V. (2007), 'Role of Black Carbon on Global and Regional Climate Change', *Testimony to the House Committee on Oversight and Government Reform, October 18, 2007, 17 pp* .

Ramanathan, V. and Carmichael, G. (2008), 'Global and regional climate changes due to black carbon', *Nature Geocience* **1**(4), 221–227.

Righi, M., Klinger, C., Eyring, V., Hendricks, J., Lauer, A. and Petzold, A. (2011), 'Climate Impact of Biofuels in Shipping: Global Model Studies of the Aerosol Indirect Effect', *Environmental Science and Technology* **45**(8), 3519–3525.

Santoso, M., Lestiani, D. and Hopke, P. (2013), 'Atmospheric black carbon in PM2.5 in Indonesian cities', *Journal of the Air an Waste Managment Assosiation* pp. 1022–1025.

Schmid, O., Artaxo, P., Arnott, W. P., Chand, D., Gatti, L. V., Frank, G. P., Hoffer, A., Schnaiter, M. and Andreae, M. O. (2005), 'Spectral light absorption by ambient aerosols influenced by biomass burning in the Amazon Basin - I. Comparison and field calibration of absorption measurement techniques', *Atmospheric Chemistry and Physics Discussions* **5**(5), 9355–9404.

Schnaiter, M., Linke, C., Möhler, O., Naumann, K.-H., Saathoff, H., Wagner, R., Schurath, U. and Wehner, B. (2005), 'Absorption amplification of black carbon internally mixed with secondary organic aerosol', *Journal of Geophysical Research: Atmospheres* **110**(D19).

Schwarz, J. P., Gao, R. S., Fahey, D. W., Thomson, D. S., Watts, L. A., Wilson, J. C., Reeves, J. M., Darbeheshti, M., Baumgardner, D. G., Kok, G. L., Chung, S. H., Schulz, M., Hendricks, J., Lauer, A., Kärcher, B., Slowik, J. G., Rosenlof, K. H.,

Thompson, T. L., Langford, A. O., Loewenstein, M. and Aikin, K. C. (2006), 'Single-particle measurements of midlatitude black carbon and light-scattering aerosols from the boundary layer to the lower stratosphere', *Journal of Geophysical Research: Atmospheres* **111**(D16).

Stohl, A., Burkhart, J. F., Eckhardt, S., Hirdman, D. and Sodemann, H. (2007), 'An integrated internet-based system for analyzing the influence of emission sources and atmospheric transport on measured concentrations of trace gases and aerosols', *Norwegian Institute for Air Research, Kjeller, Norway, 26 pp* .

Stone, R. S., Herber, A., Vitale, V., Mazzola, M., Lupi, A., Schnell, R. C., Dutton, E. G., Liu, P. S. K., Li, S.-M., Dethloff, K., Lampert, A., Ritter, C., Stock, M., Neuber, R. and Maturilli, M. (2010), 'A three-dimensional characterization of Arctic aerosols from airborne Sun photometer observations: PAM-ARCMIP, April 2009', *Journal of Geophysical Research: Atmospheres* **115**(D13).

Strawa, A. W., Castaneda, R., Owano, T., Baer, D. S. and Paldus, B. A. (2003), 'The Measurement of Aerosol Optical Properties Using Continuous Wave Cavity Ring-Down Techniques', *Journal of Atmospheric and Oceanic Technology* **20**(4), 454–465.

U.S. EPA (2012). Report to Congress on Black Carbon, United States Environmental Protection Agency, 2012, 388 pp.

Warren, S. G. (2013), 'Can black carbon in snow be detected by remote sensing?', *Journal of Geophysical Research: Atmospheres* **118**(2), 779–786.

Weingartner, E., Saathoff, H., Schnaiter, M., Streit, N., Bitnar, B. and Baltensperger, U. (2003), 'Absorption of light by soot particles: determination of the absorption coefficient by means of aethalometers', *Journal of Aerosol Science* **34**(10), 1445–1463.

Zhang, R., Khalizov, A. F., Pagels, J., Zhang, D., Xue, H. and McMurry, P. H. (2008), 'Variability in morphology, hygroscopicity, and optical properties of soot aerosols during atmospheric processing', *Proceedings of the National Academy of Sciences* **105**(30), 10291–10296.

Erklärung

Ich versichere, dass ich die Arbeit selbstständig verfasst und keine anderen als die angegebenen Hilfsmittel benutzt habe. Insbesondere habe ich keine im Quellenverzeichnis nicht benannten Internet-Quellen verwendet. Die Arbeit habe ich vorher nicht in einem anderen Prüfungsverfahren eingereicht. Die eingereichte schriftliche Fassung entspricht der auf dem elektronischen Speichermedium.
Mit der Ausleihe an die Bibliothek bin ich einverstanden.

Hamburg, den 28. Oktober 2013   Kristina Conrady